STRUCTURE/FUNCTION ANALYSIS OF HMW2 AND PROTEOMIC ANALYSIS OF THE ELECTRON-DENSE CORE IN *MYCOPLASMA PNEUMONIAE*

by

STEPHANIE ROSS BOSE

(Under the Direction of Duncan Charles Krause)

ABSTRACT

Mycoplasma pneumoniae, a cell wall-less prokaryote, causes atypical or "walking" pneumonia and tracheobronchitis in humans. Attachment to host respiratory epithelium is mediated by a polar differentiated organelle that has an electron-dense core, which contains a thin and thick rod. The non-cytadhering mutant I-2 lacks the cytadherence-associated protein HMW2 due to a frameshift mutation, is non-motile, has morphological abnormalities, reduced levels of HMW1, HMW3, and P65, and fails to cluster P1. Another cytadherence-associated protein HMW1 exhibits a reciprocal dependency with HMW2. Mutants lacking HMW1 or HMW2, designated M6 and I-2, respectively, have no obvious attachment organelle or electron-dense core. Thus, both proteins are thought to have an early role in attachment organelle assembly. Although components of the Triton X-100 insoluble fraction of *M. pneumoniae* have been identified by mass spectrometry studies, proteins specific to the core were not assigned. HMW2 was identified as a component of that fraction. Based this and other evidence, a model was suggested where HMW2 is a major component of the electron-dense core

and interacts longitudinally with an internal translation product of the *hmw2* transcript, P28, to form the core. Structure and function analysis of HMW2 derivatives allowed for identification of distinct regions, including the C-terminus, coiled-coil domains, and leucine repeats of HMW2, required for normal cellular function and core formation.

An HMW2-GFP fusion localized this protein to the attachment organelle. However, high resolution immuno-localization studies allowed for precise localization of HMW2 to the periphery of the electron-dense core and a new model for core formation is described, where HMW2 and P28 comprise the thin rod of the core, which acts as a scaffold for formation of the thick rod. The central portion of HMW2 may act as the spokes, a structural feature of the attachment organelle in the electron-lucent space between the core and the membrane. Liquid chromatography/mass spectrometry analysis allowed for identification of the components of a core-enriched fraction. These 89 proteins included cytadherence-accessory proteins, along with those involved in transcription/translation, cell division, and metabolism.

INDEX WORDS: Mycoplasma, HMW2, P28, Cytoskeleton, Electron-dense core, Attachment organelle, Coiled-coils, Cytadherence

STRUCTURE/FUNCTION ANALYSIS OF HMW2 AND PROTEOMIC ANALYSIS OF THE ELECTRON-DENSE CORE IN *MYCOPLASMA PNEUMONIAE*

by

STEPHANIE ROSS BOSE

B.S., The University of Georgia, 2000

A Dissertation Submitted to the Graduate Faculty of The University of Georgia in Partial Fulfillment of the Requirements for the Degree

DOCTOR OF PHILOSOPHY

ATHENS, GEORGIA

2007

STRUCTURE/FUNCTION ANALYSIS OF HMW2 AND PROTEOMIC ANALYSIS OF THE ELECTRON-DENSE CORE IN *MYCOPLASMA PNEUMONIAE*

by

STEPHANIE ROSS BOSE

Major Professor: Duncan C. Krause

Committee: Anna Karls
Tim Hoover
Mark Farmer
Marcus Fechheimer

Electronic Version Approved:

Maureen Grasso
Dean of the Graduate School
The University of Georgia
May 2007

DEDICATION

This work is dedicated to my husband, Jeff. Your love and encouragement have meant the world to me and helped me to press on each day toward achieving this goal. I couldn't have done it without you and am truly blessed to have you as my husband! I also wanted to dedicate this work to my parents. Your belief in me, love, and support in everything I've pursued throughout the years has helped me to get to where I am today. I could not have done it without you, as well. Thank you for encouraging me to think big and to follow my dreams and aspirations!

ACKNOWLEDGEMENTS

I would like to thank Dr. Duncan C. Krause for allowing me to join his lab and for being such a wonderful major professor and supportive mentor. I have learned so much from you! Words cannot describe how much I've appreciated all of your advice, encouragement, and support during my career here, especially when I was working through the "gray areas" of my project and during this last semester. I also want to thank you for supporting my teaching aspirations and special life events, even though it meant that I was away from the lab at times. Thank you to my committee members, Dr. Anna Karls, Dr. Tim Hoover, Dr. Mark Farmer, and Dr. Marcus Fechheimer, for all of your helpful comments and suggestions pertaining to my project, as well.

Several former Krause lab members, Mitch, Melisa, Jarrat, and Rob offered me a lot of help, support, and friendship along the way. Mitch was a great mentor and friend. I appreciated his enthusiasm about my project and new data and his help in getting started in my work on HMW2. Melisa was also a great friend, who was very supportive and made the lab an enjoyable place to work. Thanks for passing on your EM expertise! Jarrat was always willing to offer words of advice in the lab and especially about our Georgia vs. Florida college football rivalry. All of you made our lab a great place to work!

The current Krause lab members, Kyung, How-Yi, Jason, Ed, and Clint, were also great labmates. Kyung, thank you for being the lab mom that we needed. You and

Ed keep the lab running! I am so grateful for your cloning help. Thank you!! You are a life-saver! You will never lose your cloning touch, despite what you think!! How-Yi, you have been a great friend! I have enjoyed sitting near you in the lab and our many conversations about everything concerning life, weddings, and lab. I'll miss you and will always think of you on July 29th! Jason, thanks for making me laugh almost everyday (literally) and for being a great friend! Thanks for listening to my frustrations and joys concerning my project. I look forward to hearing about your future success and I expect great things from you! Ed, you are a fountain of facts and entertaining stories! Thank you for your help with the quantitative HA data! I cannot tell you how much I appreciate all your work on that. Thank you for all you do for the lab!! Clint, good luck with the HMW2 phosphorylation project. I'm glad you will be continuing on the HMW2 lineage. To all of the present Krause lab members, I have enjoyed working with you! I love and will miss you all!

Last but certainly not least, I could not have made it this far without the love and support from all my close friends both in and outside the department. A special thanks goes to Pam Bonner and Tiffany Major, who have been my friends since the first day we started graduate school together. We've come a long way!

Thanks to all of you!!!!

TABLE OF CONTENTS

Page

LIST OF TABLES

Page

LIST OF FIGURES

Page

CHAPTER I

INTRODUCTION

Mycoplasma pneumoniae is a pathogen of the human respiratory tract, causing primary atypical or “walking” pneumonia and tracheobronchitis. The attachment organelle, a remarkably complex terminal structure that mediates adherence to host respiratory epithelium (Razin and Jacobs, 1992), is a polar tapered extension of the mycoplasma cell and is defined by its electron-dense core, which enlarges to form a terminal button. The core and terminal button are part of the mycoplasma cytoskeleton (triton shell), a filamentous network of proteins that remains following extraction of *M. pneumoniae* cells with the detergent Triton X-100 (TX) (Balish and Krause, 2002; Gobel *et al.*, 1981; Meng and Pfister, 1980). Major adhesin protein P1 is found densely clustered at the attachment organelle in wild-type *M. pneumoniae* cells (Baseman *et al.*, 1982; Collier *et al.*, 1983; Feldner *et al.*, 1982; Hu *et al.*, 1982) and alone is essential but not sufficient for cytadherence. A large group of cytadherence-accessory proteins that aid in attachment has emerged from the characterization of non-cytadhering mutants. One such protein is HMW2, an attachment organelle-localized protein (Balish *et al.*, 2003b), whose loss results in a non-cytadhering avirulent phenotype, the inability to localize P1 to the attachment organelle, and the accelerated turnover of the cytadherence-accessory proteins HMW1, HMW3, and P65 (Jordan *et al.*, 2001; Krause *et al.*, 1982; Krause *et al.*, 1997; Popham *et al.*, 1997). Based on the myriad of

downstream effects associated with the loss of HMW2, I evaluated wild-type and mutant HMW2 derivatives to identify specific regions of HMW2 that are essential for normal cellular function in *M. pneumoniae*, by examining stabilization of cytadherence-associated proteins P28, P41, P24, HMW1, HMW3, and P65, TX partitioning, P1 localization, morphology, cytadherence, and motility. I found that there were distinct requirements for the C-terminus of HMW2 and its coiled-coils and leucine repeats.

The deduced amino acid sequence of HMW2 is predicted to form dimeric and trimeric coiled-coils along its length (Balish *et al.*, 2003b; Krause *et al.*, 1997). Because of the structural features of HMW2, its localization within the attachment organelle (Balish *et al.*, 2003b), the absence of a core with the loss of HMW2 (Seto and Miyata, 2003), and a predicted length which is similar to the 250nm electron-dense core, a model was suggested where HMW2 is predicted to be a major component of core. This model predicts that dimeric and trimeric interactions of HMW2 would form a compact network with other HMW2 monomers and P28, an internal translation product of the *hmw2* transcript (Fisseha *et al.*, 1999), in a longitudinal manner (Balish *et al.*, 2003b). I tested that hypothesis by TEM analysis of thin sections and TX-insoluble fractions of wild-type and mutant HMW2 derivatives to determine if the length of HMW2 corresponded with the length of the core. HMW1 and HMW2 have a reciprocal relationship (Willby *et al.*, 2004) and are suggested to have an early role in attachment organelle assembly and core formation (Krause and Balish, 2004; Seto and Miyata, 2003). Because of this, TEM analysis of thin sections and TX fractions of HMW1 mutants were also examined. Furthermore, HMW2 was previously localized to the attachment organelle through the use of an HMW2-GFP fusion; however, because of

the size of GFP and the amount of fluorescence emitted, it was difficult to determine the exact location of HMW2 within the attachment organelle. Thus, N- and C-terminus-specific HMW2 antibodies were made and used in high-resolution immuno-localization studies to establish more precisely the position of HMW2 in the attachment organelle. These data, along with the TEM analysis, allowed me to suggest a new model for core formation.

A previous mass spectrometry study identified 41 proteins as components of the *M. pneumoniae* TX-insoluble fraction (Regula et al., 2001); however these proteins were not specifically assigned to cytoskeletal structures, such as the electron-dense core. In that study, the cores were not isolated from the associated material that remains following TX extraction. Thus, I developed a protocol for isolating a core-enriched fraction (CEF), which was used in sample preparation for liquid chromatography-mass spectrometry studies. The mass spectrometry analysis identified for the first time proteins that were part of the CEF and allowed me to make predictions concerning the components of the core. Because *M. pneumoniae* has no typical cytoskeletal proteins or homologs, such as MreB, actin, MinCDE, its cytoskeletion appears to be unlike that of other genera of bactera (Balish and Krause, 2006). Thus, determination of the components of the core may help to identify novel cytoskeletal proteins.

The aim of this dissertation project was to investigate the role of HMW2, determine its significance within the attachment organelle, and further our knowledge of the components of the electron-dense core. I accomplished these goals by evaluating HMW2 derivatives to determine regions significant for normal cellular function and core

formation. Furthermore, I developed a protocol to enrich for electron-dense cores, which enabled me to analyze a core-enriched fraction and for the first time identify its components.

CHAPTER II

REVIEW OF THE LITERATURE

History

The first mycoplasma to be cultured was later identified as the causative agent of contagious bovine pleuropneumonia (CBP) in 1898 by Edmond Nocard and Emile Roux (Nocard and Roux, 1990), and subsequently classified as *Mycoplasma mycoides* in 1956 (Edward and Freundt, 1956). Phenotypic analysis of this agent not only revealed unusually small cells, which enabled passage through a filter like a virus, but also revealed "fried-egg" shaped colonies like a bacterium (Bove, 1999). Thus, uncertainty followed concerning this peculiar phenotype and whether the agent was a virus or a bacterium (Bove, 1999). Over time, the mycoplasmas were classified into a group of organisms called pleuropneumonia-like organisms (PPLOs), which were defined as filterable organisms that could be grown on artificial media (Eaton, 1965).

Another PPLO was identified in 1945 and shown by Monroe Eaton to be a causative agent of primary atypical or "walking" pneumonia (Meiklejohn *et al.*, 1945), and thus was nicknamed the "Eaton agent". Outbreaks of this illness were prominent in young adults during WWII (Eaton, 1965), commonly occurring in crowded living areas such as military barracks (Marmion, 1990). The need for continued studies was obvious from these outbreaks. Studies indicated sensitivity of the Eaton agent to certain antibiotics, a common phenotype in bacteria (Bove, 1999), and indicating that this was a

bacterium, and in the 1960s this conclusion was confirmed by visualization of bacterial cells in tissue cultures and on the epithelial surfaces of chickens that were infected with the Eaton agent (Clyde, 1961; Goodburn *et al.*, 1963). The Eaton agent was cultured for the first time in 1962 by Chanock and Hayflick and, although initially identified in 1945, it was not designated as a PPLO until 1962 (Chanock *et al.*, 1962). Classified as *Mycoplasma pneumoniae* in 1963 (Chanock, 1963), this organism was the first PPLO found to be a human pathogen, although the first PPLO identified in humans was *Mycoplasma hominis* (Dienes, 1940). Later, PPLOs were shown to have no cell wall (van and Ruys, 1960), and because of this, PPLO was later changed to Mollicutes, meaning “soft skin” (Edward *et al.*, 1967).

By 1970, Biberfeld and Biberfeld were able to take a much closer look at the ultrastructure of *Mycoplasma pneumoniae* (Biberfeld and Biberfeld, 1970), opening the doors to the inner workings of this organism, its motility, and how it causes infection. Finally, in 1996, the genome was sequenced, allowing for the expansion of molecular techniques and the field of proteomics in exploration of *M. pneumoniae* cell and molecular biology.

Taxonomy and Phylogeny

Mycoplasma pneumoniae is grouped in the taxonomic class *Mollicutes*, the order *Mycoplasmatales*, and the genus *Mycoplasma*. Other genera of the *Mollicutes* class include *Anaeroplasma, Acholeplasma*, *Ureaplasma*, and *Spiroplasma*. The 16S rRNA analysis revealed that the mollicutes are members of the Gram-positive branch of the phylogenetic tree, sharing a common ancestor with lactobacilli, bacilli, and streptococci

with low G+C content, and are facultative anaerobes (Weisburg *et al.*, 1989; Woese *et al.*, 1980)). Later, the *Mollicutes* diverged into the AAP branch (*Acholeplasmataceae*, *Anaeroplasmataceae*, and *Phytoplasma*) with a reduction in genome size where the genes for cell wall synthesis were predicted to be lost (Maniloff, 2002; Rogers *et al.*, 1985). Another divergence event further reduced the genome necessitating the requirement of sterols for growth (Rogers *et al.*, 1985). Formation of the SEM branch containing *Spiroplasmataceae*, *Entomoplasmataceae*, and *Mycoplasmataceae* occurred at this time (Rogers *et al.*, 1985). *Mycoplasmataceae* diverged from the SEM branch into various mycoplasma branches, one of which is the δ-mycoplasma branch, which includes *Mycoplasma* and *Ureaplasma*. Phylogenetic analysis revealed *M. genitalium* and *M. gallisepticum* as the closest relatives (Maniloff, 2002).

Cellular Physiology

Mycoplasma pneumoniae was first cultured in 1962 on artificial agar media, growing as “fried-egg” shaped colonies (Chanock *et al.*, 1962). The requirement of specific nutrients in these culture conditions demonstrated the fastidious nature of the organism. Yeast extract and horse serum were necessary for growth (Chanock *et al.*, 1962), as a source of amino acids and cholesterol, respectively (Rodwell and Mitchell, 1979; Waites and Talkington, 2004). Because cholesterol is seldom found in bacterial cell membranes, its requirement for growth in these cells, where it contributes to membrane rigidity, is unusual. Liquid media used for culturing *M. pneumoniae* are Hayflick’s medium (Hayflick, 1965) or SP4 medium (Hackett and Whitcomb, 1995),

which both contain serum and yeast as essential supplements. Its optimal growth temperature is between 36-38°C (Freundt and Razin, 1984).

The complete genome of *M. pneumoniae* was sequenced in 1996 and further elucidated the physiology of the organism, its limitations, and its complexity. The *M. pneumoniae* genome is 816kbp, has 687 genes (Himmelreich *et al.*, 1996) and is considered to be among the smallest to date in self-replicating organisms (Pollack *et al.*, 1997; Wilson and Collier, 1976); for comparison, the genome of *E. coli* is five times larger (Rudd, 2000; Waites and Talkington, 2004). This minimal microbe also has a low G+C content of approximately 40% (Dybvig and Voelker, 1996).

As a result of having a reduced genome, *M. pneumoniae* has many metabolic and biosynthetic limitations. First, no cell wall is present due to the absence of cell wall synthesis genes, which were thought to have been lost as part of a genome reduction event during its evolution (Rogers *et al.*, 1985). Second, it must be provided with nucleotide precursors in its growth media because of its inability to synthesize purines and pyrimidines *de novo* (Dandekar, 2002; Himmelreich *et al.*, 1996). Third, although the enzymes required for the metabolism of glucose to pyruvate in the Embden-Myerhoff pathway are present and allow for synthesis of ATP (Himmelreich *et al.*, 1996), the metabolic processes of *M. pneumoniae* are limited by the absence of other enzymes required for metabolism. For instance, glucose-6-phosphate dehydrogenase, 6-phospho-gluconate dehydrogenase, and transaldoslase, are required in the pentose phosphate pathway, an alternative pathway in glucose metabolism, but are not present in *M. pneumoniae* (Himmelreich *et al.*, 1996). Furthermore, synthesized pyruvate is not metabolized by the tri-carboxylic acid (TCA) cycle, because most of the enzymes

needed for this pathway are absent as well, except for malate dehydrogenase (Dandekar, 2002; Pollack, 2002). Metabolism of pyruvate by *M. pneumoniae* most often occurs by either: formation of lactate by lactate dehydrogenase, or formation of acetyl–CoA by the pyruvate dehydrogenase complex, which is then metabolized to acetate by phosphotransacetylase and acetate kinase (Himmelreich *et al.*, 1996). Although *M. pneumoniae* lacks quinones and cytochromes, it can recycle NAD^+ by transferring electrons from NADH through flavoproteins to oxygen (Pollack *et al.*, 1981; Pollack, 1992, 2002). Because of the absence of a typical electron transport chain, most of the ATP for the cell is synthesized by substrate-level phosphorylation in the Embden-Myerhoff pathway (Pollack *et al.*, 1981) to produce 2 moles of pyruvate, ATP, and NADH from each mole of glucose (Freundt and Razin, 1984).

Other limiting factors of *M. pneumoniae* include its inability to perform homologous recombination despite having *recA* in its genome, its inability to support plasmids (Dybvig, 1990), and its unusual codon usage where the UGA codon codes for the amino acid tryptophan (Inamine *et al.*, 1990). All of these factors contribute to difficulties in performing genetic manipulations. Since, the inability to perform homologous recombination prevents the formation of targeted knockout mutations in *M. pneumoniae*, spontaneous and chemical mutations were initially relied on to produce mutants. Success in transforming the *Staphylococcus aureus Tn*4001 transposon into mycoplasmas (Mahairas and Minion, 1989), and specifically in *M. pneumoniae* (Hedreyda *et al.*, 1993) has yielded a tool that has been used to create widespread insertion mutants in random transposon mutagenesis. Because of the difficulty in expressing large amounts of specific proteins in *M. pneumoniae*, attempts were made to

express and overproduce these proteins by transforming them into *E. coli*. However, this often led to premature termination of translation of proteins containing multiple UGA codons (Schaper *et al.*, 1987). Thus, alternative methods to accomplish this were explored, one of which led to the formation of an opal suppressor system, which increased the likelihood of translational read-through (Smiley and Minion, 1993). Despite the limitation in protein overproduction, mutations are generally constructed in *E. coli* plasmids containing the *Tn*4001 transposon, as long as no UGA codons are present, and introduced to wild-type and mutant strains of *M. pneumoniae* by transposon delivery.

Cell Division and Motility

Mycoplasma pneumoniae cells divide by binary fission with a generation time of approximately three hours (Bredt, 1968). An early model for replication showed individual images of cells in different conformations having one normal cell, then two "heads" of the cell, followed by one head in a different location than the other, and finally two individual cells (Bredt, 1968). With the advent of immunofluorescence technology, a more detailed model for cell division emerged. Using a monoclonal antibody to the protein P1 conjugated to a fluorophore to mark the attachment organelle of the cell, and DAPI nucleic acid stain to monitor the level of DNA, images of what are believed to be different stages of cell division were captured (Seto *et al.*, 2001). The different stages of cell division that were captured consisted of one normal cell, a cell at the early stages of replication with duplicated DNA and formation of a nascent tip structure, a cell with one tip structure on the side of the cell body and a second at cell poles, a cell with one tip on

either pole of the cell, and finally two new cells each with its own DNA. The images collected suggested that the DNA is replicated in a cell as a new nascent tip structure is formed, either the original tip structure or the nascent tip migrates to the opposite end of the cell, and finally cytokinesis occurs, leaving two individual cells (Seto *et al.*, 2001). The major limitation to this model is that a single cell was not monitored through each stage of cell division. Therefore, as analysis of cell division continued and with exponential increase in visualization technology, new views of the cell division process have been possible in *M. pneumoniae*, expanding on what was the basic model for cell division. A new model has suggested an expanded pathway for cell division (Hasselbring *et al.*, 2006a). In this model, gliding stops while a nascent tip structure forms, as demonstrated by visualization of a possible adhesin protein P30 fused to YFP, as a marker for the attachment organelle and its formation. In contrast to the previous model for cell division, where only 1 or 2 attachment organelles were present, this study demonstrates that cells often form multiple tip structures before cytokinesis occurs. Separation of the tips coincides with restoration of gliding, where the initial tip displaces the nascent tip with the tip structures releasing from glass to allow movement of the cell body for cell division to occur. Significantly, terminal organelles never separate in a non-motile mutant. Finally, evidence supports a cell division event, where an entirely new tip structure forms *de novo*, instead of by a semi-conserved mechanism, as has been proposed (Seto *et al.*, 2001).

An important aspect of cell division is the ability of the cells to move. Originally, *M. pneumoniae* was considered to be non-motile, based on the lack of structures typically identified for movement, such as flagella or pili. However, microscopic analysis

aided in visualization of cells moving in many different directions at an estimated 1μm/sec in medium containing gelatin (Bredt, 1968), with the attachment organelle always at the leading end (Kirchoff, 1992). A subsequent motility study found that the average speed of a cell in medium containing 3% gelatin ranged from 0.2 to 0.5μm/sec. The cells moved in alternating periods of gliding and rest, with gliding occurring over varying lengths of time. This study also demonstrated various environmental elements to influence motility, such as viscosity, pH, and temperature (Radestock and Bredt, 1977). Motility has been thought to coincide with the ability to hemadsorb, however, attachment to glass in non-motile and motile strains indicate that motility and hemadsorption (HA) may not directly correlate with each other (Hasselbring et al., 2005). Recently, the P30 protein was shown to be required for motility, as P30 mutants are non-motile or exhibit reduced motility (Hasselbring *et al.*, 2005). Furthermore, cytadherence accessory proteins B and/or C as well as HMW1 are also thought to be required for motility. Other proteins have also been implicated in motility because of their absence in*Tn*4001.2065 insertion mutants exhibiting reduced or inhibited movement (Hasselbring *et al.*, 2006b). Other reports have indicated that attachment by a major adhesin P1 is necessary for gliding, as an anti-P1 monoclonal antibody reduces the gliding speed of motile cells and causes the cells to detach from glass over time in an antibody concentration-dependent manner. Non-gliding cells are not affected by this antibody, suggesting that the epitopes of P1 are inaccessible to antibody binding, due to possible conformation changes of P1. Because of this, it was suggested that P1 may be involved in a “power stroke” that allows the cell to glide (Seto *et al.*, 2005).

Morphology and Ultrastructure

The morphology of *M. pneumoniae* is described as pleomorphic, however, cells are often flask-shaped, slender and tapered at one end. This tapered polar end is a specialized structure know as the attachment organelle, and as its name would imply, is involved in attachment and believed to function in gliding motility (Krause and Balish, 2001). Several other pleomorphic pathogenic mycoplasmas also have flask-shaped cells, including *Mycoplasma genitalium* and *Mycoplasma gallisepticum*, whose attachment organelle is referred to as a bleb (Carson, 1992). Being among the smallest known bacteria at 1.0-2.0μm in length (Krause and Balish, 2001), the fine details of the attachment organelle of *M. pneumoniae* have at times exceeded the limitations of light microscopy necessitating the use of electron microscopy.

As early as 1964, “protrusions”, or extensions of the cell were seen in electron micrographs of *M. gallisepticum* and *M. pneumoniae* (Domermuth *et al.*, 1964). Several years later, these “protrusions” were suggested to have a more intricate structure than described previously (Biberfeld and Biberfeld, 1970). Transmission electron micrographs of thin sections revealed a differentiated polar structure with a distinct electron-dense rod and electron-lucent space between the rod and the membrane. A knob-like structure on the distal end of the attachment organelle was also observed (Biberfeld and Biberfeld, 1970) and later coined the terminal button (Krause, 1996). A periodicity to the electron-dense core was observed, in which repeating striations were apparent during examination of thin sections of wild-type cells (Biberfeld and Biberfeld, 1970; Wilson and Collier, 1976) and freeze fracture replicas (Wall *et al.*, 1983).

Removal of the membrane material surrounding the electron-dense core allowed for a less obstructed examination of the details of the core. Triton X-100 (TX), a nonionic detergent, was used to remove this material, leaving behind the TX insoluble fraction, often called the Triton shell. This treatment has been previously used to isolate cytoskeletal components of the eukaryotic cytoskeleton (Herrmann and Wiche, 1983; Starger and Goldman, 1977; Steinert *et al.*, 1978) and more recently the bacterial cytoskeleton, which acts as a backbone for the cells. Electron microscopic analysis was used to visualize TX-extracted cores and confirm previous observations of the presence of striations perpendicular to the core, as well as filaments in parallel with the core (Gobel *et al.*, 1981; Meng and Pfister, 1980). Treatments with various concentrations of KCl and KI removed membrane material also. The 0.6 M KCl treatment allowed for the appearance of a more isolated, but stable core, whereas an isolated but destabilized core was apparent with the 0.6 M KI treatment (Gobel *et al.*, 1981).

Cross-sections of the attachment organelle exposed two rods in parallel that appeared to form the core. Other cytoskeletal features included spokes surrounding the edge of the core and a wheel-like structure at the base of the core toward the cell body. Striations of the core were also observed in this study and for the first time, seven major striations were identified (Hegermann *et al.*, 2002). Recently, images from tomography experiments, in which the samples were plunge-frozen in liquid ethane, have shown that the two rods that make up the core are not identical and that one rod is thicker and longer than the other (Henderson and Jensen, 2006), in contrast to previous predictions (Hegermann *et al.*, 2002). Interestingly, previous observations of the presence of spoke-like structures surrounding and protruding from the core (Hegermann *et al.*,

2002) were not observed in this work (Henderson and Jensen, 2006). Based on the differences between the rods, a model was suggested for the role of the core in motility, where the two rods change in shape and distance from each other to allow for "inch-worm"-like movement.

Strains with mutations and/or reduced levels of some of the cytadherence-accessory proteins, HMW1 (Stevens and Krause, 1991), HMW2 (Balish *et al.*, 2003b), HMW3 (Stevens and Krause, 1992), P200 (Hasselbring *et al.*), P1 (Collier *et al.*, 1983; Feldner *et al.*, 1982; Hu *et al.*, 1982), P30 (Baseman *et al.*, 1987), and B and C (Franzoso *et al.*, 1993), which all localize to the attachment organelle, have allowed for structure and function analysis of each protein and analysis of the influence each has on core formation (Table 2.1). For instance, some strains lacking the C-terminus of HMW1 and HMW2 have been shown to have an unusual morphology, distinct from wild-type (Balish *et al.*, 2003a; Hahn *et al.*, 1998), where no electron-dense core is apparent (Seto and Miyata, 2003), implicating both proteins in core stability and/or core formation. However, a strain lacking HMW3 does have a distinct core, but its rods are split apart toward the cell body in a "chevron" shape, also indicating a requirement for HMW3 in normal core formation (Willby and Krause, 2002). Mutant strains which form cores that appear normal but function improperly are those lacking B and C (M5/III-4), P1, B, C (IV-22), expressing a truncated P30 (M7/II-7), and lacking P200 ($P200^{-}$) (Hasselbring *et al.*, 2006a; Seto and Miyata, 2003), and are therefore predicted to have no role in core stabilization or formation. Recent studies have demonstrated that cores can be found in other locations of the cell in wild-type *M. pneumoniae* prior to localization at the cell pole

(Henderson and Jensen, 2006), although, in mutants lacking HMW1 and HMW2, no such cores were viewed (Henderson and Jensen, unpublished data).

Interest in core formation and the identity of proteins involved has extended to studies to establish the precise components of the core. Mass spectrometry analysis of Triton X-100 insoluble fractions has identified many proteins that are associated with the electron-dense core and the membrane material that remains attached to the proximal end of the core following TX extraction. Cytadherence-accessory proteins identified in this fraction included HMW1, HMW2, HMW3, P65, B, C, P1, and P200. The fraction also included proteins involved in energy metabolism, transcription, translation, heat shock, and those of unknown function, containing leucine zippers and coiled-coil domains (Regula *et al.*, 2001). Further studies involving isolation of the electron-dense core structure alone and mass spectrometry studies will be necessary to identify the precise components of the core.

Pathogenesis

Mycoplasma pneumoniae is a causative agent of atypical “walking” pneumonia and tracheobronchitis. Attachment to the respiratory epithelium is a requirement for colonizing the host and causing infection in humans (Talkington *et al.*, 2001). This attachment is mediated by the attachment organelle, in which many cytadherence-accessory proteins and a major adhesin protein, P1, are localized. The cell attaches to the host via sialyated-glycoproteins and glycolipids (Roberts *et al.*, 1989). Attachment is necessary for colonization because of host cell mechanical defense mechanisms, such as mucocilliary clearance, which will remove unattached cells away from the lungs

Table 2.1. Relative levels of cytadherence-associated proteins in mutant *M. pneumoniae* strains. Modified from Balish and Krause (2002); +++, ++, +, - are relative protein levels, where +++ indicates wild-type levels and – indicates none is detected; Δ indicated truncated P30.

Strain	P1	B/C	P30	HMW1	HMW2	HMW3	P65
WT	+++	+++	+++	+++	+++	+++	+++
I-2	+++	+++	++	+	-	+	+
II-3	+++	+++	-	+++	+++	+++	++
II-7	+++	+++	++Δ	+++	+++	+++	++
III-4	+++	-	+++	+++	+++	+++	+++
IV-22	-	-	+++	+++	+++	+++	+++
M6	+++	+++	++Δ	-	+	+	+
***hmw3*$^{-}$**	+++	+++	+++	+++	+++	-	++

(Waites and Talkington, 2004). The HA assay is a convenient test to assess the attachment ability of *M. pneumoniae* strains by evaluating their adherence to erythrocytes, although *M. pneumoniae* is not believed to encounter erythrocytes typically during infection. Recently, motility has also been shown to be an essential element for efficient colonization, by allowing for movement toward and subsequent interaction with host cells (Krause *et al.*, 2007). In these studies, normal human bronchial epithelial (NHBE) cells were used to examine the ability of specific *M. pneumoniae* strains to colonize. These ciliated cells produce mucus, providing a barrier to non-motile strains and those with reduced motility. Thus, colonization of NHBE cells by strains with significantly reduced motility occurs much less efficiently than it does with wild-type strains (Krause *et al.*, 2007).

In response to colonization, the host mounts an immune response where invading mycoplasmas are opsonized and destroyed by the complement system. Infection of host cells activates the adaptive immune response to produce *M. pneumoniae*-specific IgA, IgM, and IgG antibodies, as well (Krause and Taylor-Robinson, 1992). Production of antibodies promotes increased phagocytosis of mycoplasmas and inhibition of adhesin-receptor binding, cytadherence (Krause and Taylor-Robinson, 1992). However, the adaptive immune response can also be harmful to host cells causing delayed hypersensitivity to mycoplasmas and significant lung damage in hamsters and guinea pigs by lymphocytes (Jacobs *et al.*, 1990; Krause and Taylor-Robinson, 1992; Taylor *et al.*, 1974). Because *M. pneumoniae* lacks the catalase and superoxide dismutase enzymes, hydrogen peroxide and toxic oxygen radicals are not broken down. Thus, mycoplasma infection can lead to local cytotoxicity

of the host cells, due to oxidative damage (Waites and Talkington, 2004). *M. pneumoniae* has been shown to bind host cell lactoferrin (Tryon and Baseman, 1987), and because of this, oxidative damage of host cells may occur due to generation of hydroxyl radicals in the presence of iron complexes (Waites and Talkington, 2004). Some effects of oxidative damage include erythrocyte lipid peroxidation, hemoglobin denaturation, loss of reduced gluthathione, and cell lysis (Waites and Talkington, 2004). Local damage can lead to cytopathic effects of the host cells including the loss of ciliary motion of the host cell and eventually complete loss of the cilia (Collier and Clyde, 1971). Further host injury typically involves the appearance of vacuoles, and reduced ability to consume oxygen, take up amino acids, synthesize macromolecules needed by the cell, and utilize glucose (Clyde, 1979; Collier and Baseman, 1973; Waites and Talkington, 2004).

Aerosol transmission of this pathogen, commonly found in the nose, throat, trachea, and sputum of those infected (Waites and Talkington, 2004), facilitates the spread of the illness (Clyde, 1979). Cases of *M. pneumoniae* are most prominent in areas of close quarters, such as military barracks and college dorms (Talkington *et al.*, 2001). Thus, it is not surprising that many cases occur in young adults. It has also been shown to affect the elderly and children between the ages of 5 and 15 (Alexander *et al.*, 1966). The incubation period of the illness can vary from several days to over 3 weeks (Waites and Talkington, 2004). Symptoms of the infection are reminiscent of the flu with aches and pain, headache, chills, and a dry cough (Krause and Taylor-Robinson, 1992). Tetracycline, macrolide, and fluoroquinolone derivatives can be used to treat the illness (Waites and Talkington, 2004).

Adhesin-Related Proteins

P1. Attachment of *M. pneumoniae* to host epithelial cells is essential for colonization and subsequent infection (Hu *et al.*, 1975, 1976). For this reason, research by Hu et al. (1977) focused on examining the attachment entity and its mechanism. In those studies, surface exposure of the attachment entity was established because attachment was greatly reduced when mycoplasmas treated with trypsin were incubated with tracheal rings. Following trypsin treatment, reincubation of mycoplasmas in fresh media restored attachment, although not in media containing the protein synthesis inhibitor erythromycin. Together, these experiments suggested that attachment was dependent on a mycoplasma surface protein (Hu *et al.*, 1977). This prompted SDS-PAGE analysis, which showed that levels of the protein P1 increased with restored attachment and decreased with reduced attachment, indicating a direct association between this protein and cytadherence (Hu *et al.*, 1977). Immunoblot analysis followed, where monoclonal antibodies to surface antigens of *M. pneumoniae* were produced and specifically reacted with P1. Furthermore, attachment was inhibited in the presence of P1 monoclonal antibodies, confirming the role for P1 as a major adhesin (Baseman *et al.*, 1982; Collier *et al.*, 1983; Feldner *et al.*, 1982; Hu *et al.*, 1982). Using a P1 monoclonal antibody conjugated to ferritin, P1 was localized to the surface of the attachment organelle and in low levels elsewhere in the cell body (Feldner *et al.*, 1982; Hu *et al.*, 1982). P1 was also shown to cluster at the tip of the attachment organelle, along with a nap-like structure that seemed to correlate with clustering of P1 (Baseman *et al.*, 1982). Immunofluorescence (IF) studies of P1 have confirmed its localization at

one cell pole (Seto *et al.*, 2001), as well as its co-localization with cytadherence associated proteins B and C (Seto and Miyata, 2003).

P1 was thought to be necessary for cytadherence. However, isolates of chemically mutagenized strains of *M. pneumoniae* (Hansen *et al.*, 1979a), which produced P1, were found to be cytadherence-negative. This indicated that the presence of P1 alone is necessary, but not sufficient for cytadherence to occur. The inability of these mutants to cytadhere despite the presence of P1 suggested the need for additional proteins to assist P1, or a requirement for a specific conformation of P1 for attachment (Hansen *et al.*, 1979b). Evidence toward both requirements was established. First, analysis of antibody binding sites using five different monoclonal antibodies to P1 allowed for a closer examination of the conformation requirements of P1, identifying three regions of P1 that are important for adherence: an N-terminal region, a region in the middle of the protein designated D1, and a region at the C-terminal end designated D2. Patterns of antibody binding suggest that the protein takes on a conformation in which the N-terminus, D1 and D2, are in close proximity to each other for attachment to occur (Gerstenecker and Jacobs, 1990). Second, spontaneous HA-negative mutants were isolated and divided into classes based on their mutations. Strain IV-22 is the only representative of the Class IV mutants, which lack P1 and cytadherence accessory proteins B and C. Strain III-4 is member of the Class III mutants, which lack cytaherence proteins A, B, and C and are also unable to cytadhere, suggesting a role for these proteins in assisting P1 in attachment (Krause *et al.*, 1982). Class II and I mutants are discussed below.

A functional and physical link between P1, B, and C was revealed as the proteins were characterized. P1 is 1627 amino acids in length and has a calculated molecular mass of 176-kDa as the precursor protein, which is processed to form the mature protein with a deduced size of 170-kDa. It has no cysteines, a high proline content in its C-terminus, and has multiple antigenic sites, as predicted previously (Su *et al.*, 1987). The first 59 amino acids are part of a leader sequence of P1 and are cleaved to form the mature protein (Inamine *et al.*, 1988a). The *p1* gene (MPN141; (Inamine *et al.*, 1988a) was found to be a component of the P1 operon, where it is surrounded by orfs on either side, designated orf-4 (MPN140) and orf-6 (MPN142) (Inamine *et al.*, 1988b). MPN142 encodes a precursor protein, whose observed size is 130-kDa by SDS-PAGE, that is cleaved to form proteins B and C, which migrate at 90 and 40-kDa, respectively (Layh-Schmitt, 1993). The genes encoding P1 and B and C are thought to be transcriptionally coupled, and transcription of P1 is required for restoration of B and C to wild-type levels in IV-22 (Waldo and Krause, 2006). B and C, along with several other proteins, were shown to interact with P1 in cross-linking studies aimed at identifying such proteins (Layh-Schmitt *et al.*, 2000). Thus, it was not surprising that the spatial distance between P1 and B and C was predicted to be 0.1 nm (Layh-Schmitt and Herrmann, 1994). B and C were also shown to be important for normal partitioning of P1 in the presence of TX. P1 partitions in small amounts in the TX-insoluble fraction (Kahane *et al.*, 1985), only in the presence of B and C (Layh-Schmitt and Harkenthal, 1999). Thus, in mutant III-4, lacking B and C, P1 is completely TX-soluble, suggesting a physical interaction of B and C with P1, possibly with B and C being the link between P1 and its interaction with the cytoskeleton (Layh-Schmitt and Harkenthal, 1999).

Several other proteins are thought to interact with or have an effect on P1, based on cross-linking experiments used to identify them (Layh-Schmitt *et al.*, 2000). A potential adhesin protein, P30, that is localized to the attachment organelle also (Baseman *et al.*, 1987) and interacts with P1 (Layh-Schmitt *et al.*, 2000), is not required for P1 to cluster at the tip of the terminal structure (Hahn *et al.*, 1998). However, P30 may have an accessory role in attachment, based on the inability of P30 mutants to attach (Romero-Arroyo *et al.*, 1999). HMW1, specifically the C-terminus, apparently aids in trafficking of P1 to the attachment organelle and in maintaining a normal morphology (Balish *et al.*, 2003a; Hahn *et al.*, 1998; Willby *et al.*, 2004). Finally, HMW3 may aid in proper localization of P1 directly or indirectly by stabilizing the electron-dense core (Willby and Krause, 2002).

Portions of the gene, encoding P1, are repeated elsewhere in the genome (Collier *et al.*, 1983; Hu *et al.*, 1982). Indeed, P1 is believed to undergo antigenic variation involving sequences that repeat as many as 10 times each in the genome (Ruland *et al.*, 1990). It is believed that recombination occurs between these sites found throughout the genome, leading to a change in P1 sequence following translation. Due to this recombination, a new P1 variant can be made leading to antigenic variation and avoidance of the host immune response (Dallo *et al.*, 1990; Dorigo-Zetsma *et al.*, 2001; Kenri *et al.*, 1999; Rocha and Blanchard, 2002; Su *et al.*, 1990). Although there is antigenic variation among the repeats of P1, this protein has still been targeted as a good vaccine candidate. Dallo identified a single-copy 13-amino acid epitope of P1 in *M. pneumoniae* as a potential vaccine candidate (Dallo *et al.*, 1988).

Homologs of P1 have been identified and characterized. A 140-kDa protein, MgPa, isolated in *M. genitalium*, is a homolog of P1 (Morrison-Plummer *et al.*, 1987). This protein was shown to share many features with P1 including surface-exposure at its tip structure, the presence of a nap region, sensitivity to trypsin (Hu *et al.*, 1987), and the presence of a signal sequence and hydrophobic region (Mader *et al.*, 1991). The MgPa protein is also thought to be part of an operon, like P1, with open reading frames on either side (Inamine *et al.*, 1989). Two proteins (GapA and Mgc-1) in *M. gallisepticum* were also shown to be homologs of P1 in *M. pneumoniae*. Mgc-1 is a 150-kDa protein with homology to P1 of *M. pneumoniae* and MgPa of *M. genitalium*. It has been shown to be surface-exposed, based on sensitivity to trypsin, and has an upstream transcription start site inside of another orf (Keeler *et al.*, 1996). GapA is 105-kDa protein with homology to P1 of *M. pneumoniae*, MgPa of *M. genitalium*, and the P1-like adhesin in *M. pirum*. It is surface exposed, sensitive to trypsin, transcribed in an operon, in a single copy in its genome, and antisera to GapA inhibits attachment (Goh *et al.*, 1998). Other P1 homologs were identified as well, including P30 of *M. pneumoniae*, Clone MS-1 of *M. synoviae*, and a P1-like adhesin in *M. pirum* (Dallo *et al.*, 1990; Morsy *et al.*, 1993; Tham *et al.*, 1994).

P30. This 32-kDa protein was initially thought to be involved in attachment based on its presence in an HA^+ strain and absence in an HA^- strain. Surface-localization of P30 in immunogold labeling experiments supported this notion (Baseman *et al.*, 1987). A predicted transmembrane domain was identified and thought to anchor this protein by spanning the membrane (Dallo *et al.*, 1990). Further characterization identified three six-amino acid, proline-rich repeats at the C-terminus of the protein.

P30 shows homology to other proteins thought to be involved in cytadherence, including P1 in *M. pneumoniae*, P32 in *M. genitalium*, and PvpA in *M. gallisepticum*. P32 and PvpA, like P30, are also surface-exposed and have proline-rich regions in their C-termini (Boguslavsky *et al.*, 2000; Reddy *et al.*, 1995). It was initially thought that the gene encoding P30 may be part of a larger coding region (Dallo *et al.*, 1990). This later was confirmed to be the case as the gene encoding P30 is in the *hmw* gene cluster, which consists of *hmw1* (MPN447), *hmw3* (MPN452), *rpsD* (MPN446), and six other open reading frames of unknown function (Waldo *et al.*, 1999). Interestingly, the gene for P32 in *M. genitalium* is also organized in an transcription unit (Reddy *et al.*, 1995) and other evidence suggests this may be true for PvpA in *M. gallisepticum* also (Boguslavsky *et al.*, 2000).

Various mutants of P30 have been isolated and have aided in structure and function analysis of the protein. Sequence analysis of previously isolated class II mutants, II-3 and II-7 (Krause *et al.*, 1982), revealed a frameshift mutation, causing the loss of P30, and a 144 bp internal deletion at the C-terminus of P30, producing a truncated protein, respectively (Dallo *et al.*, 1996; Layh-Schmitt *et al.*, 1997; Romero-Arroyo *et al.*, 1999). Revertants of the II-3 mutants restored their HA capacity to wild-type, again demonstrating the importance of P30 in cytadherence. This was also evident in II-3 and II-7, where P1 localized to the attachment organelle, but cytadherence did not occur (Romero-Arroyo *et al.*, 1999). Thus, P1 localization alone was not sufficient for attachment. Another spontaneously-arising P30 mutant, designated M6, was identified, which lacks HMW1, due to a frameshift caused by a deletion of one thymidine, and expresses a truncated P30, due to its 144 bp internal

deletion. It is noteworthy to mention that this P30 deletion is the identical deletion found in II-7 (Layh-Schmitt *et al.*, 1995). P30 also functions in maintaining normal morphology and motility. First, a star-shaped morphology was attributed to the deletion or truncation of certain regions of P30, specifically its C-terminus (Romero-Arroyo *et al.*, 1999). Second, the requirement of P30 for motility was supported by motility studies, where P30 mutants II-3 and II-7 were non-motile or motile at a reduced rate, respectively (Hasselbring *et al.*, 2005). Other studies confirmed that P30 co-localizes with P1 and, based on the localization patterns in various mutants, suggest that P30 is incorporated into the attachment organelle after HMW1 and HMW2 (Krause and Balish, 2004; Seto *et al.*, 2001; Seto and Miyata, 2003).

Cytadherence-Associated Proteins

HMW1. HMW1 is a 112-kDa protein that migrates as an apparently much larger protein (210-kDa) by sodium dodecyl sulfate-polyacrylamide gel electrophoresis (SDS-PAGE), which is most likely attributed to its high number of acidic and proline residues (Ogle *et al.*, 1992; Proft *et al.*, 1996). It is encoded in the *hmw* gene cluster, which includes the genes for P30 and HMW3, along with several other genes expressing proteins of unknown function (Dirksen *et al.*, 1996; Krause and Lee, 1991; Waldo *et al.*, 1999). The genes in this cluster are thought to be co-transcribed based on RT-PCR analysis (Waldo *et al.*, 1999). Like cytadherence accessory proteins HMW3, P65, and P200 discussed later in this section, HMW1 has an acidic and proline rich (APR) domain and, as in P200, also contains a region enriched in aromatic and glycine residues (EAGR box) (Balish *et al.*, 2001; Proft *et al.*, 1996). HMW1 is divided into 3

domains, Domain I contains the EAGR box, Domain II has the APR domain, and Domain III consists of coiled-coil motifs. As a peripheral membrane protein, HMW1 has no predicted transmembrane domain (Balish *et al.*, 2001; Dirksen *et al.*, 1996; Proft and Herrmann, 1994), but also lacks a typical signal peptide. It is phosphorylated at certain threonine residues by a predicted serine/threonine kinase (Dirksen *et al.*, 1994; Krebes *et al.*, 1995). Analysis on sucrose density gradients demonstrated that HMW1 is part of a multi-protein complex, now known as the cytoskeleton (Stevens and Krause, 1991). A homolog of HMW1 was identified in *M. genitalium*, and like HMW1, it lacks homology with any protein of known function (Balish *et al.*, 2001).

A derivative of HMW1 exists called HMW4, which is a heat-altered form of HMW1 (Hahn *et al.*, 1996). It appeared as a band migrating at 215-kDa in wild-type cells and decreased in intensity in mutants lacking HMW1-3 (Krause *et al.*, 1982). A relationship between HMW1 and HMW4 was first suggested when antisera against HMW1 reacted specifically with HMW1 and HMW4 (Krause *et al.*, 1983). Furthermore, an increase in HMW4 in pre-boiled wild-type protein samples was coupled with a decrease in HMW1 levels (Stevens and Krause, 1991). Later, this relationship was elucidated when the HMW1-HMW4 mutant strain transformed with recombinant truncated HMW1 was shown when boiled to have decreased levels in truncated HMW1 with the appearance of increased levels of recombinant truncated HMW4 (Hahn *et al.*, 1996).

The stability of HMW1 is greatly affected by the absence of HMW2, as shown in mutant I-2 (Balish *et al.*, 2001). This mutant is the result of a frameshift due to the addition of an adenine to a poly-adenine tract in the coding region of *hmw2* (MPN310)

(Fisseha *et al.*, 1999). Initial characterization of I-2 revealed the absence of HMW1-HMW4 (Krause *et al.*, 1982). However, HMW1, HMW3, and P65 were later shown to be present at reduced levels (Krause *et al.*, 1997; Popham *et al.*, 1997). Slot blot and pulse chase studies showed that HMW1 was transcribed and translated, respectively, but lost by proteolysis over time. The C-terminus of HMW1 was shown to be required for targeting by proteolysis, based on experiments where the absence of HMW2 allowed for reduction of full-length HMW1, but recombinant HMW1, lacking the C-terminus, remained stable. A repeating motif of four paired serine residues, which has been shown to be a protease recognition signal in P1 and HMW3, was identified in the C-terminus of HMW1 (Hahn *et al.*, 1996).

HMW1 is TX-insoluble (Proft and Herrmann, 1994), and therefore part of the *M. pneumoniae* cytoskeleton. However, its partitioning in the insoluble fraction occurs over time. Initially, HMW1 primarily partitions in the TX-soluble fraction in wild-type with only a portion distributed in the insoluble fraction. Pulse- chase studies indicated that its partitioning in the soluble fraction decreases over time, as its partitioning in the insoluble fraction increases, indicating an incorporation of HMW1 into the insoluble fraction. In the absence of HMW2, the initial distribution of HMW1 is similar to wild-type; however, over time while the soluble fraction decreases, the insoluble fraction never increases, indicating that HMW1 is never incorporated into the insoluble fraction. A model was suggested, based on these data that TX-insoluble proteins initially move between the soluble and unstable insoluble fractions, but are eventually incorporated and remain in the stable insoluble fraction. In the absence of HMW2, incorporation into the stable insoluble fraction does not occur, and as a result the soluble fraction is degraded by

proteases. The same process is thought to occur with cytadherence accessory proteins, HMW3 and P65, as well (Balish *et al.*, 2001).

The spontaneous HA- negative mutant M6 lacks HMW1 as the result of a frameshift mutation in the *hmw1* (MPN447) coding region, and produces a truncated P30 derivative, resulting from a 144 nucleotide deletion in MPN453 (Layh-Schmitt *et al.*, 1995). M6 has an aberrant morphology and fails to localize P1 to the attachment organelle (Hahn *et al.*, 1998). The II-7 strain also is HA- negative and results from the same P30 deletion as in M6 but expresses wild-type HMW1 (Dallo *et al.*, 1996). These two mutant strains were used to determine a function for HMW1. First, transformation of recombinant P30 into II-7 restored its ability to hemadsorb. However, transformation of recombinant P30 into M6 (M6/P30) did not restore its hemadsorption ability, thus indicating a role for HMW1 in cytadherence (Hahn *et al.*, 1998). Second, immunogold labeling of P1 in M6 and M6/P30 strains showed a randomly distributed pattern of gold particles, whereas M6 transformed with recombinant HMW1 (M6/HMW1) restored normal P1 localization (Hahn *et al.*, 1998). Therefore, HMW1 is also required for P1 clustering. Finally, HMW1 was found to be important for normal cell morphology, when a near wild-type morphology was restored in M6/HMW1, not in M6 alone or M6/P30. P1 localization and cell morphology were not restored when a slightly truncated HMW1 derivative lacking the normal C-terminus was transformed into M6. Thus, the C-terminus of HMW1 is essential for these normal cellular processes (Hahn *et al.*, 1998).

HMW1 localizes to the exterior and interior of the leading and trailing filaments of wild-type *M. pneumoniae* cells (Stevens and Krause, 1991), although other reports indicated that HMW1 was only localized to the attachment organelle (leading filament)

(Seto *et al.*, 2001). HMW1 also localized properly in mutants II-7 and III-4, lacking proteins B and C, indicating that the presence of P30, B, or C has no effect on HMW1 localization (Seto *et al.*, 2001). In the I-2 mutant, where full-length HMW2 is not made, HMW1 is at reduced levels and is not localized (Stevens and Krause, 1991), although other reports have indicated HMW1 is localized in I-2 (Seto and Miyata, 2003). HMW1 is not only required for its localization, but it is required for localization of cytadherence accessory proteins HMW3, P90, P40, and P65 (Seto *et al.*, 2001). Because HMW1 functions in stabilizing many proteins in the attachment organelle and does not rely on many for its own stability, it is believed that HMW1 has an early role in the assembly process of the attachment organelle (Krause and Balish, 2004; Seto *et al.*, 2001).

HMW2. HMW2 is a 216-kDa phosphorylated protein, most likely phosphorylated by an ATP-dependent serine/threonine kinase (Dirksen *et al.*, 1994; Krause *et al.*, 1997). This protein is 1818 amino acids in length and is predicted to consist of coiled-coils and five leucine zipper motifs. Disruptions in the coiled-coils allow for flexibility, perhaps enabling predicted dimeric and trimeric interactions to occur (Fig. 1). HMW2 partitions in the TX-insoluble fraction, which indicates its incorporation into the cytoskeleton, and shows homology with the eukaryotic cytoskeletal component myosin II heavy chain, excluding its ATP binding domain (Krause *et al.*, 1997; Stevens and Krause, 1990).

HMW2 is part of a cytadherence regulatory locus (crl), which was identified through a transposon *Tn*4001 mutagenesis screen for proteins important in cytadherence (Hedreyda and Krause, 1995). Six HA-negative crl transformants (A3, B7, C1, G19, H9, and D3) were isolated from this mutagenesis event and found to have

insertions within the *hmw2* gene. The HA-negative phenotype of these transformants and the restoration of cytadherence with excision of the transposon suggested that HMW2 may regulate cytadherence. Later, a transcriptional start site and a predicted promoter region were identified upstream of the gene encoding P65, which begins the transcriptional unit (now called the P65 operon), consisting of the genes encoding P65, HMW2, P41, and P24 (Krause *et al.*, 1997). An additional, internal translation start site was also found near the 5' end of the coding region of *hmw2* (MPN310), which encodes a 28kDa protein, P28 (Fisseha *et al.*, 1999). A disulfide-linked dimer of HMW2 (HMW5) has been observed under non-reducing conditions by SDS-PAGE at around 340kDa (Krause *et al.*, 1997; Stevens and Krause, 1990).

HMW2 has 57.9% identity with MG218 in *Mycoplasma genitalium*, which is the closest known relative to *M. pneumoniae* (Dhandayuthapani *et al.*, 1999, 2002). Both proteins are composed of predicted coiled-coils and five leucine zipper motifs, and are important for cytadherence (Dhandayuthapani *et al.*, 1999; Krause *et al.*, 1997). Unlike HMW2, MG218 does not contain an internal translation start site at its C-terminus or express a homolog of P28 (Dhandayuthapani *et al.*, 2002). MG218, is essential for stabilizing and for maintaining a proper conformation of P140 (homolog of P1) and P110 (homolog of cleavage products B and C) (Dhandayuthapani *et al.*, 1999), in contrast to HMW2, which is essential for stabilizing HMW1, HMW3, and P65 and proper localization of P1, B, and C.

Spontaneous HA-negative mutants of HMW2, including mutant I-2, were isolated in a study to identify proteins involved in virulence (Krause *et al.*, 1982). This mutant was found to lack HMW2 as a result of a frameshift mutation, where an adenine is

inserted into a poly-A tract of *hmw2* corresponding to amino acid 936. This mutant has reduced levels of HMW1, HMW3, and P65 (Fisseha *et al.*, 1999). I-2 transformed with recombinant wild-type HMW2 restores HMW1, HMW3, and P65 to wild-type levels (Fisseha *et al.*, 1999) and restores cytadherence (Krause *et al.*, 1982), suggesting that HMW2 is required for their stabilization and cytadherence. HMW1, HMW3, and P65 are not stably incorporated into the cytoskeleton in the absence of HMW2, but instead are subject to accelerated proteolytic degradation (Balish *et al.*, 2001; Jordan *et al.*, 2001; Popham *et al.*, 1997). Mutant I-2 has also been shown to have an aberrant morphology (Balish *et al.*, 2003a), and an electron-dense core is not apparent (Seto and Miyata, 2003). Immunoblot studies examining crl transformants (A3, B7, C1, D3, G10, and H9), using both N-terminal and C-terminal HMW2-specific antisera showed that no HMW2, either full-length or truncated, was detected in A3, C1, D3, G19.

An excision revertant of the C1 insertion mutant (C1R1) contains an in-frame 858 bp deletion in MPN310, the gene encoding HMW2, which removes the two possible translation start sites for P28. This strain expresses an 185-kDa HMW2 derivative and no P28 and is HA-positive (Fisseha *et al.*, 1999; Krause *et al.*, 1997). Thus, P28 is not a requirement for cytadherence (Fisseha *et al.*, 1999). There are two potential translation start sites for P28 predicted for expression of a 28-kDa protein at the 5' end of MPN310. Purification of P28 is necessary to identify its actual translation start site within MPN310. Because of this, several constructs were made with a variety of promoters and coding regions of MPN310 to attempt expression of P28 alone, although none were unsuccessful (Balish *et al.*, 2003a).

An HMW2-GFP sandwich fusion was constructed, to circumvent previous difficulties in the localization of HMW2 due to epitope inaccessibility or the lack of immunogenicity (Balish *et al.*, 2003b; Dirksen *et al.*, 1994; Krause *et al.*, 1983; Stevens and Krause, 1990). This construct was transformed into mutant I-2, restoring a near wild-type phenotype, with the exception of intermediate hemadsorption and motility. Although the morphology of the cells was generally normal, there appeared to be a large population of cells with two attachment organelles (bifurcated tips), which was suggested to result from a defect in the cell division process, due to the GFP insertion. Fluorescence studies indicated for the first time that HMW2 localizes to the attachment organelle (Balish *et al.*, 2003b). Later, an HMW2-EYFP fusion was constructed by another group and used to confirmed its localization within the attachment organelle (Kenri *et al.*, 2004). Due to the size of GFP and the amount of fluorescence emitted, it was difficult to determine the precise location of HMW2 within the attachment organelle and emphasized the need for immunofluorescence analysis of HMW2 in the attachment organelle. However, previous antisera to HMW2 were ineffective in immunofluorescence studies, due to a weak signal (Balish *et al.*, 2003b; Dirksen *et al.*, 1994; Krause *et al.*, 1983; Stevens and Krause, 1990). In the current studies, new HMW2 antisera are much more reactive to HMW2 than previous antisera and have allowed for more precise analysis of the location of HMW2 within the attachment organelle.

HMW2 is hypothesized to be a major component of the electron-dense core, due to its structural features, as well as a predicted length which is similar to the 250 nm core (Balish *et al.*, 2003b). A model was suggested for how this arrangement could

allow for core formation, where the predicted dimeric and trimeric interactions of HMW2 form a compact network with P28 and other HMW2 monomers (Figure 2.1). Based on this model, HMW2 would line up in parallel bundles to form the core. Thus, a shorter HMW2 derivative would be predicted to form a shorter core, and this possibility is explored in the current study, including TEM analysis of thin sections of the various HMW2 mutants. It has already been shown that I-2 does not have an obvious electron-dense core (Seto and Miyata, 2003), suggesting that certain regions of HMW2, possibly the C-terminus, may always be required for core formation (Balish *et al.*, 2003b).

HMW1-HMW2 Dependency. HMW1 and HMW2 have been shown to have a co-dependent relationship, based on studies using HMW1 and HMW2 mutants. In mutant I-2, where HMW2 is absent, HMW1 levels are reduced, along with levels of HMW3 (Popham *et al.*, 1997) and P65 (Jordan *et al.*, 2001), due to the inability to incorporate efficiently into the TX-insoluble fraction (Balish *et al.*, 2001). In mutant M6, lacking HMW1, HMW2 is found to be at greatly reduced levels and not localized properly (Willby *et al.*, 2004). Thus, it was shown that the C-terminus of HMW1 is essential for stabilization of HMW2 and normal HMW2 localization.

The C-terminus of HMW1 is also important for normal attachment organelle formation, as seen in mutant M6 (Hahn *et al.*, 1998) or mutants lacking the C-terminus HMW1, where the morphology of the cells is aberrant and branching (Willby *et al.*, 2004). Since these proteins stabilize each other, have numerous downstream effects when they are absent, and localize to the attachment organelle, they are believed to be among the earliest proteins involved in attachment organelle formation. Other evidence towards this assertion includes the apparent absence of an electron-dense core, a

Figure 2.1. Previous model for HMW2-bundling in the attachment organelle. From Balish *et al.*, 2003b. Long vertical lines represent HMW2 with its predicted dimeric coiled-coil interactions. Regions highlighted in gray represent predicted trimeric coiled-coil interactions of HMW2, including P28 (short lines with the diagonal lines representing the N-terminal portion).

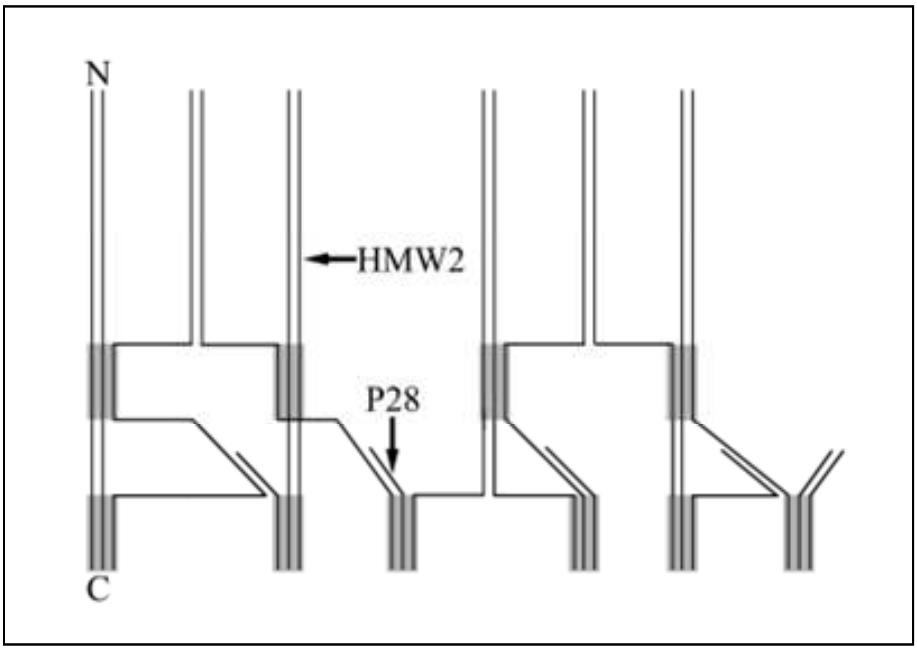
N
HMW2
P28
C

defining structure of the attachment organelle, in HMW1 mutant M6, and HMW2 mutant I-2 (Seto and Miyata, 2003). Additional evidence is discussed in the results and discussion sections.

HMW3. HMW3 was identified as a third high molecular weight protein absent in SDS-PAGE analysis of the class I mutants isolated in 1982 (Krause *et al.*, 1982). Characterization of HMW3 followed, after it was shown to be expressed as an independent product from other high molecular weight proteins identified at the same time (Krause *et al.*, 1983). It is a 672-amino acid cytadherence accessory protein, whose approximate molecular mass is 74-kDa, but migrates by SDS-PAGE at 140kDa (Ogle *et al.*, 1992). This abnormal migration pattern is attributed to the presence of two APR domains, also found in HMW1, P65, and P200, which likewise migrate aberrantly (Balish *et al.*, 2001; Ogle *et al.*, 1991, 1992; Proft *et al.*, 1996). The gene for HMW3 (MPN452) is near that of *hmw1* on the chromosome (Krause and Mawn, 1990; Ogle *et al.*, 1991) as part of the *hmw* gene cluster that includes *p30*, *hmw1*, *rpsD*, and six open reading frames (orfs) of unknown function (MPN446 to MPN455) (Dirksen *et al.*, 1996). The *hmw* gene cluster is transcriptionally linked, based on the presence of transcriptional terminators on either side of the cluster, identification of an upstream promoter shown to be important for P30 and HMW3 transcription, and results from RT-PCR studies showing the genes in the cluster to be transcribed as a unit (Waldo *et al.*, 1999). However, several promoters appear to direct the expression of the genes in the cluster based on primer-extension studies (Waldo *et al.*, 1999).

Since HMW3 partitions in the TX-insoluble fraction, it is thought to be a component of the network of proteins that form the *M. pneumoniae* cytoskeleton (Proft

and Herrmann, 1994; Stevens and Krause, 1992). Further analysis by immunogold labeling of HMW3 in the triton shell confirmed this localization specifically to the terminal button of the attachment organelle, as well as around the core, appearing to wrap around it. Immunofluorescence microscopy confirmed this localization pattern of HMW3 and showed that it is unaffected by the loss of proteins B and C or the C-terminus of P30, yet requires HMW1 for its localization (Seto *et al.*, 2001). Further immunofluorescence studies showed that HMW1 and HMW3 co-localize (Seto and Miyata, 2003). Immunolabeling analysis of thin sections and whole cells using HMW3-specific antiserum and anti-rabbit secondary antiserum conjugated to 10 nm gold particles showed minimal labeling on the cell surface (Stevens and Krause, 1992). However, despite its absence on the cell surface, HMW3 was isolated in a complex with P1 and suggested to aid in cytadherence (Krause and Baseman, 1982; Layh-Schmitt *et al.*, 2000). In efforts to determine which proteins were responsible for maintaining the integrity of the triton shell, TX-insoluble fractions were treated with various concentrations of the chaotropic agent KI, probed with specific antiserum for immunogold labeling, and viewed under the scanning electron microscope (SEM). These treatments were shown to dissociate the fraction, removing HMW3 as well as other cytadherence accessory proteins, as indicated by the gold labeling, implicating that those proteins were necessary for maintaining a normal cytoskeletal structure (Stevens and Krause, 1992).

The stability of HMW3 is attributed to the presence of HMW2. The loss of HMW2 has been shown to have many downstream effects on other cytadherence proteins, including reduced levels of HMW3 and HMW1 (Krause *et al.*, 1982). Slot blot analysis

showed that the gene for HMW3 was transcribed in HMW2$^-$ mutants, and pulse chase studies indicated that HMW3 was expressed, but its levels were reduced over time in the absence of HMW2, presumably by proteolysis. For HMW1, this proteolysis occurs only in the presence of its C-terminus, which contains paired-serine motifs that are thought to act as a degradation signal to housekeeping proteases. HMW3 has the same motifs in its C-terminus, and therefore, is thought to be degraded over time in a similar manner. Thus, the levels of HMW1 and HMW3 are reduced when HMW2 is not present (Popham *et al.*, 1997), and in the absence of HMW2, HMW3 is also not localized (Stevens and Krause, 1992).

HMW3 is homologous to several other mycoplasma proteins, including P69 of *M. genitalium* (Reddy *et al.*, 1995) and MGA_0928 (May *et al.*, 2006) and PvpA of *M. gallisepticum* (Boguslavsky *et al.*, 2000) that have been characterized. Like HMW3, P69 is also part of a transcriptional unit. P69 has no transmembrane domains, with no evidence of membrane-association. It has many inverted repeats in its coding sequence and 64% identity to HMW3. PvpA has 49% identity with a region spanning 205 amino acids in HMW3, is localized to the cell surface as part of its terminal organelle, and is thought to be an adhesin protein (Boguslavsky *et al.*, 2000).

An HMW3$^-$ mutant, formed by transposon insertion of *Tn*4001 within *hmw3*, was isolated and at the time, shown to have reduced levels of P65 only (Willby and Krause, 2002). Phenotypic features of this mutant included intermediate hemadsorption, V-shaped (“chevron”) cores, where the vertex of the V faces away from the cell body, and no localization of P65. The separation of the two rods of the core suggests that HMW3 maintains the close proximity of the rods of the core to each other (Willby and Krause,

2002). Recently, it was shown that the HMW3$^-$ mutant has another insertion and an in-frame deletion in cytadherence accessory protein P200, forming a double mutant (Hasselbring *et al.*, 2006a). The excision revertant isolated previously from the HMW3$^-$ mutant, restored HMW3 but not P200, forming a P200$^-$ mutant (Hasselbring *et al.*, 2006a; Willby and Krause, 2002). Normal cores are formed in this mutant, confirming that V-shaped cores result from the loss of HMW3 only.

P65. P65 is a 47-kDa protein and has an abnormal migration pattern in SDS-PAGE, where it migrates with an apparent size of 65 and 68-kDa in the M129 and FH strains of *M. pneumoniae*, respectively (Proft and Herrmann, 1994; Proft *et al.*, 1995). Presumably, as in HMW1 and HMW3, this is due to its APR domain, located in the N-terminal region of the protein (Proft *et al.*, 1995). This protein is divided into 3 domains, each containing a sampling of several different secondary structures, including turns or coils in domain I, predicted coiled-coils in Domain II, and α-helices, β-sheets, and turns in Domain III (Proft *et al.*, 1995). P65 also has a predicted region for interaction with extracellular matrix proteins, known as the RGD sequence containing Arg-Gly-Asp in the C-terminus. It is found in the TX-insoluble fraction and is thus considered a part of the mycoplasma cytoskeleton (Proft and Herrmann, 1994). It is also surface exposed, as shown in studies where proteases removed a portion of P65 from whole cells, and immunofluorescence studies of whole cells using P65 antiserum where signal was apparent on the cell surface (Proft *et al.*, 1995). P65 homolog PlpA of *M. gallisepticum* is also surface exposed (May *et al.*, 2006).

The gene encoding P65 is part of the P65 transcriptional unit, which also includes HMW2, P41, and P24 (Krause *et al.*, 1997). The 65kDa protein P65 was

shown to correspond to the first gene in this unit, based on reactivity with antiserum against a portion of the first gene product fused to dehydrofolate reductase (Krause *et al.*, 1997). Production of truncated HMW2 derivatives, due to *Tn*4001 transposon insertions in *hmw2* led to a reduction in levels of some cytadherence accessory proteins, including P65. This protein has no paired-serine motifs, as in HMW1 and HMW3, but is thought to follow the same fate as the HMW1 and HMW3 in the absence of HMW2 (Jordan *et al.*, 2001).

P65 is localized to the attachment organelle in wild-type *M. pneumoniae* with scattered signal in the filamentous extension as well (Seto *et al.*, 2001). It also localized normally in mutants missing P90 (B), P40 (C), truncated P30, and P1, suggesting that these proteins are not required for its stabilization. However, HMW1 and HMW2 are required for P65 stability and proper localization, with reduced P65 levels in immunoblots and no signal in immunfluorescence studies (Jordan *et al.*, 2001; Seto and Miyata, 2003). P30 and P65 were found to localize to the distal portion of the attachment organelle in the region of the terminal button and possibly interacting with it. A P65-EYFP fusion confirmed the distal localization of P65. Although HMW2 localized near to P65, P41 and P24 had a more proximal localization (Seto and Miyata, 2003).

P65 levels were reduced in an HMW3^{-} mutant (Willby and Krause, 2002). Because P65 has reduced levels in other mutants where HMW3 is reduced, the stability of P65 is believed to be dependent on HMW3 (Willby and Krause, 2002). In this mutant, P65 has a scattered signal with a denser region near the cell poles (Willby and Krause, 2002). It has also been shown that P30 is required for the stabilization of P65, based on the loss of P65 in the absence of P30 (Jordan *et al.*, 2001). Until recently, no

P65 deletion mutants had been isolated, making functional analysis of this protein challenging. However, a transposon insertion mutant, in which a modified Tn4001.2065 from the pMT85 vector was inserted into P65, was recently isolated, and characterization is in progress (Hasselbring *et al.*, unpublished data).

P200. P200 is a 117-kDa protein, partitions into the TX-insoluble fraction (Proft *et al.*, 1995), and is thought to be part of the mycoplasma cytoskeleton. It has an APR domain, like HMW1 and HMW3, but shares no amino acid sequence homology with either protein (Proft *et al.*, 1996). Because of the presence of its APR domain, P200 has an abnormal SDS-PAGE migration pattern, as seen in HMW1, HMW3, and P65, migrating at 200-kDa (Dirksen *et al.*, 1996; Ogle *et al.*, 1992; Proft *et al.*, 1995). P200 has no coiled-coil domains or transmembrane regions, and like HMW1, contains several EAGR box domains scattered throughout the protein (Balish and Krause, 2002). An ortholog of P200, MG386 in *M. genitalium* is a part of the TX-insoluble fraction and contains APR and EAGR box domains, like P200. Although P200 is localized to the attachment organelle in wild-type cells, immunofluorescence studies have demonstrated irregular signal distribution in strains lacking HMW2 (I-2), full-length P30 (II-3), HMW1 and full-length P30 (M6), B and C(III-4), and P1, B, and C (IV-22), despite having wild-type levels in all mutant stains on immunoblots (Jordan *et al.*, 2007). This suggests a dependence on many proteins for its localization, but not stabilization.

Until recently, a P200$^-$ mutant had not been isolated. However, continued analysis of an HMW3$^-$ *Tn*4001 insertion mutant isolated in 2002 (Willby and Krause, 2002), revealed an additional insertion of an IS256 insertion element into the *p200* gene (MPN567), as well as a 36 bp in-frame deletion adjacent to the insertion. This created a

HMW3$^-$/P200$^-$ double mutant. A revertant isolate restoring wild-type HMW3 levels only maintained the P200 deletion, thus forming a P200$^-$ mutant. No immunofluorescence signal was detected in either of these mutants for P200 (Jordan *et al.*, 2007). This strain allowed for functional analysis of P200. P200 is not required for HA, adherence to A549 cells, or normal electron-dense core formation (Jordan *et al.*, 2007). Motility is reduced in this mutant, as compared with wild-type, and its ability to colonize on normal human bronchial epithelium was also reduced, suggesting a role in motility and a requirement for full-motility for colonization of differentiated respiratory mucosa (Jordan *et al.*, 2007). MG386 in *M. genitalium*, ortholog of P200, is also required for gliding motility, but not for cytadherence (Pich *et al.*, 2006).

P41 and P24. P41 and P24 are gene products of the P65 transcriptional unit, whose genes MPN311 and MPN 312, respectively, are adjacent and downstream of *hmw2.* They were so named based on the predicted size of their proteins, not on their SDS-PAGE migration. Immunoblots indicate that P41 migrates as a 47-kDa protein and P24 migrates as a 41-kDa protein. P41 and P24 levels are reduced in *Tn*4001 insertion mutants, B7, G19, H9, and D3, and both proteins are completely absent in A3 and C1. Revertants of these transformants restored these proteins to wild-type levels, suggesting downstream effects due to the transposon insertion in the gene for HMW2 (Krause *et al.*, 1997).

P41 and P24 have no particularly striking structural motifs, although P41 has two short predicted coiled-coil motifs and two hydrophobic regions, but no transmembrane domain. The genes of the P65 operon are conserved in *M. genitalium*, however P24

shares no homology with its corresponding protein MG219. The homolog for P41 is an intergenic region between MG218 and MG219 with 57.1% similarity to P41 (Krause *et al.*, 1997).

EYFP-P41 and EYFP-P24 localize to the proximal-end of the attachment organelle (Kenri *et al.*, 2004) in the same location as the wheel-like complex visualized in electron micrographs (Hegermann *et al.*, 2002), or inverted bowl shape as described elsewhere (Henderson and Jensen, 2006). Recently, a transposon insertion mutant in MPN311 was identified and characterized (Hasselbring and Krause, 2007). In this transformant, P41 and P24 are both absent, the morphology is aberrant with coccoid chains of cells and irregular formation of the attachment organelle, and the P30 immunolabeled attachment organelle seems to detach from the cell body during gliding. Complementation of this transformant with both proteins individually aided in functional analysis of P41 and P24, revealing specific roles for each. Restoration of P41 restored the normal gliding phenotype where the cell body remains intact, suggesting a role for P41 in attachment of the tip structure to the cell body. Furthermore, restoration of P24 restored normal attachment organelle formation (Hasselbring and Krause, 2007).

B and C. Cytadherence accessory proteins B and C were identified during two-dimensional gel analysis as present in a virulent strain of *M. pneumoniae* but absent in an avirulent derivative of that strain (Hansen *et al.*, 1979a, b; Hansen *et al.*, 1981). The avirulent strain was reduced in its ability to attach to hamster tracheal rings, to cause infection in hamsters (Hansen *et al.*, 1979b; Hansen *et al.*, 1981), and to HA, suggesting that B and C may aid in cytadherence and virulence (Hansen *et al.*, 1979b). Shortly thereafter, several groups of spontaneous HA negative mutants were isolated, one of

which lacked the proteins B and C. This strain was designated Class III (hereafter called III-4) and resulted from an insertion of one nucleotide in MPN142 (orf6), causing a frameshift and the loss of the precursor protein cleaved to form B and C (Layh-Schmitt, 1993; Waldo *et al.*, 2005). Another strain was designated Class IV (hereafter called IV-22) lacking A, B, C, and P1. *M. pneumoniae* attaches to sialic acid residues on glycoproteins of the host cell, allowing the bacterium to colonize and cause infection (Roberts *et al.*, 1989). Neuraminidase treatment can be used to disrupt these residues on hamster tracheal rings and prevent low levels of attachment. However, this did not prevent attachment of III-4 or IV-22, suggesting an alternate receptor for binding. Despite retaining a reduced ability to attach, these strains were still unable to cause infection in hamsters (Krause *et al.*, 1982). Revertants of both mutant strains were isolated and restored protein levels, cytadherence, virulence in hamsters, and attachment to hamster tracheal rings (Krause *et al.*, 1983). This evidence suggested that B and C are necessary for cytadherence and virulence (Layh-Schmitt, 1993).

A homolog of orf6 identified in *M. gallisepticum* is a 120-kDa protein called Mrc3 and then later cytadhesin related molecule A (CrmA). The gene for this protein is located downstream from the gene encoding the P1 homolog, Mrc1, now called GapA. Unlike orf6, CrmA is present in only a single copy in the genome and is not cleaved (Yoshida *et al.*, 2000). GapA and CrmA are both required for normal cytadherence and virulence in chickens, as shown in experiments where GapA is absent and cytadherence and virulence are not restored to wild-type levels (Papazisi *et al.*, 2002).

The P1 gene (MPN141) is part of a three-gene transcriptional unit (Inamine *et al.*, 1988b). Primer extension analysis revealed the transcriptional start site, and further

analysis aided in the identification of the likely promoter, ribosome binding site, and terminator sequence regions. The downstream ORF (MPN142) was predicted to encode a 130-kDa membrane protein with a signal sequence consisting of 25 amino acids and a hydrophobic region thought to anchor the protein to the membrane (Inamine *et al.*, 1988b). This 130-kDa protein is cleaved to form two proteins, P90 and P40, which correspond to proteins B and C, respectively (Waldo *et al.*, 2005). Another study confirmed that B and C are membrane proteins, based on their partitioning in the Triton X-100 soluble fraction (Layh-Schmitt and Herrmann, 1992).

B and C are surface-exposed membrane proteins. Evidence to indicate surface exposure of B and C includes trypsin treatment, which altered the structure of B and C or completely removed these proteins from *M. pneumoniae* cells. In addition, radioactive iodination, immunofluorescence, and immunogold experiments provide further evidence that protein B is surface exposed (Franzoso *et al.*, 1993; Hansen *et al.*, 1979a; Layh-Schmitt and Herrmann, 1992). Protein C antiserum did not produce any signal when reacted with whole *M. pneumoniae* cells, possibly due to epitope inaccessibility, but like B, C is thought to be surface-exposed (Franzoso *et al.*, 1993). Immmunogold labeling also localized protein B, and by extension protein C, to the attachment organelle (Franzoso *et al.*, 1993), as had been shown previously for P1 (Collier *et al.*, 1983; Feldner *et al.*, 1982; Hu *et al.*, 1982). In fact, spatial localization studies revealed that P1 and B and C are spatially oriented at a distance of 0.1 nm in relation to each other (Layh-Schmitt and Herrmann, 1994), suggesting potential for these proteins to interact.

P1 has been previously shown to partition partially in the TX-soluble fraction with some remaining in the insoluble fraction (Layh-Schmitt and Harkenthal, 1999). Analysis of P1 partitioning after TX treatment of mutants M5 (lacking B and C), M6 (lacking HMW1 and expressing a truncated P30), and M7 (expressing a truncated P30), demonstrated that B and C are required for P1 partial partitioning into the insoluble fraction, which was completely solubilized in their absence. HMW1 or P30 had no effect on the localization of P1. These data suggested that B and C are the link between P1 and the cytoskeleton. The loss of B and C resulted in altered morphology of *M. pneumoniae* cells and indicated that these proteins aid in attachment organelle formation as well (Layh-Schmitt and Harkenthal, 1999). The interaction of P1 with B and C was confirmed in cross-linking studies, along with MALDI mass spectrometry to identify proteins that interact with P1, as well as its interaction with other cytadherence accessory proteins. Given the importance of P1 localization for cytadherence, and the proteins involved in the P1 complex, it is not surprising that in mutants of HMW1, HMW2, HMW3, B, and C, P1 is not properly localized, most likely due to the lack of binding partners to stabilize it (Layh-Schmitt *et al.*, 2000). Immunofluorescence studies confirmed that B and C localize to the attachment organelle with scattered signal in the cell extension (Seto *et al.*, 2001). Other studies confirmed that the loss of HMW2 (Seto and Miyata, 2003) and separately the loss of HMW1 (Seto *et al.*, 2001) results in scattered P1 signal and no signal from B and C. HMW1, HMW3, P65, and P30 were unaffected by the loss of P1, B, and C. P1, B, and C co-localize to the attachment organelle, supporting the notion that P1 interacts with the cytoskeleton through proteins

B and C (Seto and Miyata, 2003). Later, it was shown that B and C are required for P1 to function normally (Waldo and Krause, 2006). It was also found that P1, B, and C are not required for normal core formation (Seto and Miyata, 2003). These data together suggest that B and C participate at a later stage in the attachment organelle assembly process (Seto *et al.*, 2001).

Formation of the Attachment Organelle

The assembly process of the attachment organelle has been the subject of much interest because of the number of proteins that localize to the attachment organelle, the intricate protein interactions that occur there, and the complex stoichiometry that is required for normal function of the proteins in this structure. The order of assembly was previously proposed implicating HMW1 as the initial protein in the pathway, followed by other cytadherence accessory proteins, HMW3, P1, P30, B and C, in no specific order of assembly, and finally P65, which was shown to require the proteins prior to it in the assembly pathway for stabilization (Seto *et al.*, 2001). Shortly after that, two separate pathways were suggested for the initial steps in the assembly process, converging later in assembly, where P1, B, and C assemble in a separate pathway from the rest of the cyadherence-accessory proteins. The P1 pathway was predicted to merge with the main assembly path at the point of P1 localization (Krause and Balish, 2001). For the other pathway, a specific order of assembly is suggested, in contrast to previous predictions. HMW1 and HMW2 are thought to be the initial proteins in assembly, followed by HMW3 and P30, and finally P65. Recently, fluorescence localization studies indicated that P41 may be involved in the pathway prior to P30 and P65

(Hasselbring *et al.*, 2006a). An order of assembly indicating how each protein interacts and stabilizes another has been suggested, based on previous data (Krause and Balish, 2004).

CHAPTER III

MATERIALS AND METHODS

Bacterial Strains and Culture Conditions

The *M. pneumoniae* strains used in this study were grown to mid-log phase in Hayflick's medium (Hayflick, 1965) at 37°C in tissue culture flasks until the phenol red pH indicator was red-orange in color. Gentamicin and chloramphicol was added to the medium (18 μg/ml and 24 μg/ml, respectively) as appropriate for transformant cultures (Hedreyda *et al.*, 1993). Mycoplasmas were harvested as described previously (Stevens and Krause, 1991). The protein concentration of each sample was determined by using the bicinchominic acid (BCA) protein assay (Pierce, Rockford, Ill.).

Preparation of HMW2 Antibodies

The peptide encoding the first 18 amino acids of the N-terminus of HMW2 (MNDTDKKFPLQPVYDTGF) and the peptide encoding 17 amino acids of the C-terminus of HMW2 (PAFLATQQSISKQQIAQ) were synthesized and coupled separately to keyhole limpet hemocyanin (KLH) using glutaraldehyde. Each KLH-peptide fusion was injected into a pre-screened rabbit, and antiserum collected following several boosters. Antiserum against each peptide was used for immunoblot analysis, and antibodies were affinity-purified as described previously (Stevens and Krause, 1992), for use in immunocytochemistry studies.

Protein Profile and Immunoblot Analysis

Protein profiles were analyzed by sodium dodecylsulfate-polyacrylamide gel electrophoresis (SDS-PAGE) (Laemmli, 1970) and western immunoblotting (Towbin *et al.*, 1979) using antibodies against the N- and C-terminus of HMW2 both at dilution 1:1000 (Balish *et al.*, 2003a), HMW1 at 1:10,000 dilution (Stevens and Krause, 1991), HMW3 at 1:10,000 dilution (Stevens and Krause, 1992), P65 at 1:3000 dilution (Jordan *et al.*, 2001), P41 and P24 at 1:1000 and 1:250 dilutions, respectively (Hasselbring and Krause, 2007). Protein profiles were also analyzed by silver staining (Oakley *et al.*, 1980) following SDS-PAGE.

Generation of C1/HMW2Δmid Tranformants

Plasmid pKV185, containing the HMW2Δmid construct (Balish *et al.*, 2003a), was amplified by PCR using the upstream primer CAAGCTTGCATGCCTGGATCCAGAGAT GCG and downstream primer CCCCGGATCCTTATTTAGCTGCTTTTTGGGC to create BamHI sites (underlined). The PCR product was cloned into the corresponding site of *Tn*4001cat (Hahn *et al.*, 1999) in pKV304 to form plasmid pKV316. Random colonies were picked and insertion was confirmed by sequencing. Plasmid DNA was transformed into M. pneumoniae mutant C1 (*hmw2*::*Tn*4001; Hedreyda and Krause, 1995; Krause et al., 1997) by electroporation, plated on PPLO agar plates containing gentamicin and chloramphenicol (18 μg/ml and 24 μg/ml, respectively), and incubated at 37°C for 7-10 days. Following incubation, plates were overlaid with 12.5% sheep blood, 1% Noble agar, and 0.85% NaCl and incubated at 37°C for 2-3 days for

hemolytic plaque formation to visualize colonies. Afterwards, chloramphenicol and gentamicin resistant colonies were selected and cultured in 1 ml of Hayflick's medium and expanded.

Triton X-100 Extraction and Trichloroacetic Acid Precipitation

Mycoplasma cells were extracted with 2% Triton X-100 (TX) in 20 mM Tris (pH 7.5)/150 mM NaCl (TN buffer) (Stevens and Krause, 1991) at 37°C for 30 min, then centrifuged at 14,000 rpm for 30 min to separate the TX-insoluble fraction from the TX-soluble fraction. The TX-insoluble pellet was suspended in TN buffer. One-tenth volume of 100% Trichloroacetic acid (TCA) was added to the TX-soluble fraction and incubated on ice for 5 min to precipitate the protein. Following a 5 min centrifugation at 14,000 rpm, the supernatant was removed and 500 μl acetone was added to the pellet to remove the TCA. After another 5 min centrifugation, the pellet was suspended in 50 μl TN buffer.

Immunofluorescence (IF) Experiments

Detailed protocols for IF analysis of *M. pneumoniae* are described elsewhere in detail (Balish et al., 2003, Willby et al., 2004). Briefly, mycoplasmas were incubated for 2 h in SP4 broth or Hayflick's medium on 0.01% poly-L-lysine- coated coverslips. Following wash steps with 0.05% TX in PBS and blocking with 5% non-fat dry milk in wash solution for 1 h at RT, coverslips were incubated with a 1:20 dilution of monoclonal anti-P1 primary antibody at 4°C overnight. Following washes to remove excess primary antibody, Cy3 conjugated donkey anti-mouse (Jackson Immunologicals,

West Grove, Pa) at 1:100 dilution was added and incubated at RT for 1 h. Coverslips were washed again to remove excess antibody and then attached to glass slides and examined as described above using the tetramethyl rhodamine filter cube (Leica, Wetzlar, Germany). Digital images by phase-contrast and fluorescence microscopy were captured separately and merged using Adobe Photoshop (Adobe Systems Incorporated, San Jose, CA).

Qualitative and Quantitative Hemadsorption Assays

The protocol for the quantitative (Fisseha *et al.*, 1999; Hasselbring *et al.*, 2005) and qualitative (Krause *et al.*, 1982) assays have been described in detail previously. Briefly, in the qualitative assay, *M. pneumoniae* strains were inoculated on PPLO agar plates and incubated at 37°C for 7-9 days, after which 1 ml of chicken blood diluted 1:5 in 0.85% NaCl was overlaid on each plate and incubated 30 min at 37°C. Excess erythrocytes were removed with several washing steps and colonies were imaged using a Nikon Diaphot inverted phase contrast microscope (Nikon, Garden City, NY).

In the quantitative assay, *M. pneumoniae* strains were incubated in 30 ml of Hayflick's medium with 400 μCi [^{3}H]-thymidine for approximately 72 h at 37°C. Following the incubation, 50 μl of 4% chicken blood in PBS was added to labeled mycoplasma cells which had been passed through a needle repeatedly and centrifuged to remove aggregates. This mycoplasma cell/chicken blood mixture was incubated at 37°C for 30 min with mixing and then overlaid on 200 μl of 40% sucrose solution at room temperature and centrifuged for 20 sec at 7000 rpm. The pellet was collected and placed in a scintillation vial, where it was treated with 1% SDS, 3% H_2O_2 overnight.

Scintiverse scintillation fluid (Fisher Scientific, Pittsburgh, PA) was added, and radioactivity was measured using an LS 6500 scintillation counter (Beckman Instruments, Fullerton, CA).

Satellite Growth Assay

The protocol for assessing satellite growth as an indicator of gliding motility has been previously described (Hasselbring *et al.*, 2005). *M. pneumoniae* strains were inoculated in 600 μl of SP4 medium (Tully *et al.*, 1977) with 3% gelatin (pH. 7.6) in a 4-chambered glass slide (Hasselbring *et al.*, 2005) and incubated at 37°C for 24 h prior to examination. Images were digitally captured using the ORCA-ER charge-coupled device camera (Hamamatsu Photonics, Hamamatsu City, Japan) and OPENLAB 4.0 software (Improvision, Lexington, MA).

Scanning Electron Microscopy (SEM)

Wild-type and mutant strains of *M. pneumoniae* were grown and harvested as described above. Final pellets were suspended in fresh Hayflick medium and passed through a 25G needle five times and a 0.45 μm pore syringe filter to disperse cell clumps, and then incubated in a tissue culture dish with 0.01% poly-L-lysine- coated glass coverslips (Stevens and Krause, 1992) for 2-4 h at 37°C, allowing for attachment to the coverslips. Coverslips were rinsed with phosphate-buffered saline (PBS, pH 7.2) six times and immediately incubated in 1% glutaraldehyde, 1% paraformaldehyde, and 0.1% picric acid in 0.1 M sodium cacodylate buffer, pH 7.2 fixative for 30 min at room temperature. Following fixation, coverslips were rinsed as described above, then

dehydrated in a graded ethanol series (30%, 50%, 70%, 85%, 95%, 100% 2X), with one 10-min incubation each. Finally, coverslips were critical point dried in liquid CO_2, coated with chromium, and examined using a LEO 982 SEM.

Transmission Electron Microscopy (TEM)

Thin sections. Mycoplasmas were cultured and harvested as described above except that the final pellet was suspended and fixed in 500 μl of 2% formaldehyde/2% glutaraldehyde in 0.1 M phosphate buffer, pH 7.3. After fixation, mycoplasmas were washed in PBS, enrobed in 3% noble agar (Difco Laboratories, Detroit, MI) at 58-60°C, agitated, and centrifuged at 13,000 rpm for 10 min. Samples were post-fixed in 1% OsO_4 for 1 h, dehydrated in a graded ethanol series (30%, 50%, 70%, 85%, 95%, and 100% 2X), washed twice in propylene oxide, infiltrated overnight in a propylene oxide and Mollenhauer's Epon-Araldite (Mollenhauer and Whaley, 1963) 1:1, at room temperature, and then 2 h in 100% Epon-Araldite. Samples were embedded in fresh Epon-Araldite plastic using flatbed molds and allowed to polymerize at 75°C overnight. One-μm sections were obtained using a Reichert Ultracut S Ultramicrotome (Leica, Inc., Deerfield, IL), placed on glass slides, and allowed to dry with moderate heat before staining with 1% toluidine Blue O in 1% sodium borate. Selected blocks were trimmed, and sections approximately 65 nm thin were generated and placed on 200-mesh Cu Veco hex grids (Electron Microscopy Sciences, Fort Washington, PA). Sections were post-stained with 5% methanolic uranyl acetate and Reynolds' lead citrate (Reynolds, 1963), and grids were viewed using a JEM-1210 transmission electron microscope (JEOL USA, Inc., Peabody, MA).

Triton-X-100 (TX) extracted cells. Samples were prepared using a protocol modified from Regula et al. (Regula *et al.*, 2001). Wild-type and mutant mycoplasma stocks were passed through a 25G needle 10X to disperse clumps, then inoculated in Hayflick medium in 24-well tissue culture dishes containing 0.01% poly-L-lysine-coated, 2% parlodion-coated copper grids. Following incubation at 37°C for 2-6 h, the grids were washed 3X by replacing the growth medium with PBS at room-temperature, and then incubated in TN buffer with 2% TX for 30 min at 37°C. Grids were washed 3X with PBS at room temperature, fixed for 10 sec with 0.2% glutaraldehyde and 0.2% (para)formaldehyde in PBS at room temperature, and immediately post-stained with 3% aqueous phosphotungstic acid (pH 6.8-7.0) for 45 sec and air-dried. Grids were viewed as described above for thin sections. Length of the cores in each fraction was measured using ImagePro Plus Imaging software (MediaCybernetics, Silver Spring, MD).

Immunocytochemistry

Thin sections. Mycoplasmas were fixed as described above for thin sections except that post-fixation with OsO4 was omitted. After fixation the cell pellets were washed 3X in PBS and 3X in deionized water for 10 min each, dehydrated in a graded ethanol series (50%, 75% 2X), and infiltrated overnight with 50% L.R. White resin (Polysciences, Inc., Warrington, PA) in 75% ethanol, then in 100% L.R. White resin for 2 h. The samples were embedded in fresh gelatin capsules (Ted Pella, Inc., Redding, CA) and fresh L.R. White resin using flatbed molds and allowed to polymerize at 58-60°C for 24 h. Thin sections were incubated for 10 min in wash buffer [0.2 M Tris-

buffered saline (TBS) pH 8.2 with 1% crystallized bovine serum albumin (BSA, Sigma-Aldrich, St. Louis, MO)], then in TBS with 3% BSA for 30 min. After washing in wash buffer for 1 min, grids were incubated in a 1:15 dilution of affinity-purified HMW2 N-terminal-specific antibody in wash buffer overnight at 4°C. Grids were washed for 1 min in wash buffer and incubated in 0.2 M TBS for at least 1 min. Following washes, grids were incubated with a 1:20 dilution of goat anti-rabbit antibody conjugated to 10 nm colloidal gold (Amersham Biosciences, Piscataway, N.J.) in wash buffer for 30 min. Sections were obtained, stained, and viewed as for thin sections above.

TX fractions. TX fractions were prepared as described above except that samples were probed with antibodies prior to post-staining. Following TX extractions, gold-labeling was performed as for thin sections and grids were viewed as described above.

Quantitation of Gold Particles on TX Fractions

Using the ImagePro Plus Imaging software (MediaCybernetics, Silver Spring, MD), distances were measured from each gold particle to the edge of the core for each colloidal gold-labeled TX fraction. We used 20 nm as the maximum distance between the antigen and the gold particle, based on antibody flexibility [(8); 10 nm as the length of the primary antibody, plus 10 nm as the length of the secondary antibody (Amersham Biosciences, Piscataway, NJ)]. Thus, any gold particle with a distance measurement $\leq$ 20 nm was considered to correspond to the core. We measured the width of the attachment organelle at the base toward the cell body to be 110 $\pm$ 13 nm and the width of the core at the base to be 46 $\pm$ 8 nm. Subtracting these two widths, we found that the

electron-lucent region in the attachment organelle between the core and the membrane was 64 nm with the space between one side of the main rod and the membrane being 32 nm. Using this plus the maximum distance from antigen to gold particle, the particles could be up to 52 nm away from the core and still be associated peripherally to the main rod. Therefore, any gold particles 20-52 nm from the core were not considered to correspond to the core, but instead to the peripheral region. Gold particles on the edge of the core were grouped with those found directly on the core. Particles located between 52 and 150 nm from the core were thought to be outside the range of the terminal organelles, while particles greater than our arbitrary maximum distance (150 nm) from the core were excluded, as were the rare particles that were found with membrane material not associated with the core. All measurements were analyzed in Microsoft Excel (Microsoft Corporation, Redmond, WA).

Electron-Dense Core Purification

Mycoplasmas were grown and harvested, and protein concentrations were determined as described above. Cells were subjected to various treatments including 0.5-4% sodium deoxycholate, 0.5-4% CHAPS, 2-4 M potassium thiocyanate, 0.2-1.8 M potassium chloride, 0.6-1.8 M potassium iodide, 0.1-2 M guanidine-HCl, 1 M sodium perchlorate, 2% Triton X-100, 1% digitonin with 4 mM $MgCl_2$, 20% sucrose in combination with guanidine-HCl and KI, and 2% TX/DNaseI (50 μg/ml) in a variety of combinations and sequences. Protein profiles of rifampin (5 μg/ml) treated wild-type cells were also analyzed. The three treatments used in the final protocol were chosen based on the removal of any material not directly associated with the core, such that the

resulting fraction was enriched for cores. By this protocol, cells were suspended in 2% TX/0.6 M KCl in TN and incubated at 37°C for 30 min. Insoluble and soluble fractions were separated by centrifugation at 14,000 rpm for 30 min. The insoluble fraction was further extracted with 0.6 M KI/20% sucrose in TN, followed by 1.5 M Guanidine-HCl in TN, as described above. The final insoluble fraction was suspended in TN, urea was added to a concentration of 8 M and the sample was incubated for 10 min at 37°C, followed by incubation in 3X sample buffer (0.3 M Tris-HCl (pH 6.8), 6% sodium dodecylsulfate, 60% glycerol, 13% 2-mercaptoethanol, 0.06% bromophenol blue) for 10 min at 37°C. The urea aided in solubilizing the samples prior to SDS-PAGE. Following electron-dense core purification, the insoluble fractions were analyzed on 4-8% and 8-12% gradient SDS-PAGE (Laemmli, 1970), and silver-stained (Oakley et al., 1980).

Assay to Measure Efficiency of Membrane Removal

Mycoplasmas were grown in Hayflick medium supplemented with 10 nM of ^{3}H-palmitic acid (Amersham Biosciences, Piscataway, NJ) on poly-L-lysine- coated coverslips and incubated until red-orange in color at 37°C. After incubation, each coverslip was washed in PBS 3X and counted for radioactivity or incubated with 2% TX/0.6 M KCl, 0.6 M KI/20% sucrose, or 1.5 M Guanidine-HCl for 30 min at 37°C and washed 3X again. Coverslips and associated washes were placed in scintillation vials and counted for each step of the purification process. Control coverslips incubated in the absence of mycoplasmas were carried through the entire purification process in parallel. Radioactivity was measured in a LS 6500 scintillation counter (Beckman Instruments, Fullerton, CA).

TEM Analysis of the Efficiency of Core Purification

Wild-type mycoplasmas were grown on grids as in steps prior to TX extraction for fractions above. The specific treatments that extracted the most protein bands from the TX-insoluble fraction (above) were subsequently used in TEM analysis to determine if the cores were intact and enriched. Grids were treated with 1ml of 2% TX/0.6 M KCl in TN for 30 min at 37°C and washed once with PBS at room temperature. Grids were subsequently treated with 0.6 M KI/20% sucrose in TN, followed by 1.5 M Guanidine-HCl in TN as described above. After the final treatment, grids were washed 3X with PBS at room temperature and fixed, post-stained, and viewed as described above for TX fractions.

Mass Spectrometry Analysis

Cell suspensions were extracted with detergent and salts as described above and subjected to SDS-PAGE. The isolated core samples were subjected to SDS-PAGE, just into the 5% separating gel but before protein band separation occurred. The entire band of unresolved proteins was excised from the gel, separated into three 1.7 ml microcentrifuge tubes for better manageability, and incubated in a 1:1 concentration of 100 mM potassium ferricyanide and 100 mM sodium thiocyanate for 10 min, shaking. Gel pieces were washed with distilled water 3 x 5 min, hydrated/dehydrated with 25 mM ammonium bicarbonate and 50% acetonitrile, and dried by vacuum centrifugation for approximately 1 h. Trypsin (Promega, Madison, WI) (30 ng/ul) in 25 mM ammonium bicarbonate absorbed into the gel bands while incubating overnight at 37°C. After incubation, peptides were extracted with 25 mM

ammonium bicarbonate wash for 15 min, followed by 2 x 15 min washes in 75% acetonitrile, 0.5% trifluoroacetic acid in distilled water. Each wash was collected and, finally, vacuum centrifuged to dryness to concentrate the peptides.

A reversed-phase HPLC spray column (75 μm × 10 cm; tip 15 ± 1 μm, PicoTip EMITTER, New Objective, Woburn, MA) was prepared by packing silica C18 resins (Rainin Microsorb MV, 5 μm, 300 Å pore size) with 50% isopropanol and 50% methanol. The protein samples were loaded onto the column using a pressurized stainless steel bomb and nitrogen gas at 1,000 psi for 30 min. Peptides were rinsed in 0.1% formic acid and eluted at a flow rate of approximately 400 nL/min with a 65-min linear gradient of 5 to 60% acetonitrile in 0.1% formic acid/water. The spectra were acquired by nano elecrospray ionization on a Finnigan LTQ Linear Ion Trap Mass Spectrometer (Thermo Finnigan, San Jose, CA) at 1.92 kV spray voltage and 220°C capillary temperature, which was directly coupled to the reversed-phase HPLC system. Following detection in MS mode, the nine most abundant ions were independently selected to undergo MS/MS analysis. Spectra obtained from this analysis were compared with theoretical MS/MS spectra of all peptides in the database to provide the most probable peptide sequence for each precursor ion (Alvarez-Manilla *et al.*, 2006; Weatherly *et al.*, 2005).

CHAPTER IV

RESULTS

HMW2 Functional Analysis

Determination of expression levels of HMW2 derivatives, P28, and other proteins of the P65 operon in mutant strains. The loss of HMW2 has numerous downstream effects on the cell. Previous studies have shown that spontaneously arising mutant strain I-2, in which HMW2 is not produced due to a frameshift mutation, has reduced levels of cytadherence accessory proteins HMW1, HMW3, and P65 (Fig. 4.1) (Fisseha *et al.*, 1999). Introduction of HMW2 restores these proteins by allowing for their stable incorporation into the cytoskeleton (Balish *et al.*, 2001; Fisseha *et al.*, 1999; Popham *et al.*, 1997). Furthermore, in the absence of HMW2, the major adhesin P1 does not cluster at the tip of the cells, the cellular morphology is aberrant, and the cells are non-motile. Given the fundamental importance of HMW2, I examined other HMW2 derivatives to determine possible functional domains of the protein. An earlier study reported the isolation of six *Tn*4001 insertion mutants, A3, B7, C1, D3, G19, H9, in which transposon insertion in MPN310 encoding HMW2 yielded no detectable truncated HMW2 derivatives, as seen by immunoblots using antisera against a dehydrofolate reductase-HMW2 fusion (Krause *et al.*, 1997). However, here new antiserum specifically against the N-terminus of HMW2 allowed for detection of truncated HMW2 derivatives in the B7 and H9 strains (data not shown and Fig. 4.1 and

Figure 4.1. Schematic of wild-type, engineered, and mutant HMW2 derivatives. Regions in black indicate the deleted portion of each protein. Approximate start site of P28 translation indicated by black arrows above the protein. Inverted red triangles are the sites of transposon insertion. Amino acid residues corresponding to each truncation or deletion are indicated beneath each protein. Strain name is indicated to the left of each protein.

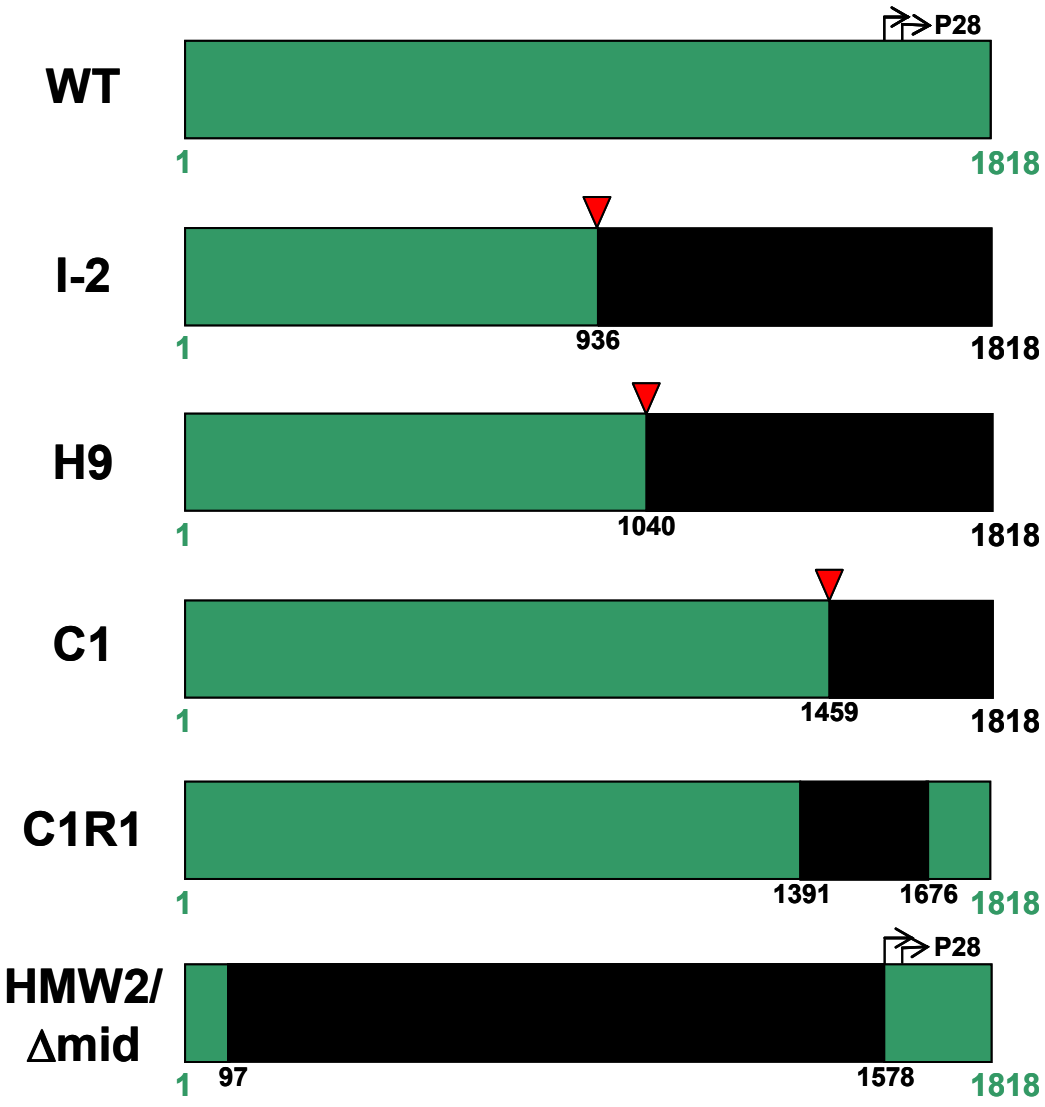
WT
P28
1
1818
I-2
936
1818
H9
1040
1818
C1
1459
1818
C1R1
1391
1676
1818
HMW2/
Δmid
P28
97
1578
1818

Figure 4.2. Immunoblot analysis of levels of proteins of the P65 operon in wild-type *M. pneumoniae* and MPN310 mutant strains. WT, wild-type; I-2, spontaneous MPN310 mutant (Krause *et al.*, 1982); H9, MPN310::*Tn*4001 insertion mutant (Krause *et al.*, 1997); C1, MPN310::*Tn*4001 insertion mutant (Krause *et al.*, 1997); HMW2Δmid, transformants of the indicated mutants producing the recombinant HMW2 deletion derivative (Balish *et al.*, 2003a); Size standards are indicated to the left. Numbers in parentheses indicate different clonal isolates. 30μg of protein was used in each lane. (A) N-terminus-specific HMW2 antiserum (upper) was used at 1:1000 dilution and C-terminus-specific HMW2 antiserum (lower) was used at 1:1000 dilution. (B) Anti-P41 antiserum (upper) was used at 1:1000 dilution and anti-P24 antiserum (lower) was used at 1:250 dilution.

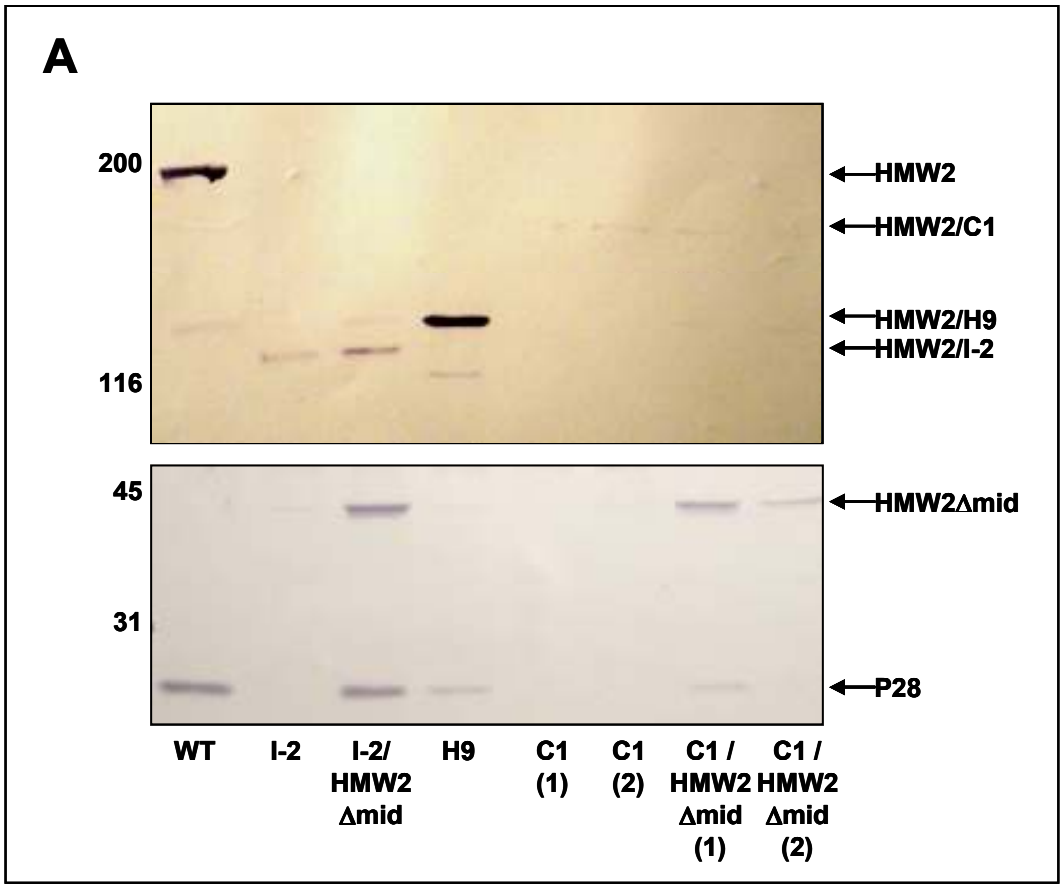
A
200
116
HMW2
HMW2/C1
HMW2/H9
HMW2/I-2
45
31
HMW2Δmid
P28
WT
I-2
I-2/ HMW2 Δmid
H9
C1 (1)
C1 (2)
C1 / HMW2 Δmid (1)
C1 / HMW2 Δmid (2)

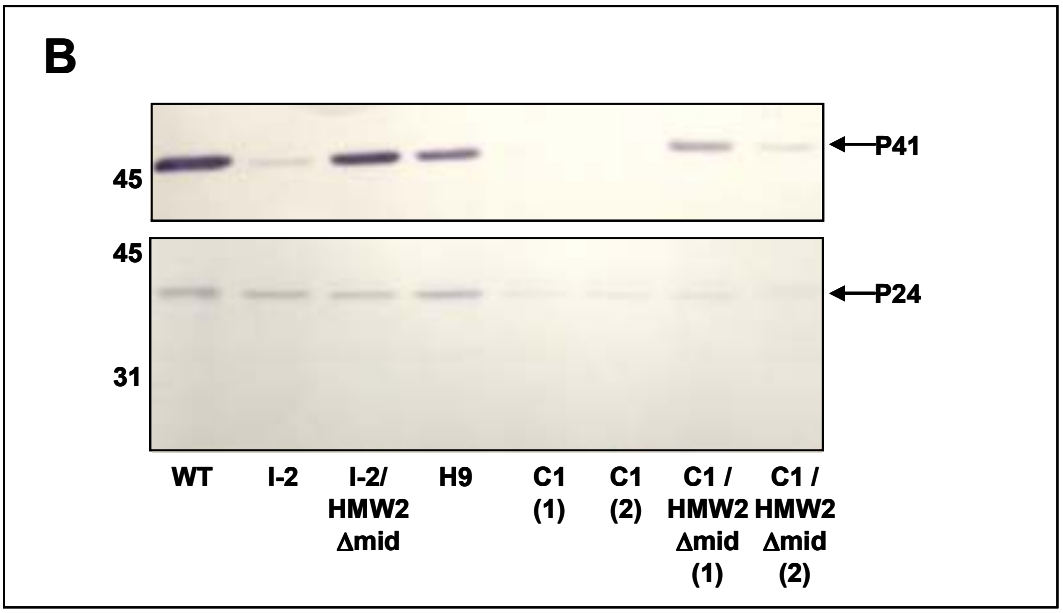
B
45
45
31
P41
P24
WT
I-2
I-2/ HMW2 Δmid
H9
C1 (1)
C1 (2)
C1 / HMW2 Δmid (1)
C1 / HMW2 Δmid (2)

Fig. 4.2A, respectively). Truncated HMW2 was present at wild-type levels in H9, while variably reduced levels of truncated HMW2 were observed in B7, comparable to the results reported for the HMW2 derivative in mutant I-2 (Fisseha *et al.*, 1999). Because of variability in the level of the HMW2 derivative in mutant B7, further analysis was only continued with mutant H9. No HMW2 derivatives were detected in the other MPN310:Tn4001 mutants, using this antiserum (data not shown). However, antiserum against the N-terminus of HMW2 revealed very low levels of truncated HMW2 in the C1 mutant (Fig. 4.2A). The C1 excision-revertant C1R1 has an in-frame 858-bp deletion in MPN310 and produces a slightly truncated (~185kDa) HMW2 derivative at wildtype levels (Fig. 4.1) (Krause *et al.*, 1997).

The recombinant HMW2 derivative HMW2Δmid has an internal in-frame deletion of nearly 80% of the MPN310 coding region. Transformation of this construct into mutant I-2 results in production of a 38-kDa HMW2 derivative at wildtype levels (Fig. 4.1, 4.2A; (Balish *et al.*, 2003a)). Mutant I-2 has a high rate of reversion, restoring a wild-type phenotype and limiting the value of this mutant (S. Bose, unpublished data). Therefore, HMW2Δmid was also transformed into mutant C1, in which reversion is much less likely as long as gentamicin selection is maintained. The levels of HMW2Δmid varied among C1/HMW2Δmid transformants (Fig. 4.1, 4.2A); such variability is also seen with expression of recombinant full-length HMW2 in mutant I-2 (Fisseha *et al.*, 1999).

Internal translation initiation near the 3'end of MPN310 allows for production of a 28-kDa protein, P28, in wild-type *M. pneumoniae* (Fig. 4.1) (Krause *et al.*, 1997). There are two potential translational start sites for P28 within MPN310; the actual start site is

yet to be determined. Production of P28 was detected in immunoblots using antiserum against the C-terminus of HMW2 in the wild-type strain (Krause *et al.*, 1997); Fig. 4.2A). However, in MPN310 mutants I-2 and H9, P28 levels were reduced (Fig. 4.2A). Interestingly, P28 levels were lower in mutant I-2 than in H9, which could be due to greater stability of truncated HMW2 in the latter. The transposon insertion in the C1 transformant is located near the two potential translation start sites, which presumably prevents expression of P28, as none is detected on immunoblots (Krause *et al.*, 1997); Fig. 4.2A). Production of P28 was restored in mutants I-2 and C1 when these strains were transformed with HMW2Δmid. Levels of P28 were shown to correlate with the levels of HMW2Δmid in different transformants. For example, in one I-2/ HMW2Δmid transformant, HMW2Δmid and P28 were observed at wild-type levels, while in a C1/HMW2Δmid transformant, HMW2Δmid and P28 were both at reduced levels. It is important to make the distinction that this variability in P28 levels was only seen in the HMW2Δmid transformants where P28 levels are restored, and not in the I-2 and C1 mutant strains lacking HMW2Δmid, where P28 is reduced or not present, respectively. Lastly, C1R1 lacks P28 as a result of an imprecise excision of *Tn*4001 mutant from the C1 mutant (Fig. 4.1) (Fisseha *et al.*, 1999).

The gene encoding P41 is located downstream of the gene encoding HMW2 and P28 in the P65 operon. The levels of this protein correlated with the stability of P28. As the levels of P28 decreased, the levels of P41 likewise decreased accordingly, where H9, for example, had higher levels of P41 than I-2 and C1 (Fig. 4.2B), such that the levels of P41 were H9 > I-2 > C1. P24 is also encoded in the P65 operon and is downstream of the gene encoding P41. Here, the levels of P24 correlated with only the

presence P41, not its levels, such that P24 was apparent in mutants H9 and I-2 in which P41 is made, but greatly reduced in mutant C1, where minimal levels of P41 were detected (Fig. 4.2B). This result was not surprising considering that P41 and P24 may be translationally coupled (Hasselbring *et al.*, 2006a; Kenri *et al.*, 2004).

In I-2/HMW2Δmid and C1/HMW2Δmid transformants, P41 levels varied based on the levels of HMW2Δmid, as was the case for P28. Thus, the levels of HMW2Δmid and P41 were I-2/HMW2Δmid > C1/HMW2Δmid(1) > C1/HMW2Δmid(2) (Fig. 4.2B). However, HMW2Δmid did not restore P24 levels in I-2/HMW2Δmid and C1/HMW2Δmid above the levels initially present in I-2 and C1, respectively (Fig. 4.2B). Table 4.1 summarizes the results from this section.

The C-terminus of HMW2 is essential for normal Triton X-100 partitioning and stabilization of cytadherence-associated proteins. Wildtype HMW2 partitions primarily into the Triton X-100 (TX) insoluble fraction (Fig. 4.3) (Proft and Herrmann, 1994), where it appears to be stably incorporated into the cytoskeleton. In the absence of the C-terminus of HMW2 in H9, HMW2 partitioned largely in the TX-soluble fraction; however, some stable association with the cytoskeleton did occur with poor efficiency (Fig. 4.3). In I-2/HMW2Δmid, the presence of the C-terminus of HMW2 conferred normal partitioning into the TX-insoluble fraction (Fig. 4.3), indicating a requirement for the C-terminus but not the central domain of HMW2, regardless of HMW2 derivative stability, for this to occur.

Previous studies indicated that the absence of HMW2 in I-2 prevents stable incorporation of HMW1, HMW3, and P65 into the cytoskeleton (Balish *et al.*, 2001) (Fig. 4.4A); as a result, HMW1, HMW3, and P65 are subject to accelerated proteolytic

Table 4.1 Summary of relative protein levels of cytadherence-associated proteins. n/a, strains in which this construct was not transformed; nt, not tested. ++++, +++, ++, +, +/-, and - are relative protein levels.

Strain	HMW1	HMW2	HMW2 Δmid	P28	P41	P24	HMW3	P65
WT	++++	++++	n/a	++++	++++	++++	++++	++++
I-2	+	+	n/a	+/-	+/-	++	+	+
I-2/ HMW2 Δmid	+	++	++++	++++	++++	++	++++	++++
H9	+	++++	n/a	++	+++	++	+	+
C1	+	+/-	n/a	-	+/-	+/-	+	+
C1/ HMW2 Δmid	+	+/-	++	+	++	+/-	++++	++++
C1R1	++++	++++	n/a	-	nt	nt	++++	nt

Figure 4.3. Immunoblot analysis of Triton X-100 partitioning in wild-type (WT) and HMW2 derivative strains. HMW2 N-terminus-specific antiserum was used at 1:1000 dilution. TX-insoluble and -soluble fractions (TX-insol and TX-sol, respectively) are indicated along the bottom. From Balish et al., 2003b.

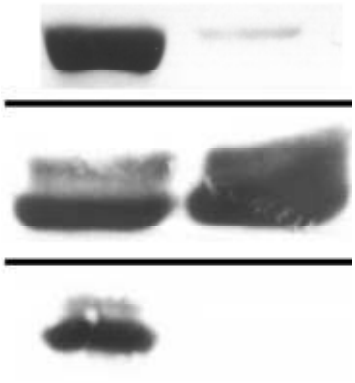
WT
H9
I-2/HMW2Δmid
TX-insol
TX-sol

Figure 4.4. Immunoblot analysis of HMW1, HMW3, and P65 levels in wild-type (WT) and HMW2 derivative strains. 30μg of protein was used in each lane. (A) Two C1 and two C1/HMW2Δmid transformants were used indicated by numbers in parentheses. Anti-HMW1 (upper) and anti-HMW3 (middle) antisera were used at 1:10,000 dilution. Anti-P65 antiserum (lower) was used at 1:3,000 dilution. (B) Anti-HMW1 (upper) and anti-HMW3 (lower) antisera were used at 1:10,000 dilution.

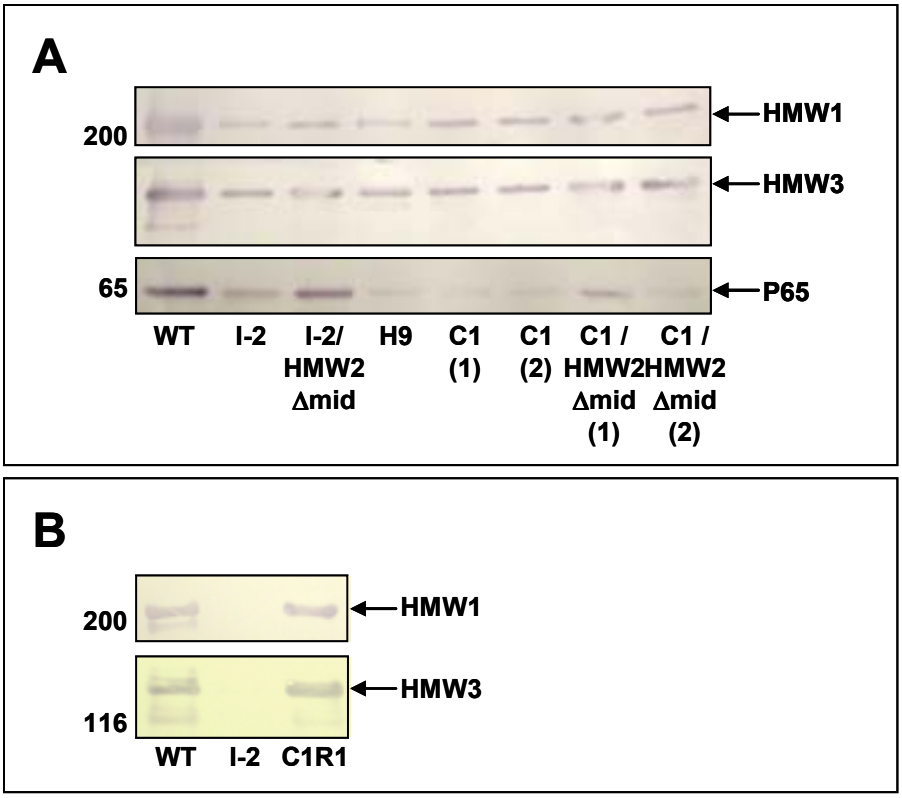
A
200
65
HMW1
HMW3
P65
WT
I-2
I-2/ HMW2 Δmid
H9
C1 (1)
C1 (2)
C1 / HMW2 Δmid (1)
C1 / HMW2 Δmid (2)
B
200
116
HMW1
HMW3
WT
I-2
C1R1

turnover and are detected at reduced steady-state levels in immunoblots (Popham *et al.*, 1997). Like I-2, mutants H9 and C1 also have reduced levels of these proteins (Fig. 4.4A) (Balish *et al.*, 2003a). However, introduction of HMW2Δmid in I-2 and C1 restored HMW3 and P65 to normal levels (Fig. 4.4A). Wild-type levels of HMW3 are also present in C1R1 (Fig. 4.4B), while P65 levels have yet to be tested in C1R1. Again, the C-terminus of HMW2, not the stability of the HMW2 derivative, is essential for stabilization.

Specific coiled-coil domains or spatial positioning between the N-terminus and the C-terminus of HMW2 is essential for stabilization of HMW1, P1 localization, normal cytadherence, motility, and cellular morphology. As mentioned previously, mutant I-2 has reduced levels of HMW1 and other cytadherence accessory proteins. Likewise, the C-terminally truncated HMW2 mutants H9 and C1 also have reduced levels of these proteins (Fig. 4.4A). Surprisingly, HMW2Δmid was not sufficient to stabilize HMW1 levels (Fig. 4.4A), although stabilization of HMW1 did occur in the C1 revertant C1R1 (Fig. 4.4B). Specific regions of HMW2 other than the C-terminus are required for HMW1 stabilization.

P1 has been shown to localize, or cluster, at the attachment organelle in wild-type *M. pneumoniae* cells, enabling cytadherence (Fig. 4.5). In immunofluorescence studies, the signal for P1 in wild-type was distinct and focused at the tip of the attachment organelle. Initially, it was thought that the absence of the C-terminus of HMW2 in strains I-2 and H9 prevented P1 clustering as evidenced by scattered P1 foci in these strains (Fig. 4.5). However, the foci for P1 remained scattered even after restoration of the C-terminus of HMW2 by transformation of HMW2Δmid into I-2 (Fig.

Figure 4.5. Indirect immunolocalization of P1 in wild-type (WT) and HMW2 derivative strains. Scale bar, 30μm; From Balish et al., 2003b.

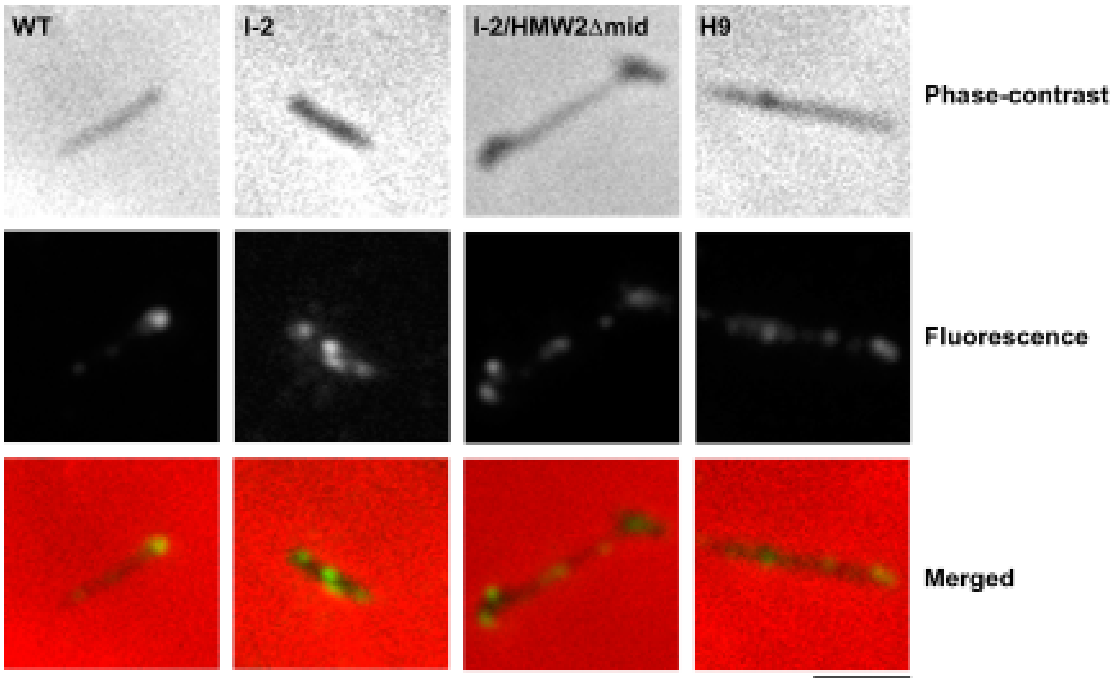
WT
I-2
I-2/HMW2Δmid
H9
Phase-contrast
Fluorescence
Merged

4.5). Earlier studies indicated the requirement for HMW1 in P1 clustering (Hahn *et al.*, 1998). I-2/HMW2Δmid, like I-2 and H9, has reduced levels of HMW1 and does not cluster P1, consistent with that finding. Thus, the same regions of HMW2 that are essential for stabilizing HMW1 appear to indirectly allow for P1 localization.

Hemadsorption (HA) is a convenient cytadherence test that correlates with the ability of *M. pneumoniae* cells to attach to respiratory epithelium. Wildtype *M. pneumoniae* is HA-positive, with qualitative analysis showing erythrocytes completely covering each colony (Fig. 4.6A). In contrast, mutants I-2 and H9 were HA-negative, while I-2/HMW2Δmid exhibited an intermediate HA (Fig. 4.6 A; 4.6C; (Balish *et al.*, 2003a)). Quantitatively, C1 and C1/HMW2Δmid, like I-2 and H9, were HA-negative as was P30 deletion mutant II-3, which served as a negative control (Fig. 4.6B; 4.6C). Contrasting results between I-2/HMW2Δmid and C1/HMW2Δmid suggest that the stability of the HMW2 expressed in these strains, where HMW2 in I-2 is more stable than in C1, is important for cytadherence. Furthermore, since C1R1 exhibits intermediate levels of HA (Fisseha *et al.*, 1999), the regions essential for HMW1 stability and P1 clustering are necessary but not sufficient for full restoration of the ability to hemadsorb, suggesting that other regions of HMW2 are also required. Interestingly, the HA ability of I-2/HMW2Δmid was greater than that of C1R1.

Like cytadherence, the ability of *M. pneumoniae* cells to glide is also believed to be a virulence factor (Jordan *et al.*, 2007). Satellite growth around colonies is an indicator of *M. pneumoniae* motility. Thus, we used this phenotype to determine the regions of HMW2 that are required for gliding motility. Filamentous, branching cells are apparent around colonies of wild-type *M. pneumoniae*, indicating that they are motile

Figure 4.6. Levels of hemadsorption for wild-type (WT) and HMW2 derivative strains. (A) Qualitative analysis, Scale bar, 60μm; from Balish et al., 2003b. (B) and (C) Quantitative analysis, where levels of HA are normalized to WT.

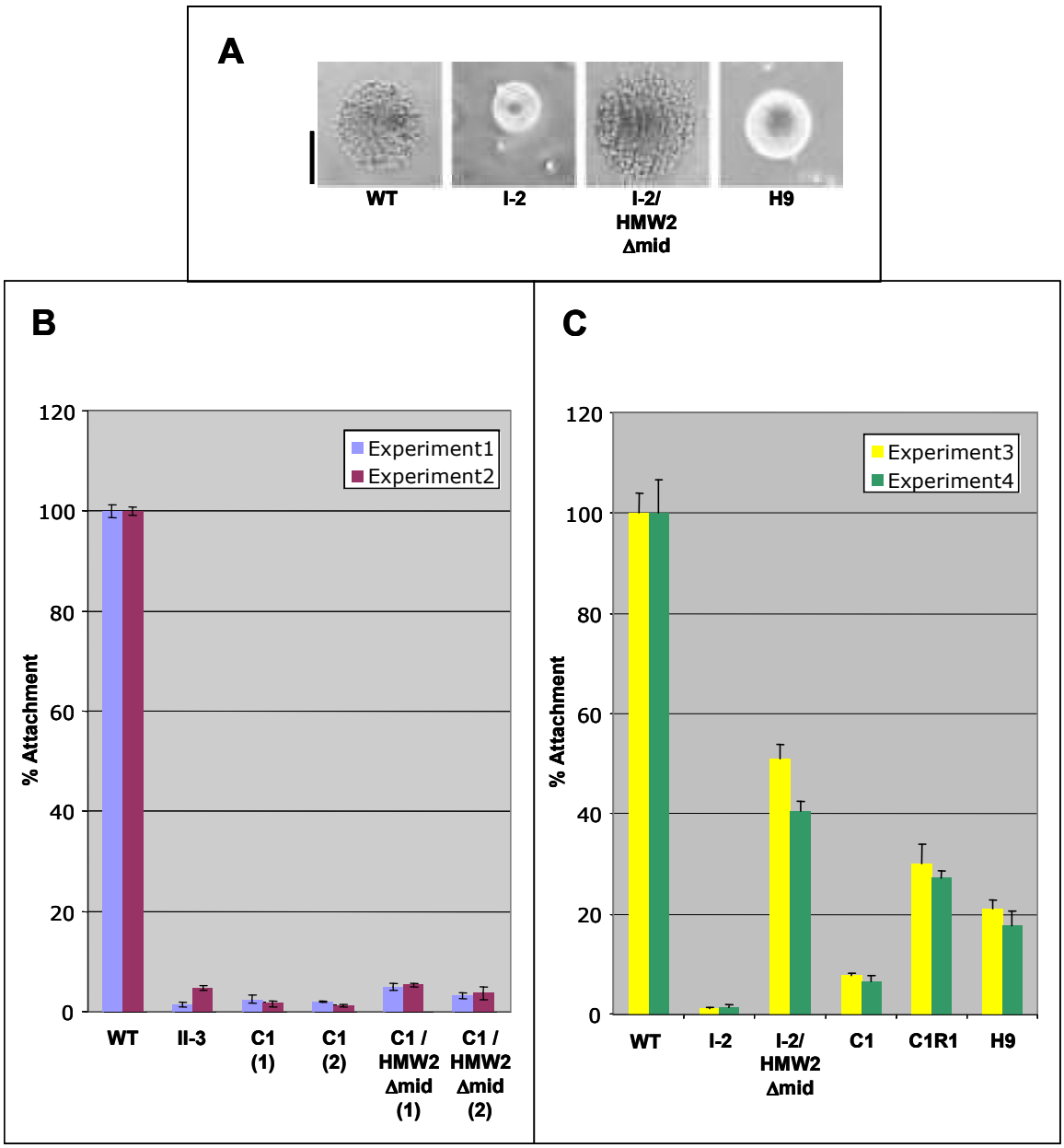
A
WT
I-2
I-2/ HMW2 Δmid
H9
B
% Attachment
120
100
80
60
40
20
0
Experiment1
Experiment2
WT
II-3
C1 (1)
C1 (2)
C1 / HMW2 Δmid (1)
C1 / HMW2 Δmid (2)
C
% Attachment
120
100
80
60
40
20
0
Experiment3
Experiment4
WT
I-2
I-2/ HMW2 Δmid
C1
C1R1
H9

Figure 4.7. Satellite growth analysis of wild-type (WT) and HMW2 derivative strains. Images were taken at the specified hours after inoculation of SP4 medium containing 3% gelatin and incubation at 37°C. Scale bar, 15μm.

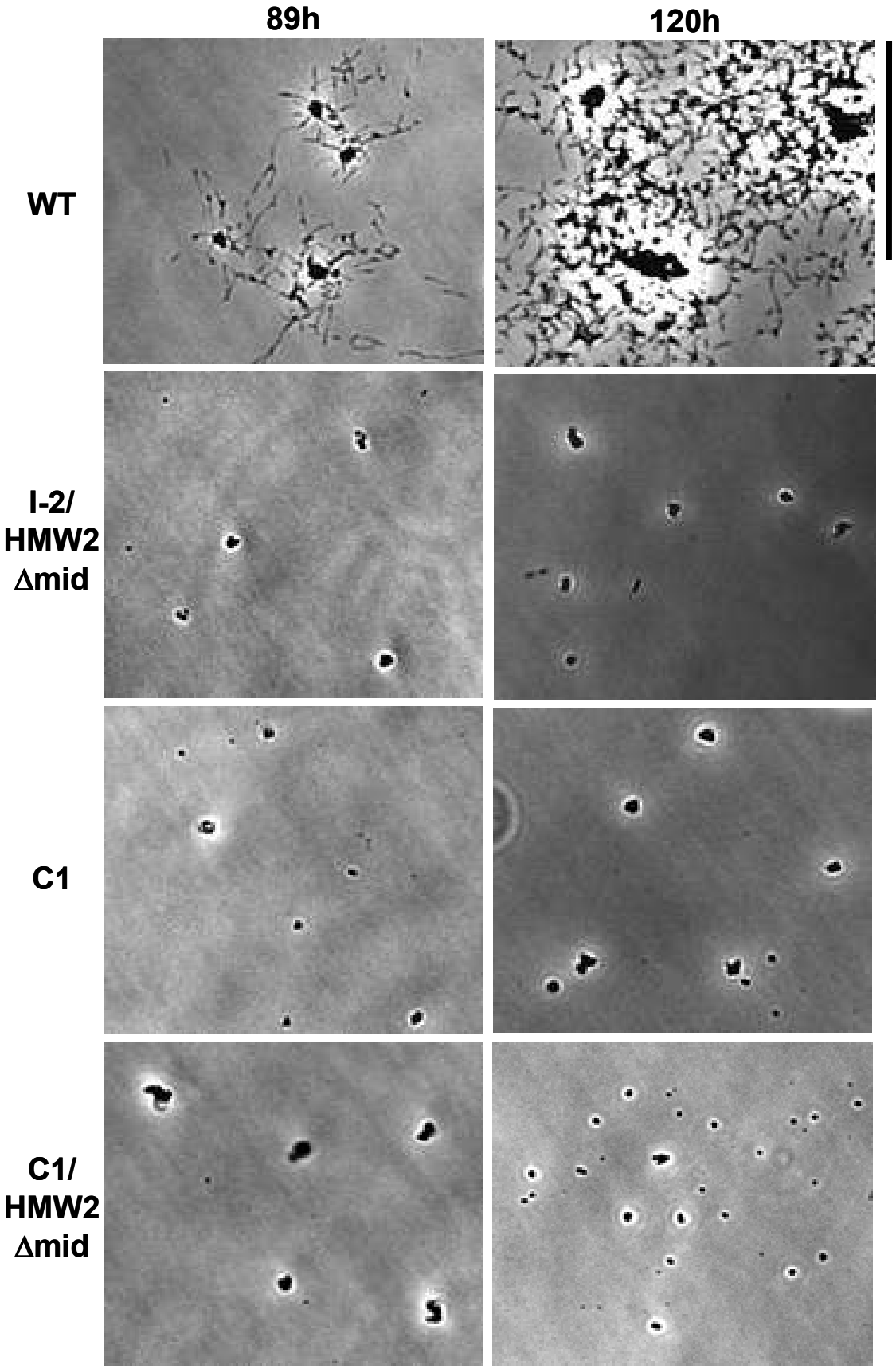
89h
120h
WT
I-2/
HMW2
Δmid
C1
C1/
HMW2
Δmid

(Fig. 4.7). In contrast, C1 colonies exhibited no satellite growth (Fig. 4.7) and HMW2Δmid failed to restore normal satellite growth (Fig. 4.7). Normal satellite growth was also not apparent in I-2/HMW2Δmid. C1R1 was tested in a motility study (Hasselbring and Krause, unpublished data) and shown to exhibit wild-type movement.

Finally, cell morphology is also altered when certain regions of HMW2 are absent. For example, the cell morphology of mutants I-2 and H9 is aberrant in SEM micrographs (Fig. 4.8), lacking the typical slender cell appearance and tapering at one end that is characteristic of wild-type (Fig. 4.8). Interestingly, although some phenotypic traits of I-2/HMW2Δmid are not wild-type, such as stabilization of HMW1, cytadherence, and localization of P1, these cells have a wild-type cell morphology with slender tapered cells. Based on the otherwise mutant phenotype of this strain, this wild-type morphology is probably not due to reversion. Thus, the requirements of specific regions of HMW2 to restore normal cytadherence and morphology are distinct from those required for HMW1 stabilization, P1 localization, and gliding motility. Table 4.2 summarizes the results of this functional analysis.

Transmission electron microscopy (TEM) analysis of HMW1 and HMW2 structure and function in core formation. Previous studies indicate that the loss of HMW1 in mutant M6, or HMW2 in mutant I-2, results in failure to assemble a stable core (Seto and Miyata, 2003). Introduction of the corresponding recombinant wild-type alleles restores a wild-type phenotype (Fisseha et al., 1999, Popham et al., 1997) and allows for normal core formation (data not shown). Lack of a normal core in the absence of HMW1 and HMW2, along with the similarity between the predicted length of HMW2 and the actual length of the core (Balish *et al.*, 2003b), led to a model proposing

Figure 4.8. Scanning electron micrographs (SEMs) of wild-type (WT) and HMW2 derivative strains. The strain is listed on each image. Scale bar, 2μm; From Balish et al., 2003b.

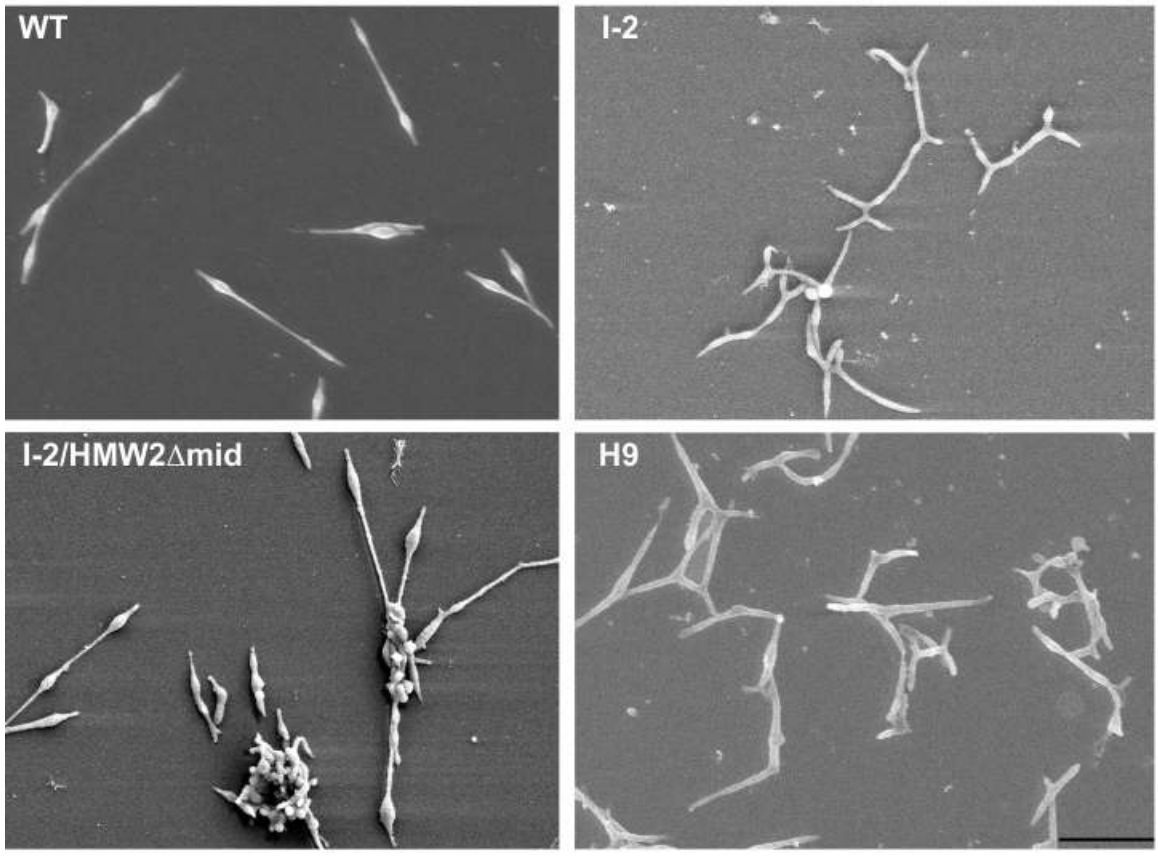
WT
I-2
I-2/HMW2Δmid
H9

Table 4.2. Summary of functional analysis. nt, not tested.

Strain	TX Partition of HMW2	P1 Localization	HA	Gliding Motility	Cell Morphology
WT	95% insoluble, 5% soluble	localized	positive	++++	normal
I-2	n/a	scattered foci	negative	+/-	aberrant
I-2/ HMW2Δmid	100% insoluble	scattered foci	intermediate	-	wild-type-like
H9	50% insoluble, 50% soluble	scattered foci	negative	nt	aberrant
C1	nt	nt	negative	-	nt
C1/ HMW2Δmid	nt	nt	negative	-	nt
C1R1	nt	nt	intermediate	++++	nt

that predicted dimeric and trimeric interactions of HMW2 and P28 promote bundling of these proteins to comprise the core. Based on that model, the length of HMW2 and the core would be directly proportional, and one would predict that strains producing a shorter HMW2 would therefore form shorter cores.

We tested this prediction by examining strains producing truncated HMW2 derivatives. Truncation of HMW2 at the C-terminus results in altered cell morphology, motility, and HA (Balish *et al.*, 2003a). Based on this, and the lack of a core in mutant I-2, we hypothesized that the C-terminus of HMW2 might also be essential for core formation. We also examined thin sections of the H9 and C1*Tn*4001 insertion mutants, which produce a stable, truncated HMW2 protein (~130kDa) or low levels of truncated HMW2 protein (~185kDa), respectively, in each case lacking the C-terminus. No cores were apparent in either of these strains, consistent with a potential requirement for the C-terminus in core formation (Fig. 4.9). Additional evidence for a requirement of the C-terminus of HMW2 was shown after examination of C1R1. Normal, wild-type-like cores were apparent in this strain, which contains the C-terminus of HMW2, but does not produce P28 (Fig. 4.9). We expected core formation to occur in I-2 transformed with the HMW2Δmid construct, which lacks 80% of the internal portion of HMW2, but produces a 38-kDa HMW2 deletion derivative with an intact C-terminus. Indeed, wild-type-like cores were apparent, albeit much less frequently than in wild-type (Fig. 4.9). Because of the high rate of reversion in this strain, we reasoned that the rare cores observed were probably due to a revertant population. Thus, we also examined C1 transformed with HMW2Δmid for the presence of cores because C1 was much less likely to revert than I-2. However, introduction of HMW2Δmid into C1 did not restore its ability to form

Figure 4.9. TEM analysis of thin sections of wild-type (WT), HMW2 derivative strains, and HMW1 derivative strains on formvar-coated, carbon-coated nickel grids. Strains are noted above or below each image; arrows indicate cores. Scale bar, 250nm.

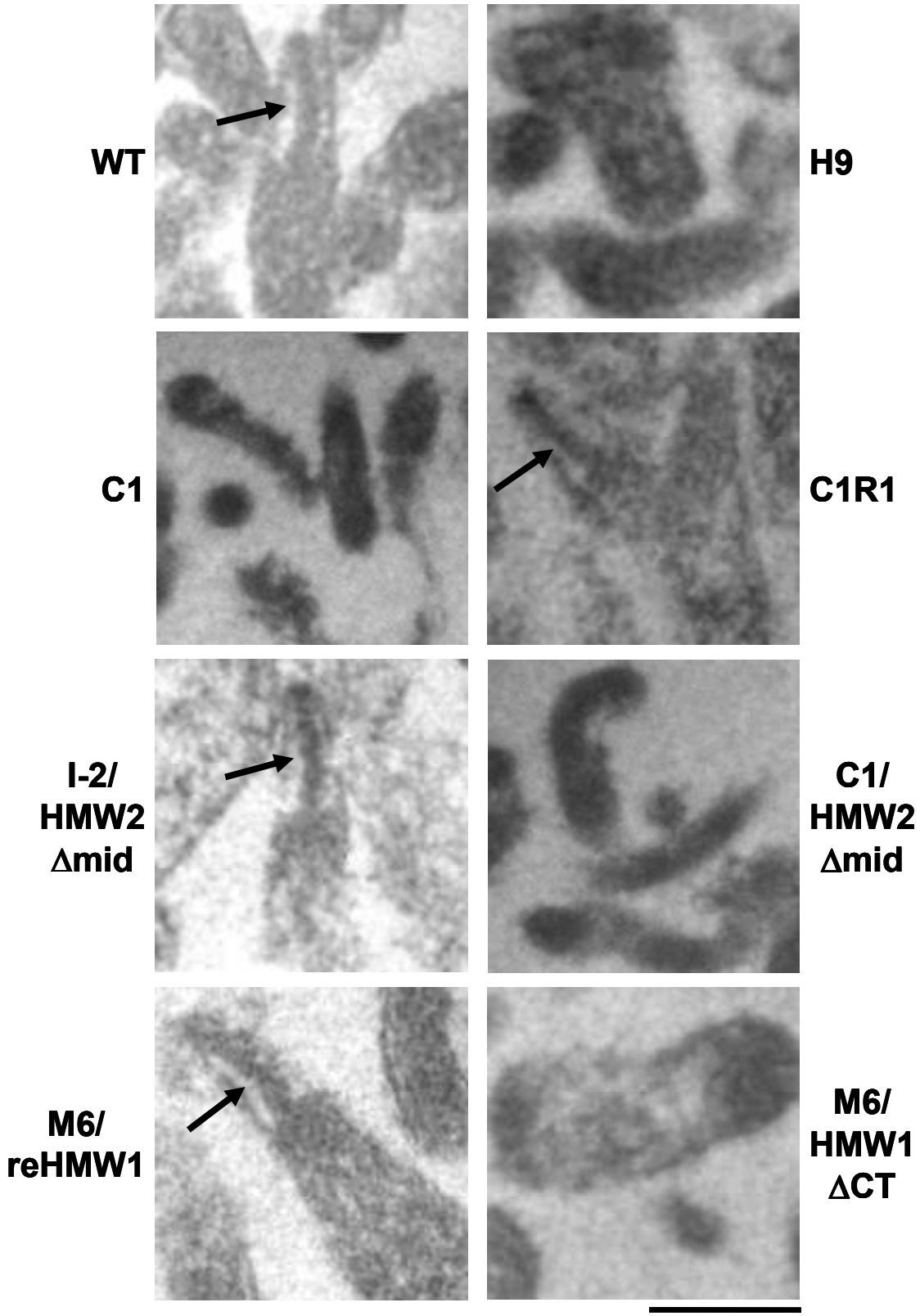
WT
H9
C1
C1R1
I-2/
HMW2
Δmid
C1/
HMW2
Δmid
M6/
reHMW1
M6/
HMW1
ΔCT

cores either (Fig. 4.9). Taken together, these data suggest that the C-terminus of HMW2 may be necessary but not sufficient for core formation. Comparison of wild-type HMW2 with HMW2 derivatives identified one predicted trimeric coiled-coil (Fig. 5.1), which is absent in truncated HMW2 derivative strains that do not form cores and present in strains that do. Thus, this region may contribute to their function, which may include maintaining spatial positioning of the protein or direct interactions with other proteins to form the core.

The M6 mutant lacks HMW1 and is also unable to form stable cores (Seto and Miyata, 2003). While recombinant full-length HMW1 restored core formation in M6 (Fig. 4.9), a recombinant HMW1 derivative truncated at the C-terminus (HMW1ΔCT) (Willby *et al.*, 2004) did not (Fig. 4.9), indicating that the C-terminus of HMW1 is essential for normal core formation, as well.

Because ultrastructural analysis of thin sections can be affected by the cut angle of the section, we also examined by TEM the appearance of cores in TX-extracted preparations. This examination of cores by TEM analysis of TX fractions has allowed for a more detailed view with visible segmented regions or striations on the core that were not visible in thin sections. Although the core has been shown actually to consist of a larger rod and a smaller rod by electron cryotomography (Henderson and Jensen, 2006), only occasionally were two rods visible in our studies, where we primarily saw a single segmented rod. The presence of two rods and striations here was consistent with observations noted in the electron cryotomography study, which mapped out the structural components within the attachment organelle (Henderson and Jensen, 2006). Also, consistent with that study and ultrastructural studies by Hegermann et al.

(Hegermann *et al.*, 2002), we occasionally saw a wheel-like (or bowl complex) structure at the proximal end of the core and a terminal button structure at the distal end. We were unable to see two additional segments of the core that were not segmented, as well as a region that connects the bowl complex to the core and the two distinct nodules of the terminal button, as described by Henderson and Jensen (Henderson and Jensen, 2006). In our studies, spokes or extensions outward from the core were apparent that were not visible in the electron cryotomography studies. Thus, our observations and measurements here were based on the regions of the core that were apparent in our analysis.

Wild-type cells extracted with TX yielded electron-dense cores, 271.75nm ± 21.59 (n=30) in length, with characteristic periodicity, as previously seen (Biberfeld and Biberfeld, 1970; Powell *et al.*, 1976) (Fig. 4.10, 4.11). In agreement with our thin section analysis, no cores were visible in the H9 TX fractions examined. In contrast, where no cores were apparent in C1 thin sections, surprisingly, cores that appeared to be falling apart were visible in the C1 TX fractions. Thus, a region including two predicted dimeric coiled-coils, three leucine repeats and a cysteine residue present in the HMW2 derivative in C1 but not H9 may also be required for core formation, in addition to the C-terminus and one predicted trimeric coiled-coil from our previous hypothesis. C1R1, which contains all of these specific regions, forms a normal core in appearance. However, when measured, its cores were 217.77nm ± 26.58 (n=26) or approximately 20% shorter than wild-type (Fig. 4.10, 4.11; p-value of 8.72×10^{-11}). Because C1R1 does not produce P28 and is also missing a second predicted trimeric coiled-coil region, which was deleted along with the amino acid corresponding to the translational start site

Figure 4.10. TEM analysis of Triton X-100-insoluble fractions of wild-type (WT), HMW2 derivative strains, and HMW1 derivative strains. Scale bar, 250nm. (A) Wild-type. (B) HMW2 and HMW1 derivative strains.

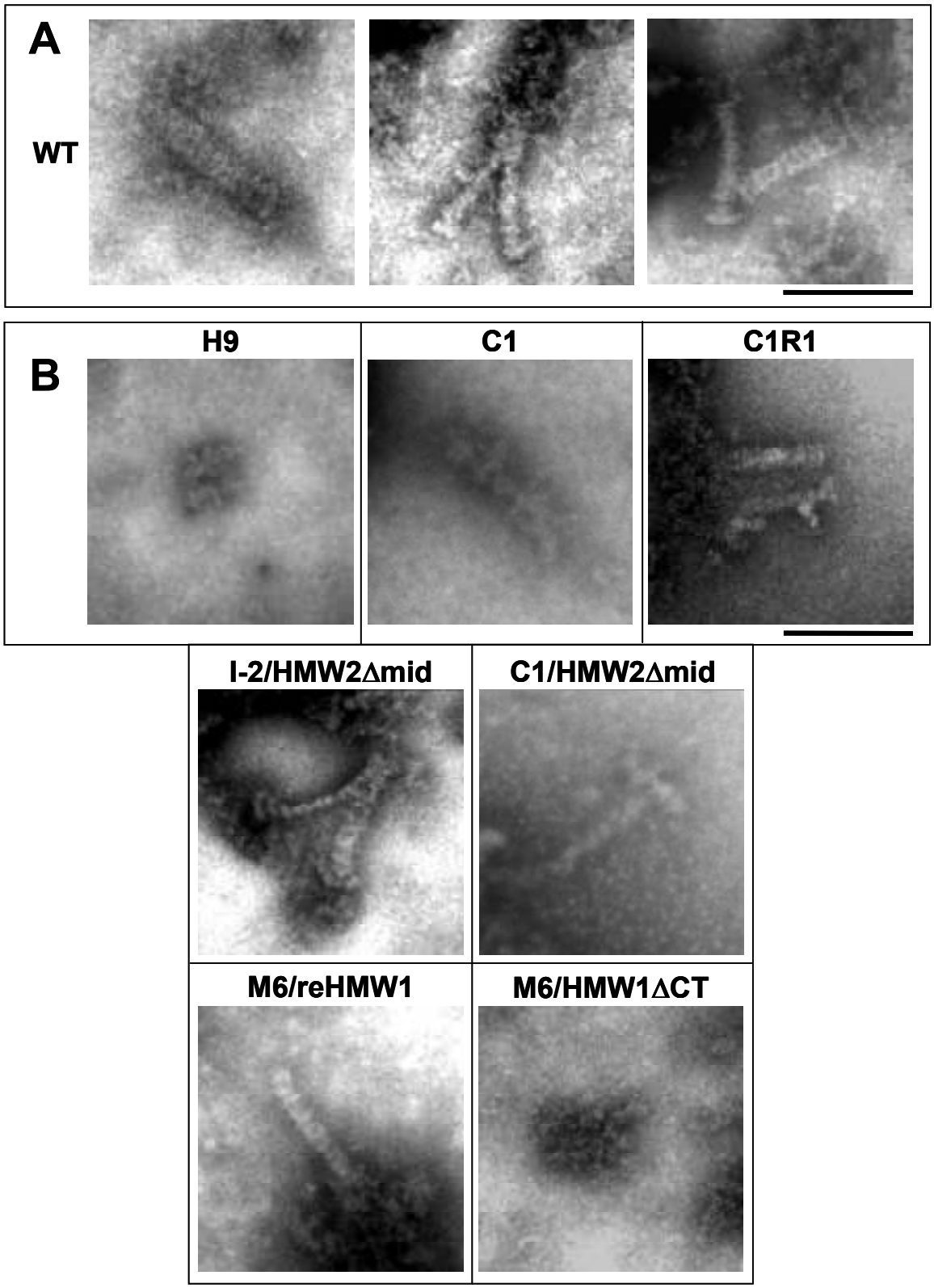
A
WT
B
H9
C1
C1R1
I-2/HMW2Δmid
C1/HMW2Δmid
M6/reHMW1
M6/HMW1ΔCT

Figure 4.11. Comparison of core lengths. TEM analysis of wild-type (WT) and C1R1 cores. Scale bar, 250nm.

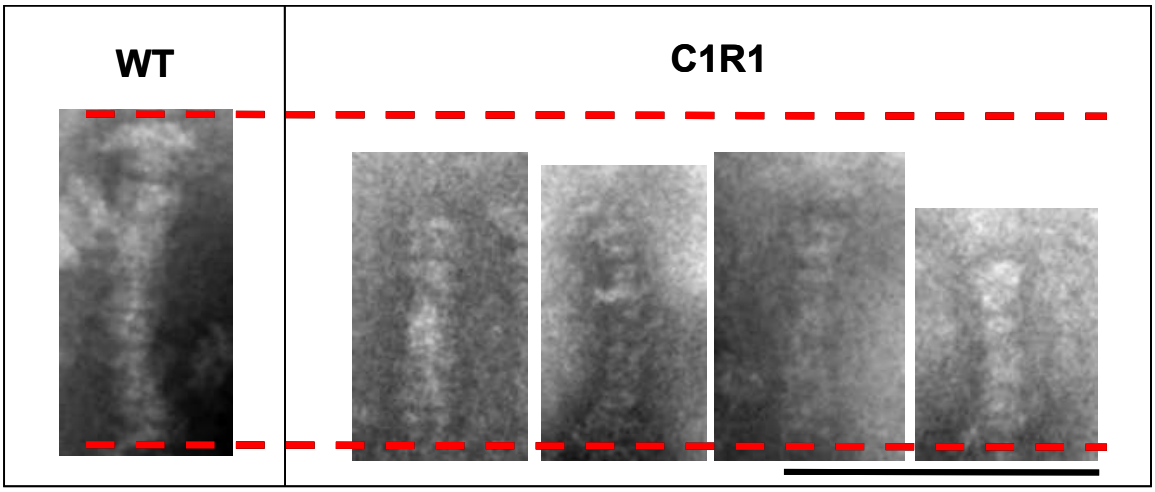
WT
C1R1

for P28, these regions of HMW2 are not required for core formation but may influence the length of the core. The HMW2∆mid construct transformed into mutant I-2 does not allow for core formation, despite occasional cores that are apparently due to a revertant population. Likewise, C1/HMW2∆mid did not stabilize the fragmented core structure observed here, suggesting that all of these specific regions must be contiguous for stabilization of the core to occur. We were unable to measure the length of the core in C1/HMW2∆mid because it was difficult to determine consistently the exact margins of the core material. Analysis of Triton fractions of M6/HMW1∆CT confirmed the absence of a stable core in this mutant lacking the C-terminus of HMW1 (Fig. 4.10). M6/reHMW1 (Fig 4.10) restored formation of normal cores, like wild-type in length.

Localization of HMW2 in thin sections of *M. pneumoniae*. Previous attempts to localize HMW2 using specific antisera have failed to yield consistent results (D. Krause, unpublished data), probably due to epitope inaccessibility rather than lack of immunogenicity because strong reactivity of these antisera with HMW2 is observed by Western immunoblotting. This necessitated analysis with an HMW2-GFP sandwich fusion (Balish *et al.*, 2003b). This fusion localized to the attachment organelle (Balish *et al.*, 2003b), but the limits of resolution by fluorescence microscopy make it difficult to establish the precise location relative to the core. In the current study, antisera directed against either the N-terminus or the C-terminus of HMW2 were affinity-purified as described previously (Stevens and Krause, 1992). Immunoblots using the affinity-purified N-terminus-specific antibody identified a band corresponding to full-length HMW2 (216-kDa) in wild-type *M. pneumoniae,* and a less intense band at approximately 117-kDa, corresponding to the truncated HMW2 in the I-2 mutant strain (Fig. 4.12A), as

Figure 4.12. Immunoblot analysis of the specificity of HMW2 antiserum. (A) Affinity-purified N-terminal HMW2 antibodies used at 1:20 dilution. Arrow, truncated HMW2 in mutant I-2. (B) Affinity-purified C-terminal HMW2 antibodies used at 1:20 dilution.

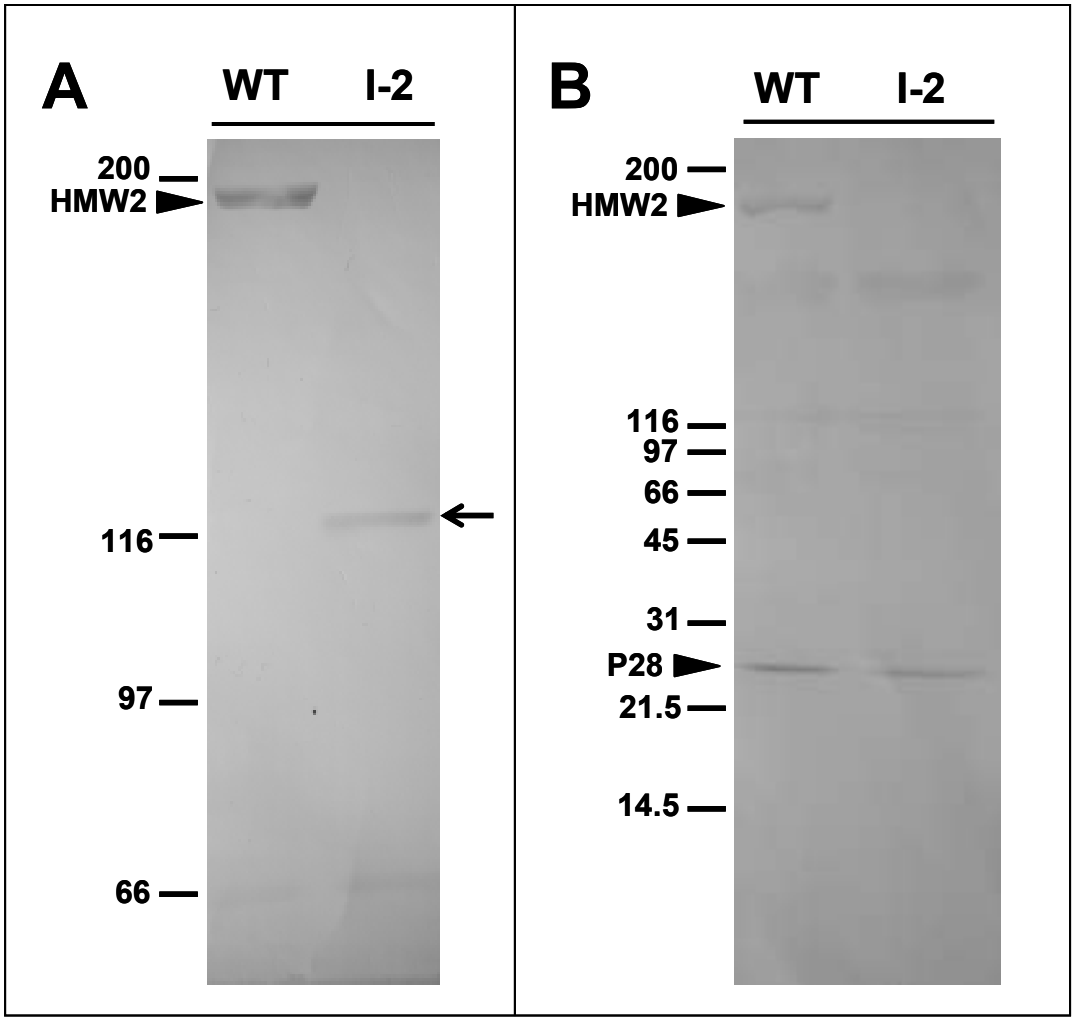
A
WT
I-2
200
HMW2
116
97
66
B
WT
I-2
200
HMW2
116
97
66
45
31
P28
21.5
14.5

in previous reports (Fisseha *et al.*, 1999). The C-terminus-specific antibody at a 1:1000 dilution identified bands corresponding to full-length HMW2 and P28 in wild-type *M. pneumoniae* (Fig. 4.12B). A band for P28 was present at reduced levels in mutant I-2, in agreement with previous data (Fig. 4.12B) (Fisseha *et al.*, 1999).

Using affinity-purified HMW2-specific antibodies, we examined HMW2 localization in thin sections of *M. pneumoniae* cells. Immunogold labeling appeared to require a specific cut angle for the exposure of HMW2 epitopes to allow for antibody binding. Furthermore, antibody titers were low based on the band intensities in immunoblots, contributing to poor signal relative to background. For both N-terminus- and C-terminus-specific HMW2 antisera, wild-type sections were only labeled with one or two gold particles and in an inconsistent pattern. Some gold labeling was also observed on sections where cores were not visible (data not shown). Similar results were obtained with thin sections of C1R1 using only the C-terminal HMW2 antibody (data not shown). As a negative control, we immunogold labeled the *Tn*4001 insertion mutant C1 and found that the non-specific labeling was similar to that for core-forming strains for both antibodies (data not shown). Multiple attempts at labeling sections using various antibody dilutions and smaller gold particles (5nm in diameter) were inconclusive. Inconsistencies in HMW2 immunolocalization were similar to difficulties seen previously (Balish *et al.*, 2003b). In order to overcome possible epitope inaccessibility issues, we examined HMW2 localization in TX-fractionated *M. pneumoniae* preparations.

Localization of HMW2 to the periphery of the electron-dense core in TX-extracted cells. Using affinity-purified antibodies specific for HMW2 we examined

HMW2 localization in TX-extracted cells. Immunogold labeling was localized to the periphery of the electron-dense core with the N-terminal antibody for wild-type *M. pneumoniae* (Fig. 4.13A), as well as for C1R1 (Fig. 4.13A). We quantitated the location of the gold based on its distance from the core; 39 wild-type cores were examined for which 64.3% of the gold particles localized adjacent to but distinct from the core (up to 52 nm; Table 4.3 and Materials and Methods). Only 2.9% of the gold particles were localized 52-150 nm from the edge of the core and were considered to have no association with the core (Table 4.3). The remaining 32.9% were found directly on the edge of the core or on the core itself (Table 4.3). TEM analysis of TX-extracted cores yielded only a 2-dimensional view and therefore did not distinguish labeling extended outward from the plane of the core. Similar data were collected for C1R1, where 34 cores were examined, with 82.4% of gold particles localizing along the core within 52 nm of the edge, 12.1% directly on the core or its edge, and 5.5% between 52 and 150 nm (Table 4.3). As our negative control, we examined immunogold-labeled *Tn*4001 insertion mutant C1 TX fractions, in which only small amounts of HMW2 are present (Krause *et al.*, 1997) and fragmented cores are visible. Using affinity-purified antibodies specific for the N-terminus of HMW2, only a few gold particles were observed for these fractions, as expected, and allowed for determination of background levels of labeling (Fig 4.13A). Because no clear core boundaries could be distinguished in this strain, no measurements were obtained.

The same analysis was performed on fractions immunogold-labeled using affinity-purified antibodies specific for the C-terminus of HMW2. As with the antibodies specific for the N-terminus of HMW2, we found that immunogold labeling was also

Figure 4.13. Immunolocalization of the N- and C-terminus of HMW2 on TX fractions of wild-type (WT) and HMW2 derivative strains. (A) Labeling using affinity-purified N-terminal HMW2 antibodies at 1:5 dilution. (B) Labeling using affinity-purified C-terminal HMW2 antibodies at 1:15 dilution. Scale bar, 250 nm.

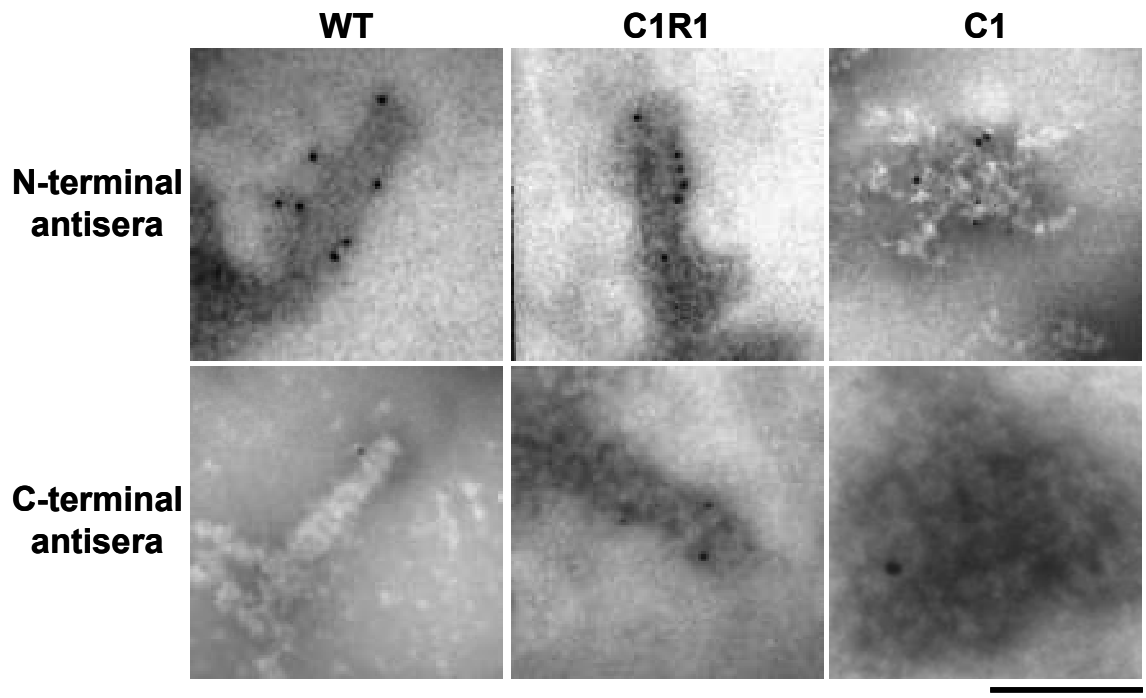
WT
C1R1
C1
N-terminal antisera
C-terminal antisera

Table 4.3. Quantitation of the localization pattern of the N- and C-termini of HMW2 on immunogold-labeled TX fractions.

M. pneumoniae Strain	Antibody	No. of cores	No. of gold particles	Avg. no. of gold particles per core	% on core, incl. on edge	% within 52nm from core	% over 52nm from core
WT	N-terminal HMW2	39	206	5.3	32.9	64.3	2.9
C1R1	N-terminal HMW2	34	165	4.9	12.1	82.4	5.5
WT	C-terminal HMW2	43	71	1.7	14.1	83.1	2.8
C1R1	C-terminal HMW2	38	71	1.9	5.6	90.1	4.2

* Due to rounding, numbers in the last three columns do not equal 100%.

localized to the periphery of the core for wild-type *M. pneumoniae* (Fig. 4.13B), as well as for C1R1 (Fig. 4.13B). Thus, 43 wild-type cores were examined, for which 83.1% of the gold particles extended out from the core up to 52 nm (Table 4.3 and Materials and Methods). Only 2.8% of the gold particles were localized 52-150 nm from the edge of the core and were considered to have no association with the core (Table 4.3). The remaining 14.1% were found to be directly on the edge of the core or on the core surface (Table 4.3). Similarly, for C1R1, 38 cores were examined, with 90.1% of gold particles localizing along the core within 52 nm, 5.6% directly on the core or edge, and 4.2% between 52 and 150 nm (Table 4.3). The negative control C1 had a few gold particles scattered on its TX-insoluble preparation (Fig. 4.13b). This was considered background labeling, as the C-terminus of HMW2 is not present, and enabled us to make more definite conclusions about the localization of HMW2.

We concluded, based on our view of the core and our localization studies, that HMW2 does not appear to be part of the core itself as it is seen in these preparations, but is perhaps peripherally associated. Although no measurements were made of the location of each gold particle along the length of the core, no pattern for localization was evident in that dimension, with gold particles being distributed all along the core, lengthwise. Thus, we were not able to indicate a preference for the positioning of the N- or C-terminus of HMW2 toward the proximal or distal end of the core. Furthermore, neither the length of HMW2 nor the loss of P28 had an effect on this localization, as seen in C1R1 with its HMW2 derivative localizing similarly to full-length HMW2 in wild-type.

Identification of the Components of the Core-Enriched Fraction

Chemical extraction of the TX-insoluble fraction. Removal of the membrane by extraction with TX was based on treatments used to isolate the cytoskeleton in eukaryotic cells, where TX detergent was used in combination with salts (Herrmann and Wiche, 1983; Starger and Goldman, 1977; Steinert *et al.*, 1978). Thus, these treatments were used as a starting point to isolate the bacterial cytoskeleton of *M. pneumoniae*, which is readily visible when whole cells are extracted with TX (Gobel *et al.*, 1981; Meng and Pfister, 1980; Stevens and Krause, 1991). Removal of the membrane reveals the electron-dense core and insoluble membrane material as components of the insoluble fraction. Mass spectrometry studies identified 40 proteins as part of this TX-insoluble fraction (Regula *et al.*, 2001), representing the first attempt to catalog proteins essential for the formation of this backbone of the cell. Proteins specific to the membrane or the core itself were not assigned. There have been no subsequent attempts to redefine the cytoskeleton or to assign specific proteins as part of the electron-dense core, although predictions concerning the components of the core have been made based upon immunolocalization data and ultrastructural analysis of cytadherence mutants (Balish *et al.*, 2003b; Regula *et al.*, 2001; Seto and Miyata, 2003). Thus, in order to identify the specific components of the core, it was necessary to explore means to extract non-core components of the TX-insoluble fraction without disrupting the core.

TEM images of the TX-insoluble fraction suggest that membrane-associated material remains in the TX-insoluble fraction. *M. pneumoniae* has cholesterol in its membrane to provide support and rigidity to the cells in the absence of a cell wall. This

extra stability of the cell membrane could explain why the membrane-associated material is not completely removed after a single treatment with 2% TX. Gobel et al. (Gobel *et al.*, 1981) treated TX-insoluble fractions with 0.6 M KCl, which resulted in the core remaining intact and removal of most of the membrane- or cytoplasmic-associated material, except for filaments attached to the core. With treatment with 0.6 M KI, the associated membrane material was removed, and the structure of the core was destabilized such that only partial cores were apparent (Gobel *et al.*, 1981). Specific proteins essential for maintaining a stable attachment organelle were revealed in subsequent studies by SDS-PAGE and silver staining, where certain proteins in the TX-insoluble fraction were partially solubilized when treated with 0.6 M KI and 1.8 M KI (Stevens and Krause, 1992). Electron micrograph images indicated that the electron-dense core appeared disorganized with the removal of the terminal button from some cores following 0.6 M KI treatment but was completely destabilized following 1.8 M KI treatment, where intact cores were not apparent (Stevens and Krause, 1992). Based on these previous observations, we chose various treatments of detergents and salts to attempt to purify further the electron-dense core of *M. pneumoniae* cells. SDS-PAGE and silver stain analysis were used to examine and compare the protein profiles after each treatment. Our analysis of each treatment was based on the removal or decrease in levels of protein bands in the profile (Table 4.4), such that we identified the treatment(s) that gave us the simplest protein profile with the core still remaining intact. Initially, we treated wild-type cells with a single detergent, salt, or a combination of the two. As expected, we found that some treatments removed more protein bands than others. Among some of the first treatments were 4% sodium deoxycholate, 2% TX

Table 4.4. Summary of treatments tested by SDS-PAGE and silver stain analysis for use in enrichment of the electron-dense core of *M. pneumoniae*. n/a, no treatment was performed; TX, Triton X-100; Gdn-HCl, Guanidine-HCl; Deoxychol., sodium deoxycholate; sucr, sucrose; slash (/) between the treatment names, both treatments were combined into one treatment. The relative extraction column indicates the amount of protein removed from the insoluble fraction following the final treatment relative to 2% TX only, as denoted by ++++, +++, ++, +, +/-, and -, where ++++ indicates a large number of proteins were removed and – indicates no proteins or only a very small number were removed.

1st Treatment	2nd Treatment	3rd Treatment	Sonication	Relative Extraction
2% TX	n/a	n/a	-	+++
2% TX with Rifampin (50 ug/ml)	n/a	n/a	-	+++
2% TX/0.6 M KCl	n/a	n/a	-	+++
2% TX/0.6 M KCl	n/a	n/a	-	+++
2% TX/0.6 M KCl	2% TX/0.6 M KCl	n/a	-	+
2% TX/0.6 M KCl	2% TX/0.6 M KCl	2% TX/0.6 M KCl	-	-
2% TX/0.6 M KCl	2% TX/0.6 M KCl	2% TX/1.8 M KCl	-	+
2% TX/0.6 M KCl	2% TX/1.8 M KCl	1 M Gdn-HCl	-	-
2% TX/0.6 M KCl	2% TX/1.8 M KCl	1 M Gdn-HCl	+	-
2% TX/0.6 M KCl	2% TX/1.8 M KCl	1% Deoxychol.	-	-
2% TX/0.6 M KCl	2% TX/1.8 M KCl	1% Deoxychol.	+	-
2% TX/0.6 M KCl	2% TX/1.8 M KCl	500 mM Gdn-HCl	-	-
2% TX/0.6 M KCl	2% TX/1.8 M KCl	500 mM Gdn-HCl	+	-
2% TX/0.6 M KCl	2% TX/1.8 M KCl	1% CHAPS	-	-
2% TX/0.6 M KCl	2% TX/1.8 M KCl	1% CHAPS	+	-
2% TX/0.6 M KCl	2% TX/1.8 M KCl	2% CHAPS	-	-
2% TX/0.6 M KCl	2% TX/1.8 M KCl	2% CHAPS	+	-
2% TX/0.6 M KCl	2% TX/1.8 M KCl	2% Deoxychol.	-	++
2% TX/0.6 M KCl	2% TX/1.8 M KCl	2% Deoxychol.	+	++
2% TX/0.6 M KCl	1% Digitonin/4 mM MgCl2	n/a	-	+/-
2% TX/0.6 M KCl	0.6 M KI	n/a	-	-
2% TX/0.6 M KCl	1.8 M KI	n/a	-	-
2% TX/0.6 M KCl	0.6 M KI/20% sucr	n/a	-	++
2% TX/0.6 M KCl	0.6 M KI/20% sucr	1 M Gdn-HCl	-	+
2% TX/0.6 M KCl	0.6 M KI/20% sucr	1.5 M Gdn-HCl	-	+
2% TX/0.6 M KCl	0.8 M KI/20% sucr	n/a	-	-
2% TX/0.6 M KCl	1.0 M KI/20% sucr	n/a	-	+
2% TX/0.6 M KCl	1.3 M KI/20% sucr	n/a	-	+
2% TX/0.6 M KCl	1.6 M KI/20% sucr	n/a	-	++
2% TX/0.6 M KCl	1.8 M KI/20% sucr	n/a	-	+++
2% TX/0.6 M KCl	2% Deoxychol.	n/a	-	+/-
2% TX/0.6 M KCl	2% Deoxychol.	1 M Gdn-HCl	-	-
2% TX/0.6 M KCl	2% Deoxychol.	1.5 M Gdn-HCl	-	-
2% TX/0.6 M KCl	100 mM Gdn-HCl	n/a	-	-
2% TX/0.6 M KCl	1 M Gdn-HCl	n/a	-	+

1st Treatment	2nd Treatment	3rd Treatment	Sonication	Relative Extraction
2% TX/0.6 M KCl	2 M Gdn-HCl	n/a	-	+++
2% TX/0.6 M KCl	2 M Gdn-HCl/20% sucr	n/a	-	++
2% TX/0.6 M KCl	2% Deoxychol.	n/a	-	++/+
2% TX/0.6 M KCl	2 M KSCN	n/a	-	+/-
2% TX/0.6 M KCl	1 M NaCLO4	n/a	-	-
2% TX/1.8 M KCl	n/a	n/a	-	+++
2% TX/1.8 M KCl	1.8 M KCl	n/a	-	-
2% TX/1.8 M KCl	1.8 M KCl	1.8 M KCl	-	-
2% TX/DNaseI(50 ug/ml)	2% TX/0.6 M KCl	n/a	-	+/-
2% TX/DNaseI(50 ug/ml)	2% TX/0.6 M KCl	0.2 M KI	-	-
2% TX/DNaseI(50 ug/ml)	2% TX/0.6 M KCl	0.3 M KI	-	-
2% TX/DNaseI(50 ug/ml)	2% TX/0.6 M KCl	0.4 M KI	-	+
2% TX/DNaseI(50 ug/ml)	2% TX/0.6 M KCl	0.5 M KI	-	+
1% Deoxychol.	2% TX/1.8 M KCl	n/a	-	-
2% Deoxychol.	2% TX/1.8 M KCl	n/a	-	-
2% Deoxychol.	2 M KSCN	n/a	-	-
4% Deoxychol.	n/a	n/a	-	++++
2% TX/2% Deoxychol./1 M KCl	n/a	n/a	-	+++
2% TX/2% Deoxychol./1 M KCl	n/a	n/a	-	+++
2% TX/2% Deoxychol./1 M KCl	n/a	n/a	+	+++
4 M KSCN	n/a	n/a	-	+++
0.5% CHAPS	n/a	n/a	-	++
1% CHAPS	n/a	n/a	-	++
2% CHAPS	n/a	n/a	-	++
4% CHAPS	n/a	n/a	-	++
2 M Gdn-HCl	n/a	n/a	-	++
2 M Gdn-HCl/20% sucr	n/a	n/a	-	++

Figure 4.14. SDS-PAGE and silver stain analysis of the effects of various detergent and salt treatments on wild-type *M. pneumoniae* insoluble and soluble protein profiles. Each treatment is designated beneath each lane. BR, broad-range marker; I, insoluble; S, soluble fraction following centrifugation at 14,000rpm after final treatment; 2x and 3x, multiple treatments. Sizes of protein standards are indicated to left.

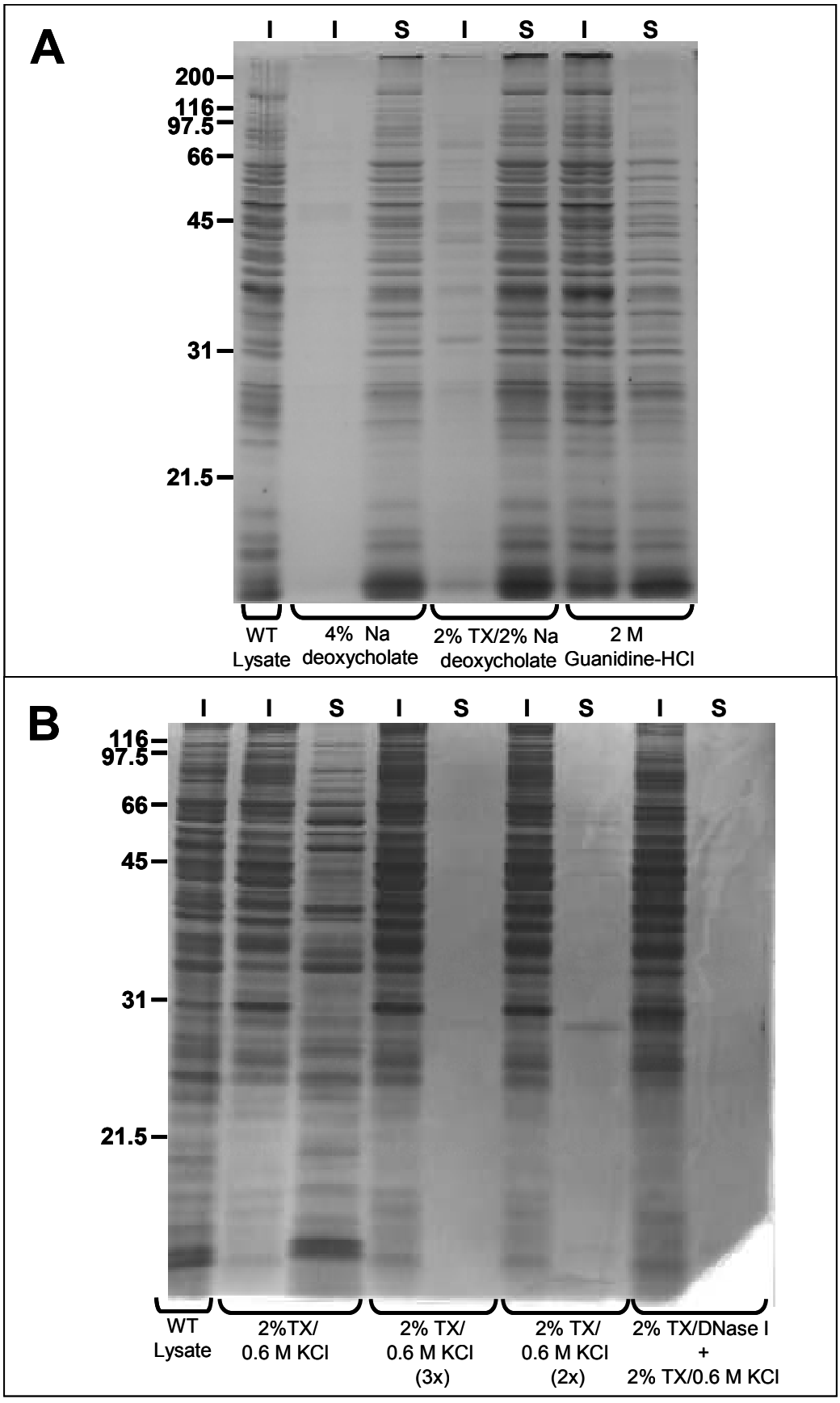
A
I I S I S I S
200
116
97.5
66
45
31
21.5
WT Lysate
4% Na deoxycholate
2% TX/2% Na deoxycholate
2 M Guanidine-HCl
B
I I S I S I S I S
116
97.5
66
45
31
21.5
WT Lysate
2%TX/ 0.6 M KCl
2% TX/ 0.6 M KCl (3x)
2% TX/ 0.6 M KCl (2x)
2% TX/DNase I + 2% TX/0.6 M KCl

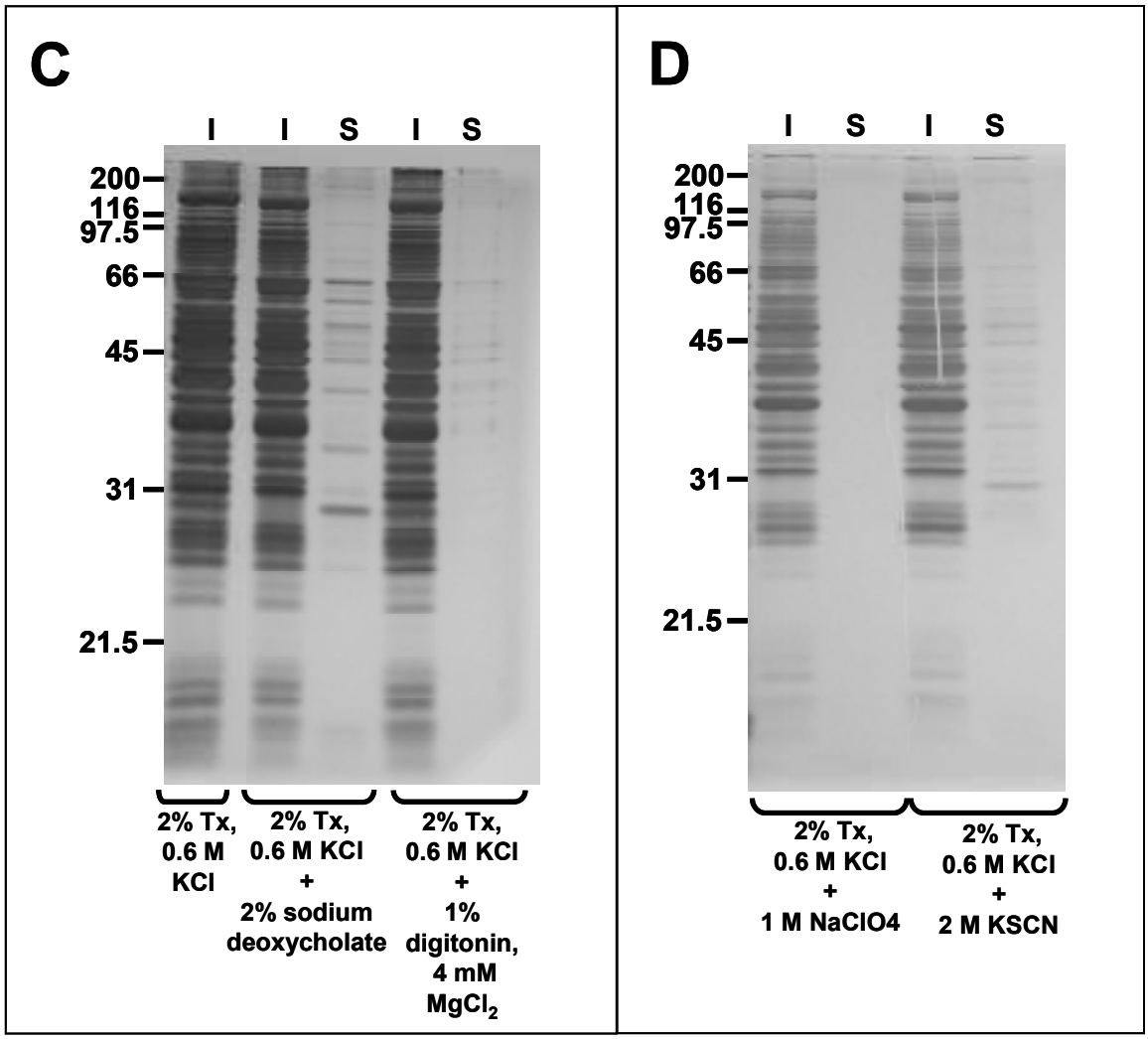
C
I I S I S
200
116
97.5
66
45
31
21.5
2% Tx, 0.6 M KCl
2% Tx, 0.6 M KCl + 2% sodium deoxycholate
2% Tx, 0.6 M KCl + 1% digitonin, 4 mM MgCl2
D
I S I S
200
116
97.5
66
45
31
21.5
2% Tx, 0.6 M KCl + 1 M NaClO4
2% Tx, 0.6 M KCl + 2 M KSCN

combined with 2% sodium deoxycholate, 2 M Guanidine-HCl (Fig. 4.14A), and 2% TX combined with 0.6 M KCl (Fig. 4.14B). We found that treatments with sodium deoxycholate, with and without 2% TX, partitioned the majority of the protein into the soluble fraction (Fig. 4.14A). The 2 M Guanidine-HCl treatment solubilized much less protein, such that most remained in the insoluble fraction (Fig. 4.14A), while the 2% TX with 0.6 M KCl appeared to partition the protein in similar quantities to both fractions (Fig. 4.14B). After testing various concentrations of sodium deoxycholate, we decided to discard this detergent as an initial treatment because it removed too many proteins and would likely solubilize the core. However, the TX and Guanidine-HCl treatments were retained.

M. gallisepticum has been shown to contain a DNA complex associated with its bleb (the equivalent to the *M. pneumoniae* attachment organelle). Thus, in attempts to remove other DNA-associated material not related to the core, we also used 2% TX with DNase I as a treatment followed by a 2% TX/0.6 M KCl treatment (Fig. 4.14B). However, minimal protein was removed from the profile, which resembled the wild-type lysate lane (Fig. 4.14B). This profile was darker than the lysate lane probably due to inherent variability in silver staining development.

After these initial tests, I chose to pursue a series of sequential treatments to purify the core to allow for a gentle removal of material associated with the core while maintaining its integrity. I chose the 2% TX/0.6 M KCl as the first treatment because, while it did not completely solubilize the sample, at least half of the total protein partitioned into the soluble fraction. Several salts and detergents that we used as a second treatment in the sequence were not strong enough to solubilize the insoluble

fraction much further. Some of our second treatments (Table 4.4) included 2% TX with 0.6 M KCl (Fig. 4.14B), 1% digitonin with 4 mM $MgCl_2$ (Fig. 4.14C), 2% sodium deoxycholate (Fig. 4.14C), 1 M sodium perchlorate ($NaClO_4$) (Fig. 4.14D), and 2 M potassium thiocyanate (KSCN) (Fig. 4.14D). Digitonin with $MgCl_2$ and sodium perchlorate removed minimal protein from the insoluble fraction (Fig. 4.14C and D, respectively). Because of the presence of cholesterol in the membrane, we thought a treatment with digitonin might remove additional membrane-associated insoluble material surrounding the core; however, this did not occur. Potassium thiocyanate and 2% TX with 0.6 M KCl removed a few protein bands (Fig. 4.14C and D, respectively) and sodium deoxycholate removed several protein bands. We tested other secondary treatments following extraction with 2% TX plus 0.6 M KCl, including 0.6 M KI with 20% sucrose. The remaining fraction could not be further solubilized by 2% TX with 0.6 M KCl as a 3rd treatment (Fig. 4.14C).

Eventually, a series of three treatments was identified that simplified the insoluble fraction in a stepwise fashion as much as possible without completely solubilizing the core. We used wild-type lysate and fractions from treatment with 2% TX only as baselines for our treatments (Fig. 4.15). The 2% TX/0.6 M KCl treatment yielded an insoluble fraction similar to that from extraction with 2%TX (Fig. 4.15). The 0.6 M KI/20% sucrose second treatment showed the same non-selective removal of proteins as 2% TX/0.6 M KCl treatment (Fig. 4.15) with an identical insoluble profile to 2% TX/0.6 M KCl with reduced band intensity (Fig. 4.15). Finally, the 1 M Guanidine-HCl treatment revealed the least intense insoluble profile (Fig. 4.15). Due to difficulties in efficient protein precipitation from the soluble fraction, protein profiles from those

Figure 4.15. SDS-PAGE and silver stain analysis of protein profiles of wild-type *M. pneumoniae* insoluble fraction following various core isolation treatments. A lysate lane was used as a control. The following treatments were used: 2% TX only, 2%TX/0.6M KCl, 0.6M KI/20%sucrose, 1M Guanidine-HCl. (A) Protein separated on a 4-8% gradient gel, (B) Protein separated on a 8-12% gradient. Red arrows indicate the prominent protein bands that remain after the final treatment.

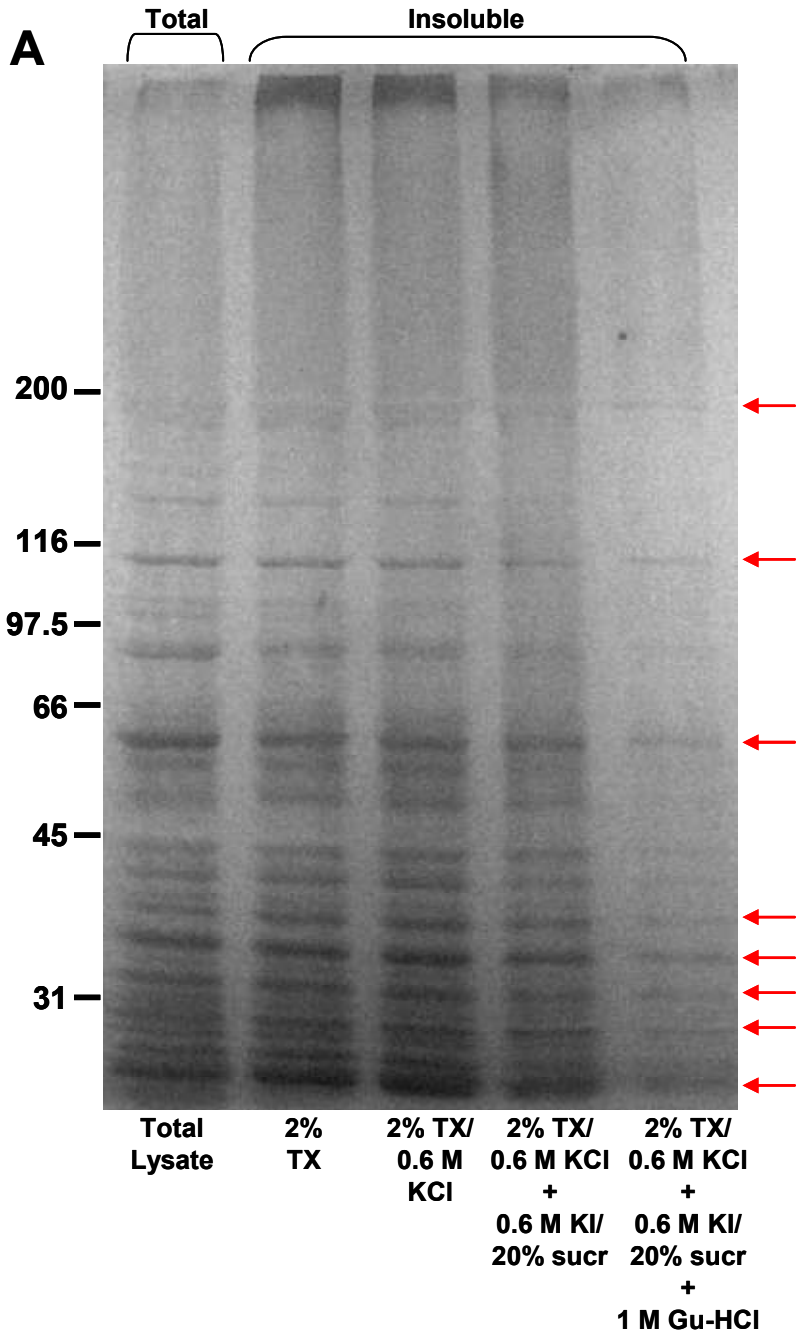
A
Total
Insoluble
200
116
97.5
66
45
31
Total Lysate
2% TX
2% TX/ 0.6 M KCl
2% TX/ 0.6 M KCl + 0.6 M KI/ 20% sucr
2% TX/ 0.6 M KCl + 0.6 M KI/ 20% sucr + 1 M Gu-HCl

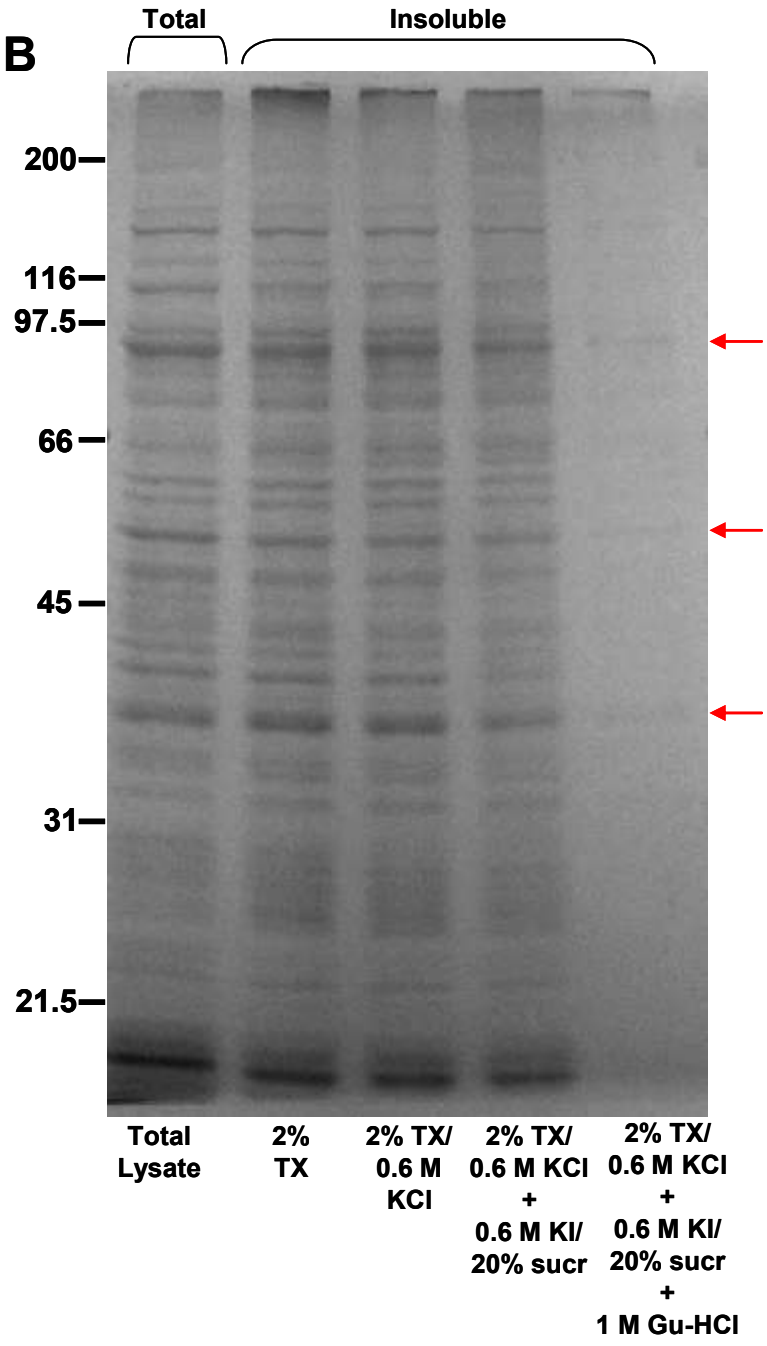
B
Total
Insoluble
200
116
97.5
66
45
31
21.5
Total Lysate
2% TX
2% TX/ 0.6 M KCl
2% TX/ 0.6 M KCl + 0.6 M KI/ 20% sucr
2% TX/ 0.6 M KCl + 0.6 M KI/ 20% sucr + 1 M Gu-HCl

HCl treatment revealed the least intense insoluble profile (Fig. 4.15). Due to difficulties in efficient protein precipitation from the soluble fraction, protein profiles from those fractions are not shown here.

Extraction with TX was previously established as a treatment to dissolve the membrane from *M. pneumoniae* whole cells. To assess the extent of membrane removal, we followed the fate of ^{3}H-palmitate, as a fatty acid marker for the membrane, in wild-type *M. pneumoniae* cells and subsequently after treatment with TX and salts. Radioactivity measurements indicated that 99.9% of the ^{3}H-palmitic acid was removed by treatment with 2% Triton/0.6 M KCl (Fig. 4.16). This removal coincided with the appearance of isolated cores on EM grids. A subsequent treatment with 0.6 M KI/20% sucrose did not appear to further remove the membrane (Fig. 4.16).

TEM analysis of extracted cores. I viewed the insoluble fractions by TEM analysis to determine if intact cores remained and were isolated. Some of the treatments that were more efficient at partitioning proteins into the soluble fraction in the SDS-PAGE analysis were used to treat wild-type cells for TEM analysis (Table 4.5). However, the primary treatments established as the potential core-enriching treatments in SDS-PAGE/silver stain analysis were the focus. Based on the [^{3}H]-palmitic acid data, the initial treatment with 2% Triton-X-100 with 0.6 M KCl in 20 mM Tris (pH 7.5)/150 mM NaCl (TN buffer) removed most of the lipids, indicating efficient membrane removal. In addition, the chaotropic effects of KCl have been shown to aid in membrane removal without disrupting the core (Stevens and Krause, 1992). Thus, it was not surprising that TX combined with KCl allowed for efficient isolation of the core as shown by TEM analysis (Fig. 4.17B). The cores appeared to be intact and complete with a terminal

Figure 4.16. Graphical representation of fatty acid removal following core isolation treatments. [^{3}H]-palmitic acid was used as a marker for the membrane. Following incorporation of ^{3}H-palmitic acid, the cells were treated with various core isolation detergents and salts. Initial counts measured were the baseline for the amount of [^{3}H]-palmitic acid associated with intact cells on the coverslips. The radioactivity associated with the soluble fraction from each treatment and subsequent PBS washes were combined and are indicated as the total solubilized material. The fractions that remained attached to the coverslip are indicated as insoluble.

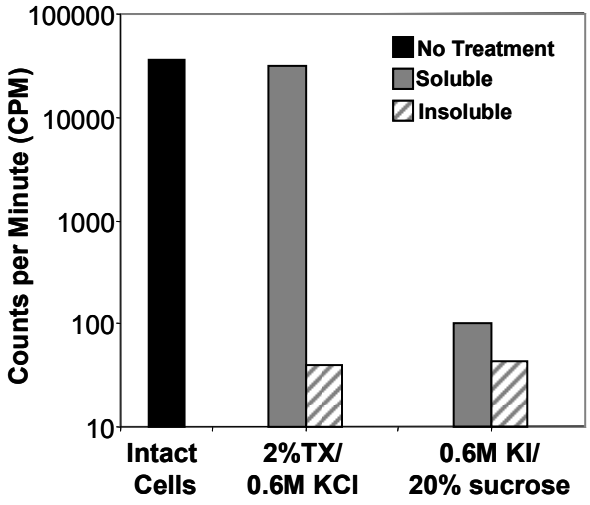
100000
10000
1000
100
10
Counts per Minute (CPM)
No Treatment
Soluble
Insoluble
Intact Cells
2%TX/ 0.6M KCl
0.6M KI/ 20% sucrose

Table 4.5. Summary of treatments tested by TEM analysis for use in enrichment of electron-dense core within cell fractions of *M. pneumoniae*. N/a, no treatment was performed; TX, Triton X-100; Gdn-HCl, Guanidine-HCl; Deoxychol., sodium deoxycholate; sucr, sucrose; slash (/) between the treatment names, both treatments were combined into one treatment. The purity column indicates the amount of residual material appearing to remain associated with the cores following the last treatment indicated, denoted by ++++, +++, ++, +, and -, where ++++ indicates the presence of the most residual material and – indicates the absence of residual material.

Treatment 1	Treatment 2	Treatment 3	Cores	Purity
2% TX	0.6 M KI	n/a	yes	+++
2% TX	1.8 M KI	n/a	no	n/a
2% TX/DNaseI (50 ug/ml)	2% TX/0.6 M KCl	n/a	yes	-
2% TX/0.6 M KCl	n/a	n/a	yes	++
2% TX/0.6 M KCl	2% TX/0.6 M KCl	n/a	yes	+
2% TX/0.6 M KCl	2% TX/0.6 M KCl	2% TX/0.6 M KCl	yes	+
2% TX/0.6 M KCl	2% TX/0.6 M KCl	2% TX/1.8 M KCl	yes	+
2% TX/0.6 M KCl	2% TX/1.8 M KCl	n/a	yes	++
2% TX/0.6 M KCl	0.6 M KI w/ 20% sucr	n/a	yes	+++
2% TX/0.6 M KCl	0.6 M KI w/ 20% sucr	1 M Gdn-HCl	yes	++++
2% TX/0.6 M KCl	0.6 M KI w/ 20% sucr	1.2 M Gdn-HCl	partial	++
2% TX/0.6 M KCl	0.6 M KI w/ 20% sucr	1.5 M Gdn-HCl	no	n/a
2% TX/0.6 M KCl	0.6 M KI w/ 20% sucr	2 M Gdn-HCl	no	n/a
2% TX/0.6 M KCl	2% Deoxychol.	n/a	yes	+++
2% TX/0.6 M KCl	2% Deoxychol.	1 M Gdn-HCl	partial	++
2% TX/0.6 M KCl	2% Deoxychol.	1.5 M Gdn-HCl	partial	+
2% TX/0.6 M KCl	2% Deoxychol.	2 M Gdn-HCl	no	n/a
2% TX/0.6 M KCl	2 M Gdn-HCl	n/a	no	n/a
2% TX/0.6 M KCl	2 M Gdn-HCl/20% sucr	n/a	partial	+
2% TX/0.6 M KCl	2 M KSCN	n/a	no	n/a
2% Deoxychol./1 M KCl	n/a	n/a	partial	+
1% CHAPS	1 M Gdn-HCl	n/a	partial	+
500 mM Gdn-HCl	n/a	n/a	partial	+
1 M Gdn-HCl	n/a	n/a	no	n/a

Figure 4.17. TEM analysis of wild-type cells extracted with various core isolation treatments. (A) 2% TX only; (B) 2% TX/0.6M KCl; (C) 0.6M KI/20% sucrose; (D) 1M Guanidine-HCl; (E) 1.2M Guanidine-HCl. Arrows, cores; arrowheads, residual material. Scale bars, 250nm.

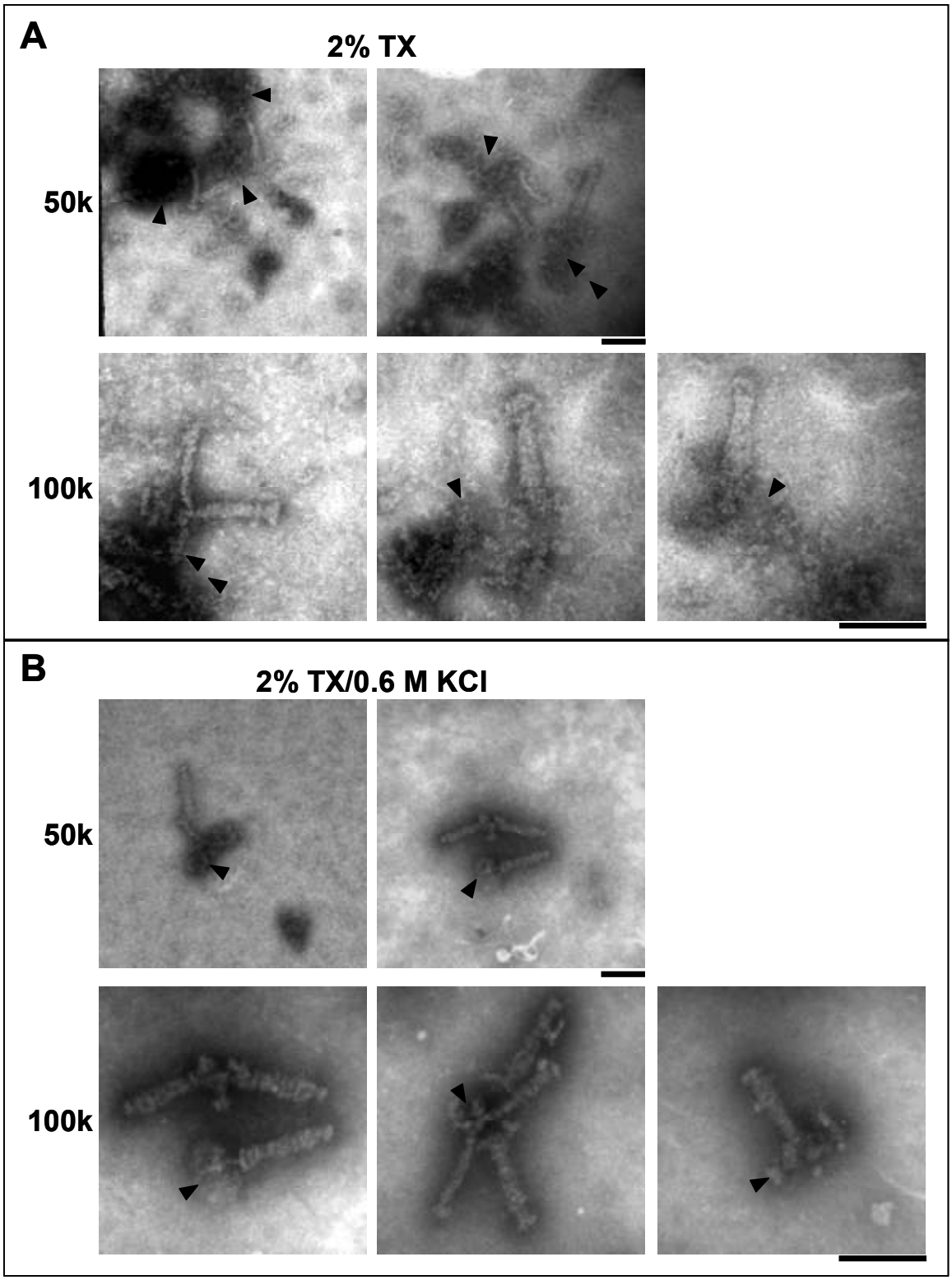
A
2% TX
50k
100k
B
2% TX/0.6 M KCl
50k
100k

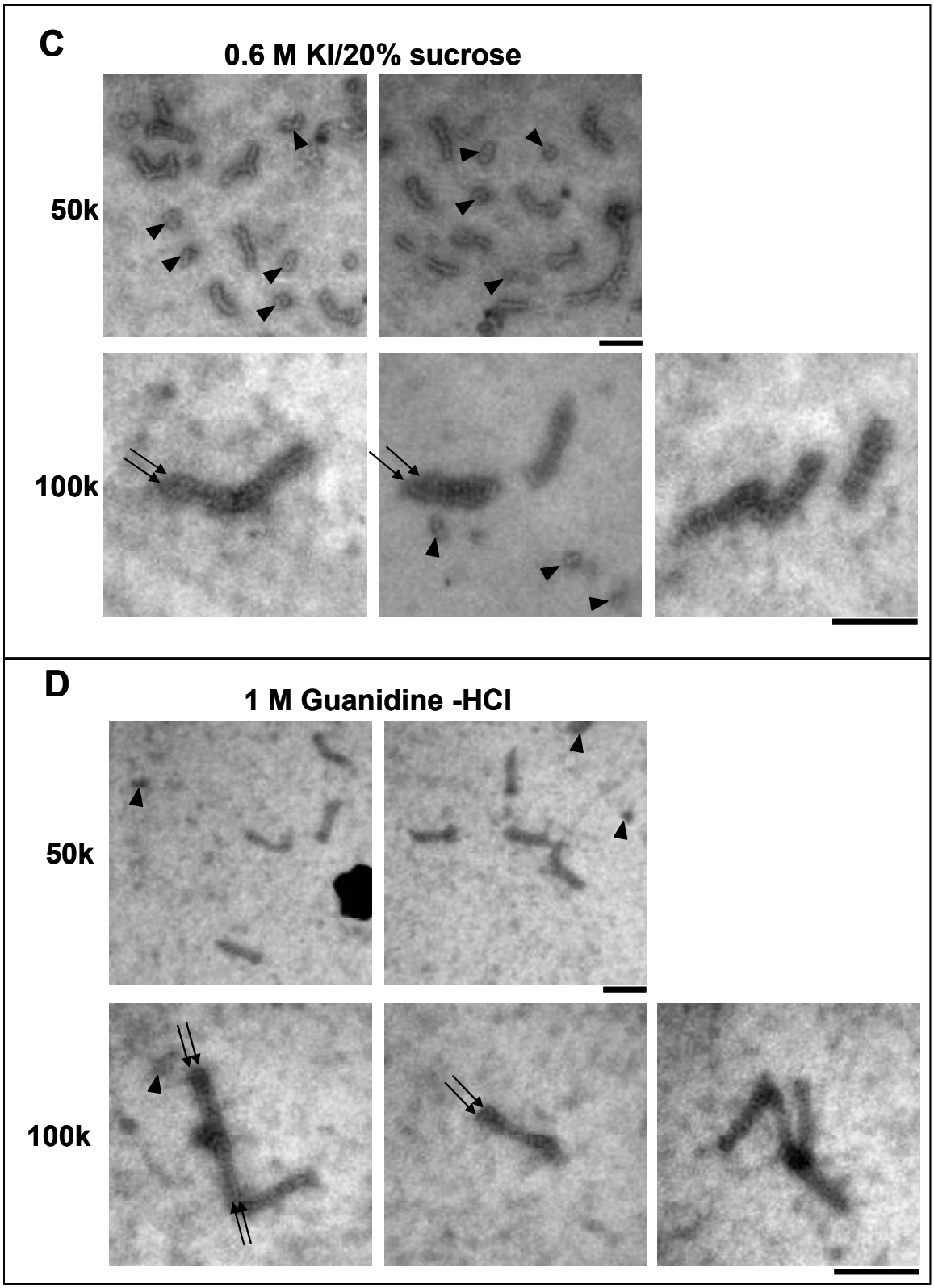
C
0.6 M KI/20% sucrose
50k
100k
D
1 M Guanidine -HCl
50k
100k

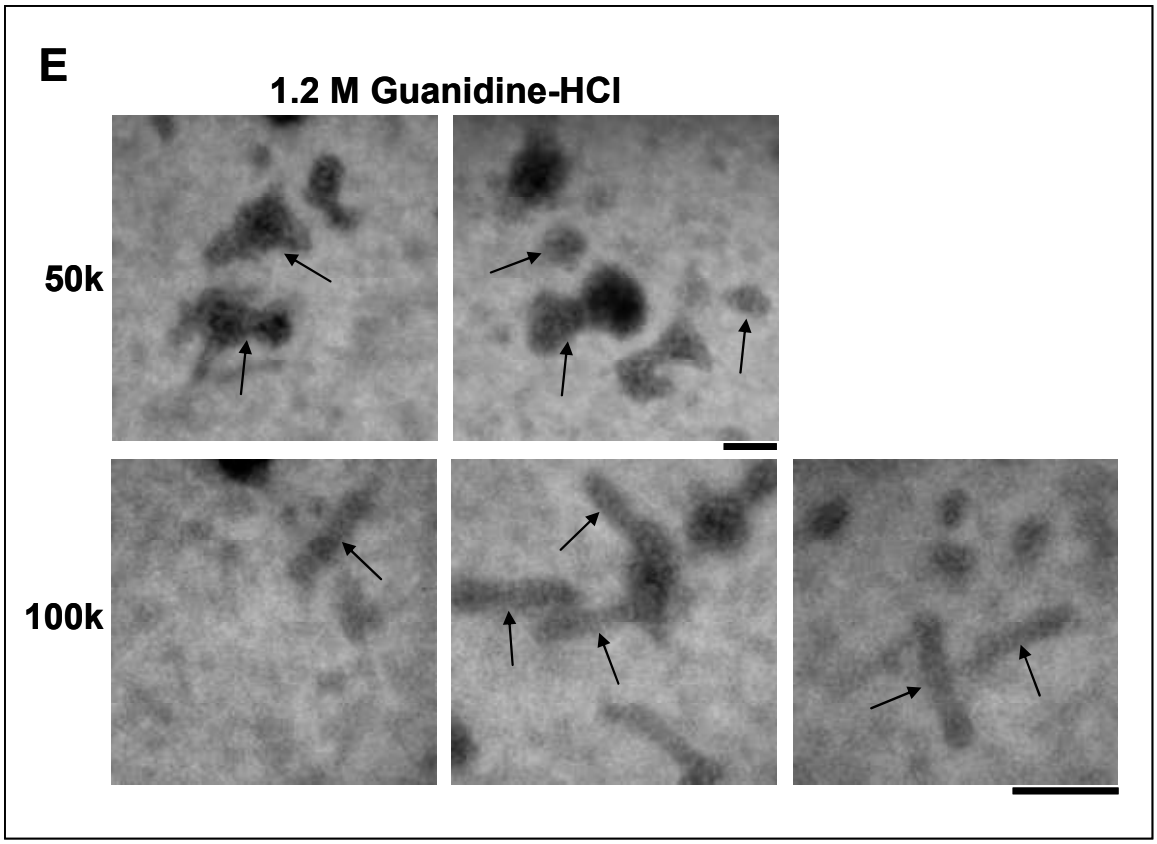
E
1.2 M Guanidine-HCl
50k
100k

button and were free from much of the material that appears to be membrane-associated and typically remains attached to each core after extraction with only 2% TX (Fig. 4.17A, arrowheads denote remaining core-associated material). However, debris still remained attached to some isolated cores and other clumps of cores (Fig. 4.17B, arrowheads denote remaining debris). Therefore, an additional treatment was necessary to remove this insoluble material from the core. However, a series of treatments using 2% TX/0.6 M KCl was not sufficient to remove the insoluble material associated with the core.

Most of the membrane was shown to be removed in our ^{3}H-palmitate experiments, using the 2% TX/0.6 M KCl treatment, where palmitate was used as a marker for the presence of membrane material. Because most of the membrane was removed with this first treatment, the material remaining associated with the core after the first treatment was probably not membrane-associated. Thus, we examined fractions treated with DNase by TEM analysis to determine if any DNA contamination could be preventing enrichment of the cores, even though no difference in the protein profile of fractions treated with DNase was noticed in our SDS-PAGE/silver stain analysis. We hypothesized that DNase treatment of the core-enriched fraction (CEF) may destabilize the surrounding insoluble network to promote further enrichment for isolated cores. As above, we used 2% TX combined with DNaseI (50 μg/ml) as the first treatment, then followed that with a 2% TX/0.6 M KCl treatment and found that the treatments did not appear to aid in removal of core-associated insoluble material (CAIM). Additionally, our previous analysis of the effects of 1% digitonin with 4 mM

$MgCl_2$ on 2% TX/0.6 M KCl extracted fractions showed minimal differences in protein profiles by SDS-PAGE/silver stain. Thus, this suggested that the CAIM was not DNA- or cholesterol-associated material.

In an effort to solubilize the remaining insoluble material associated with the core, we evaluated the effects of the stronger chaotropic agent 0.6M KI, combined with 20% sucrose in TN buffer. The sucrose is thought to mitigate partially the effects of 0.6 M KI alone, which has been shown to destabilize the cores such that they are not apparent in electron micrographs. Cores, seemingly free of CAIM, were apparent following this treatment (Fig. 4.17C). The two distinct rods that form the core were partly visible, presumably due to removal of proteins that are normally surrounding the core (Fig. 4.17C, arrows). Thus, a more defined view of the core was apparent. In the 50x and 100x images, fragments were visible that are shorter than the length of the average core and could be CAIM that was removed due to the treatment or pieces of the cores, indicating the fragile nature of the core upon removal of most of the CAIM (Fig. 4.17C, arrowheads). Our third and final treatment used 1 M guanidine-HCl in TN buffer (Fig. 4.17D). Again, isolated cores were apparent in large numbers as with the fractions treated with 2% TX/0.6 M KCl followed by 0.6 M KI/20% sucrose. The distinct rods of the core remained partially visible, as well (Fig. 4.17D, arrows). Occasionally, small fragments were visible on the grid surface that seemed smaller than those seen following the previous treatment (Fig. 4.17D, arrowheads). This material could still be parts of fragile cores that were dissociated further following this rather harsh treatment. A higher concentration of guanidine-HCl in TN buffer (1.2 M) appeared to destabilize the cores completely, such that core-like structures were apparent, but details, such as the

striations, were not as visible when compared with the 1 M guanidine-HCl treatment (Fig. 4.17D. arrows). A 1.5 M guandine-HCl treatment left the core-like structure with an almost unrecognizable appearance as if the cores were falling apart (data not shown). Thus, the 1 M guanidine-HCl treatment was determined to be the threshold treatment that enriched for the most isolated cores without completely destabilizing the core itself.

Mass spectrometry analysis of enriched cores. Having established a core preparation protocol, I had only very limited success at analyzing the proteins remaining in the insoluble fraction in silver-stained polyacrylamide gels by MALDI-TOF, and immunoblot analysis was not an option, due to a lack of specific antibodies to sufficient cytoskeletal proteins. Thus, I explored alternate methods for identifying the components of the CEF. Liquid Chromatography Mass Spectrometry (LC-MS) is a technique used to identify components of multi-protein complexes. We used this method to identify the components of the CEF because of its sensitivity and thorough coverage of the sample. After trypsin digestion and extraction, the protein complexes were analyzed by LC-MS. Common results from two separate experiments revealed 149 proteins as components of the CEF (Table 4.6), with a 5% False Discovery Rate (FDR), meaning that approximately 7-8 proteins of the 149 could possibly be a false match. The program does not identify these proteins specifically, but predicts that this percentage of protein matches is incorrect. Although a 1% FDR could be used, it would have most likely removed proteins that were actual components of the CEF, as well as those indirectly associated with the CEF. Based on the size of the genome and sample size, the MASCOT program determined our significance score to be 20, so we disregarded any peaks with a score less than 20 and included all the matches that had at least one peak

Table 4.6. Summary of liquid chromatography/mass spectrometry (LC/MS-MS) analysis of core-enriched fraction. %ab, relative abundance of the protein within the CEF; Status, number assigned based on whether the protein was a significant component of the CEF; 1, proteins retained in the CEF; 2, disgarded based on peak score below 20; 3, disgarded proteins with transmembrane domain(s); 4, disgarded ribosomal proteins.

Core-enriched Fraction Components	% ab	Status
Cytadherence high molecular weight protein 2	10.50	1
DNA-directed RNA polymerase beta chain	5.17	1
PTS system glucose-specific EIICBA component	4.24	3
Chaperone protein dnaK	4.06	1
Dihydroamide dehydrogenase (E3)	3.01	3
DNA-directed RNA polymerase beta' chain	2.82	1
Probable cytosol aminopeptidase	2.61	3
Galactoside transport ATP-binding protein mglA homolog	2.57	1
Cytadherence high molecular weight protein 3	2.49	1
Putative Xaa-Pro aminopeptidase	2.43	1
Glyceraldehyde-3-phosphate dehydrogenase	2.36	1
Pyruvate dehydrogenase E1 component subunit alpha	2.27	1
Oligopeptide transport ATP-binding protein oppF	2.13	1
ADP-ribosylating toxin CARDS	2.08	1
Hypothetical protein MPN376	1.95	3
Putative ATP-dependent helicase MG140	1.81	1
Pyruvate dehydrogenase E1 component subunit beta	1.58	3
Cytadherence high molecular weight protein 1	1.50	1
Adhesin P1 precursor	1.45	3
Elongation factor Tu	1.44	1
Hypothetical protein MG328 homolog	1.42	1
Cytadhesin P1	1.39	3
30S ribosomal protein S3	1.32	3
Enolase	1.31	1
Dihydrolipoamide acetyltransferase (E2)	1.24	3
Mgp-operon protein 1	1.22	1
Cell division protease ftsH homolog	1.21	1
Preprotein translocase secA subunit	1.14	1
DNA gyrase subunit A	0.91	1
Phosphomannomutase (PMM)	0.90	1
DNA-directed RNA polymerase alpha chain	0.88	1
Mgp-operon protein 3 precursor	0.81	1
Ribonuclease R	0.70	1
Pyruvate kinase	0.69	1
Ribonucleoside-diphosphate reductase subunit beta	0.66	1
Acetate kinase	0.64	1

Hypothetical protein MG343 homolog	0.62	1
Oligopeptide transport system permease protein oppC	0.55	3
MG130 homolog	0.54	3
Probable NADH oxidase	0.54	3
Protein P115 homolog	0.53	3
ATP synthase subunit alpha	0.51	3
Spermidine/putrescine import ATP-binding protein potA	0.49	1
50S ribosomal protein L2	0.49	4
Hypothetical protein MG075 homolog	0.48	3
Ribonucleoside-diphosphate reductase alpha subunit	0.47	1
Phosphoglycerate kinase	0.47	3
Phosphate acetyltransferase	0.47	1
30S ribosomal protein S5	0.47	4
Hypothetical protein MG210.1 homolog	0.46	1
Aspartyl/glutamyl-tRNA amidotransferase subunit B	0.44	1
Hypothetical protein MG218.1 homolog P41	0.43	1
Oligopeptide transport ATP-binding protein oppD	0.42	3
Fructose-bisphosphate aldolase	0.42	1
Hypothetical protein MG369 homolog	0.41	1
30S ribosomal protein S2	0.39	4
Hypothetical ABC transporter ATP-binding protein MG468.1 homolog	0.39	1
Asparaginyl-tRNA synthetase	0.39	3
50S ribosomal protein L1	0.39	4
Elongation factor G	0.36	1
Hypothetical protein MG422 homolog	0.36	1
ATP-dependent protease Lon	0.34	1
ABC transporter ATP-binding protein MG187 homolog	0.34	3
Protein MG054 homolog	0.34	1
GTP-binding protein era homolog	0.34	1
Protein MG468 homolog	0.33	3
Hypothetical protein MG423 homolog	0.33	3
Hypothetical lipoprotein MG040 homolog precursor	0.33	3
Oligopeptide transport system permease protein oppB	0.33	3
UvrABC system protein A	0.32	1
Putative HTH-type transcriptional regulator MG101 homolog	0.32	1
Chaperone protein dnaJ	0.30	1
Thymidine phosphorylase	0.28	1
50S ribosomal protein L5	0.26	4
Probable ATP-dependent RNA helicase MG425 homolog	0.26	3
Hypothetical protein MG116 homolog	0.25	1
50S ribosomal protein L3	0.25	4
Hypothetical ATP-dependent helicase MPN020	0.23	1
Phenylalanyl-tRNA synthetase beta chain	0.23	1
Hypothetical protein MPN491	0.23	3
ATP synthase subunit beta	0.22	3
Valyl-tRNA synthetase	0.22	1
Hypothetical protein MG105 homolog	0.22	3
RNA polymerase sigma factor rpoD	0.21	1
Transcription elongation protein nusA	0.21	1
Hypothetical protein MPN294	0.21	1

Very hypothetical mgpC-like protein MPN093	0.21	1
Cobalt import ATP-binding protein cbiO 2	0.20	1
Lipoprotein MG321 homolog precursor	0.19	3
Threonyl-tRNA synthetase	0.19	1
Hypothetical protein MG377 homolog	0.19	1
Ribose-phosphate pyrophosphokinase	0.19	1
Hypothetical protein MG255 homolog	0.19	3
Protein export, secD like	0.18	1
MG139 homolog	0.18	1
Hypothetical lipoprotein MG309 homolog precursor	0.16	3
Hypothetical protein MG123 homolog	0.16	3
Putative serine/threonine-protein kinase	0.16	3
Trigger factor	0.16	1
Hypothetical protein MG117 homolog	0.16	1
Hypothetical protein MPN407	0.15	3
Probable 1-acyl-sn-glycerol-3-phosphate acyltransferase	0.15	3
Hypothetical protein MG354 homolog	0.15	3
DNA gyrase subunit B	0.14	1
DNA topoisomerase 1	0.14	1
Deoxyribose-phosphate aldolase	0.14	1
Arginine deiminase-like protein	0.13	3
30S ribosomal protein S4	0.13	4
L-lactate dehydrogenase	0.13	3
Putative type I restriction enzyme specificity protein MPN638	0.13	1
Transketolase	0.13	1
Probable DNA helicase MPN340	0.12	3
Glutamyl-tRNA(Gln) amidotransferase subunit A	0.12	1
Hypothetical protein MG120 homolog	0.12	3
Hypothetical protein MG242 homolog	0.11	3
60 kDa chaperonin (groEL)	0.11	1
Hypothetical protein MG125 homolog	0.11	1
Hypothetical lipoprotein MPN284 precursor	0.11	3
Protein P200	0.09	1
Hypothetical protein MG409 homolog	0.09	1
Probable lipoate-protein ligase A	0.09	1
Hypothetical protein MG268 homolog	0.09	1
Probable cation-transporting P-type ATPase	0.09	3
Chaperone clpB	0.09	1
Hypothetical lipoprotein MPN152 precursor	0.09	2
Hypothetical protein MG241 homolog	0.08	3
ParA family protein MPN688	0.08	1
30S ribosomal protein S18	0.08	4
Hypothetical protein MG181 homolog	0.07	3
Glucose-6-phosphate isomerase	0.07	1
Hypothetical protein MG356 homolog	0.07	3
MG332 homolog	0.07	1
Translation initiation factor IF-2	0.06	1
DNA polymerase III subunit gamma/tau	0.06	1
S-adenosyl-methyltransferase mraW	0.06	1
Hypothetical ABC transporter ATP-binding protein MG015 homolog	0.06	3

Hypothetical protein MG039 homolog	0.05	3
Hypothetical protein MG256 homolog	0.05	3
DNA ligase	0.05	1
Hypothetical protein MG223 homolog	0.05	1
ORF8	0.04	3
50S ribosomal protein L10	0.04	4
Abc transport ATP-binding protein	0.04	1
Cysteinyl-tRNA synthetase	0.04	1
DNA polymerase III polC-type	0.04	1
Hypothetical protein MPN591	0.04	1
Elongation factor Ts	0.02	1
DNA primase	0.02	3
Hypothetical ABC transporter ATP-binding protein MG304 homolog	0.02	1
ATP synthase epsilon chain	0.02	1

with a score above 20. Only one match was disgarded, based on this criterion. Fifty known membrane proteins were also removed from the hits, considered to be membrane associated due to the presence of a transmembrane domain. In addition, nine more hits were discarded because they were ribosomal proteins, which are not likely to be found in the attachment organelle due to lack of ribosomes in the area (Biberfeld and Biberfeld, 1970; Henderson and Jensen, 2006; Wilson and Collier, 1976).

The 89 remaining proteins that comprise the CEF had a variety of functions with varying levels of abundance relative to the other proteins within the CEF (Table 4.7). As expected, several cytadherence-associated proteins were identified as part of the CEF. Transcription and translation proteins were also found including chaperone and secretion proteins. Several transport proteins were identified, as well as proteins involved in import and export. Furthermore, the CEF consists of cell division and DNA replication proteins and metabolic proteins, specifically those involved in glycolysis, the pentose phosphate pathway, acetate activation, nucleotide metabolism, and ATP synthesis. Lastly, proteins of other functions, such as RNA and protein degrading enzymes were found, along with many hypothetical proteins.

Table 4.7. Summary table of the identified components of the core-enriched fraction (CEF). Organized according to function; %ab, relative abundance of the protein within the CEF.

Cytadherence Proteins	% Abundance
Cytadherence high molecular weight protein 2	10.51
Cytadherence high molecular weight protein 3	2.49
Cytadherence high molecular weight protein 1	1.50
Hypothetical protein MG218.1 homolog P41	0.43
Protein P200	0.09
Transcription/Translation	
DNA-directed RNA polymerase beta chain	5.18
Chaperone protein dnaK (Heat shock protein 70)	4.06
DNA-directed RNA polymerase beta' chain	2.82
Elongation factor Tu	1.44
DNA-directed RNA polymerase alpha chain	0.88
Aspartyl/glutamyl-tRNA amidotransferase subunit B	0.45
Elongation factor G (EF-G)	0.36
Protein MG054 homolog	0.34
Chaperone protein dnaJ	0.30
Phenylalanyl-tRNA synthetase beta chain	0.23
Valyl-tRNA synthetase	0.22
RNA polymerase sigma factor rpoD	0.21
Transcription elongation protein nusA	0.21
Threonyl-tRNA synthetase	0.19
Trigger factor (TF)	0.16
Glutamyl-tRNA(Gln) amidotransferase subunit A	0.12
60 kDa chaperonin (Protein Cpn60) (groEL protein)	0.11
Chaperone clpB	0.09
Translation initiation factor IF-2	0.06
Cysteinyl-tRNA synthetase	0.04
Elongation factor Ts	0.02
Transport/Uptake	
Galactoside transport ATP-binding protein mglA homolog	2.58
Oligopeptide transport ATP-binding protein oppF	2.13
Preprotein translocase secA subunit	1.14
Cobalt import ATP-binding protein cbiO 2	0.20
Protein export, secD like	0.18
Abc transport ATP-binding protein	0.04
Hypothetical ABC transporter ATP-binding protein MG304 homolog	0.02
Protein with other functions	
Putative Xaa-Pro aminopeptidase	2.44
ADP-ribosylating toxin CARDS	2.08
Mgp-operon protein 1	1.22

Phosphomannomutase	0.90
Mgp-operon protein 3 precursor	0.81
Ribonuclease R	0.70
Ribonucleoside-diphosphate reductase subunit beta	0.66
Spermidine/putrescine import ATP-binding protein potA	0.49
Ribonucleoside-diphosphate reductase alpha subunit	0.47
ATP-dependent protease Lon	0.34
GTP-binding protein era homolog	0.34
UvrABC system protein A	0.32
Thymidine phosphorylase (TdRPase)	0.28
Protein MG139 homolog	0.18
Putative type I restriction enzyme specificity protein MPN638	0.13
Probable lipoate-protein ligase A	0.09
S-adenosyl-methyltransferase mraW	0.06
Cell division/DNA replication	
Cell division protease ftsH homolog	1.21
DNA gyrase subunit A	0.91
DNA gyrase subunit B	0.14
DNA topoisomerase 1	0.14
ParA family protein MPN688	0.08
DNA polymerase III subunit gamma/tau	0.06
DNA ligase	0.05
DNA polymerase III polC-type	0.04
Metabolism	
Glyceraldehyde-3-phosphate dehydrogenase	2.37
Pyruvate dehydrogenase E1 component subunit alpha	2.27
Pyruvate kinase	0.69
Acetate kinase	0.64
Phosphate acetyltransferase	0.47
Fructose-bisphosphate aldolase	0.42
Ribose-phosphate pyrophosphokinase	0.19
Deoxyribose-phosphate aldolase	0.14
Transketolase (TK)	0.13
Glucose-6-phosphate isomerase	0.07
ATP synthase epsilon chain	0.02
Hypothetical Proteins	
Putative ATP-dependent helicase MG140 homolog	1.82
Hypothetical protein MG328 homolog	1.42
Hypothetical protein MG343 homolog	0.62
Hypothetical protein MG210.1 homolog	0.46
Hypothetical protein MG369 homolog	0.41
Hypothetical ABC transporter ATP-binding protein MG468.1 homolog	0.39
Hypothetical protein MG422 homolog	0.36
Putative HTH-type transcriptional regulator MG101 homolog	0.32
Hypothetical protein MG116 homolog	0.25
Hypothetical ATP-dependent helicase MPN020	0.23
Hypothetical protein MPN294	0.21

Hypothetical mgpC-like protein MPN093	0.21
Hypothetical protein MG377 homolog	0.19
Hypothetical protein MG117 homolog	0.16
Hypothetical protein MG125 homolog	0.11
Hypothetical protein MG409 homolog	0.09
Hypothetical protein MG268 homolog	0.09
protein MG332 homolog	0.07
Hypothetical protein MG223 homolog	0.05
Hypothetical protein MPN591	0.04

CHAPTER V

DISCUSSION

HMW2 Structure/Function Analysis

Correlation of the results from our functional analysis with regions of HMW2 present or deleted in each mutant allowed us to hypothesize about specific regions required for normal cell functions and core formation to occur normally. Thus, before discussing the significance of these regions, I will compare the distinctions between each HMW2 derivative. Except for its N- and C-terminal domains, HMW2 is likely composed of disrupted coiled-coils, which allow flexibility for predicted dimeric and trimeric interactions to occur. Wild-type HMW2 contains 8 predicted dimeric coiled-coils at amino acid residues [313-358(1), 771-806(2), 813-857(3), 944-975(4), 1245-1282(5), 1285-1337(6), 1519-1603(8), and 1648-1686(9)] and 2 predicted trimeric coiled-coils at amino acid residues [1458-1485(7), 1787-1814(10)], as well as three cysteine residues [C30(1), C255(2), and C1217(3)] and five leucine repeats [starting at amino acid 542(1), 818(2), 1079(3), 1255(4), and 1389(5)] (Fig. 5.1). Two potential translational start sites for P28 have been identified corresponding to amino acids 1578 and 1619 of HMW2. The HMW2 derivative produced by mutant I-2 lacks three leucine repeats (3-5), cysteine residue 3, five predicted dimeric regions (4-6, 8-9) and both predicted trimeric regions (7,10), as well as the C-terminal domain (Fig. 5.1). Truncated HMW2 in H9 lacks the same regions as that in I-2 except the dimeric coiled coil 4 (Fig. 5.1). The truncated HMW2 produced in mutant C1 lacks two predicted dimeric coiled-coils (8-9), the two

Figure 5.1. Structural features of wild-type, engineered, and mutant HMW2 derivatives. Strains are listed to the left of corresponding HMW2. The cross-hatched regions indicate the predicted dimeric coiled-coils, and the black regions indicate the predicted trimeric coiled-coils. The translation start for P28 has not been determined, thus two arrows indicate the two potential start sites. Beneath each construct, the blue triangles represent the cysteine residues and the red boxes represent the leucine repeats. Numbers corresponding to the coiled-coil regions are above, cysteine residues are beneath each triangle in blue, leucine repeats are beneath each red box in red.

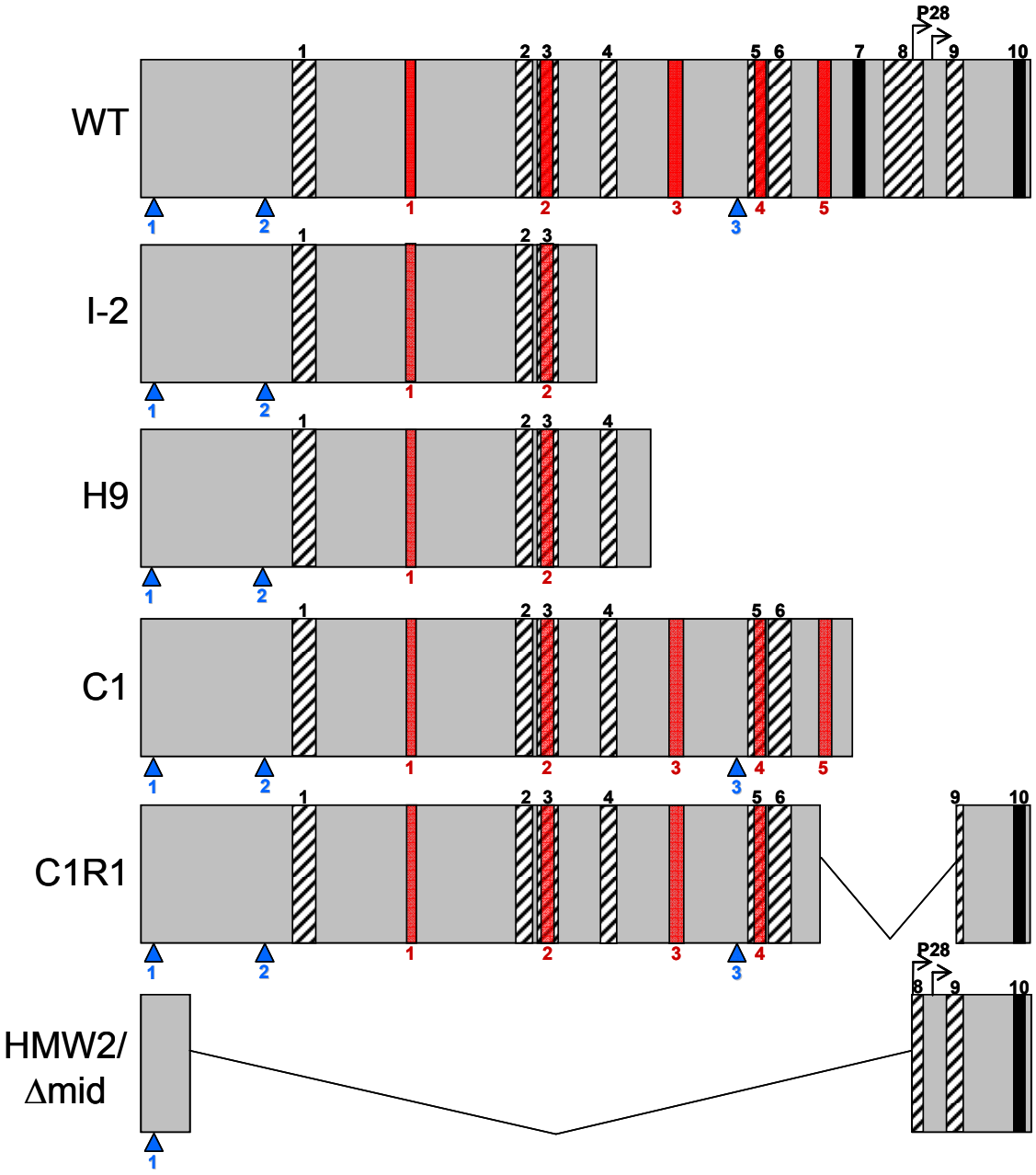
WT
I-2
H9
C1
C1R1
HMW2/
Δmid
P28

predicted trimeric coiled-coils (7,10), and the C-terminal domain (Fig. 5.1). The excision deletion that occurred in the C1 revertant C1R1 removed one entire predicted dimeric coiled-coil (8) and disrupted another (9). Furthermore, one predicted trimeric coiled-coil (7) is absent, as well as both amino acids 1578 and 1619 corresponding to the potential P28 start sites (Fig. 5.1). Lastly, the engineered HMW2Δmid construct lacks two cysteines (2-3), all five leucine repeats (1-5), six predicted dimeric coiled-coils (1-6), and one predicted trimeric coiled-coil (1), and disrupted dimeric coiled-coil (8), due to deletion of nearly 80% of the coding region (Fig. 5.1).

We found that the levels of HMW2 derivatives varied based on the strain, with wild-type levels in H9 and C1R1 and reduced levels in I-2 and C1. H9 produced the most stable HMW2 derivative and also had the highest P28 levels when compared with I-2 and C1, suggesting a correlation between P28 levels and HMW2 stability. However, the HMW2 derivative in C1R1 was stable at wildtype-levels despite the absence of P28. Thus, P28 is not required to stabilize HMW2 in C1R1. Comparison of the HMW2 derivatives in C1R1 and C1, where HMW2 is significantly reduced, identified two regions absent in C1 that may be essential for HMW2 stabilization, including the normal C-terminus of HMW2 and a nearby predicted trimeric coiled-coil, both of which regions are also found in P28. Therefore, despite their absence in the HMW2 derivative in H9, this protein is stable at wild-type levels due to the presence of these regions in P28, suggesting that the presence of these regions is required either within HMW2 or P28 to stabilize HMW2. Although P28 is not required for stabilization of HMW2 in C1R1, the presence of these regions in HMW2 is essential, and in the absence of the C-terminus of HMW2, P28 supplies these regions for stabilization to occur.

Interestingly, the production of HMW2Δmid at wild-type levels in I-2 partially stabilized the HMW2 derivative in that mutant. In contrast, the presence of HMW2Δmid in mutant C1 at reduced levels did not restore the levels of the HMW2 derivative. HMW2Δmid also allowed for production of P28, which further stabilized the HMW2 derivative in I-2. However, the HMW2 derivative in I-2 was still not completely stabilized by this construct, suggesting that a certain quantity of P28 from I-2 is required that cannot be completely provided by P28 from HMW2Δmid. This does not explain why the HMW2 derivative in C1 was not at least partially stabilized by HMW2Δmid. Perhaps the HMW2 derivative in I-2 is shorter and more stable than in C1, and thus may allow for a stabilizing interaction with HMW2Δmid that cannot occur with C1.

P41 was present at levels that correlated with the levels of the resident or recombinant P28 derivative. Thus, when P28 was produced at high levels as in WT, H9, and I-2/HMW2Δmid, P41 was likewise, and when P28 was made at reduced levels, as in I-2 and C1/HMW2Δmid, so was P41. Thus, the levels of P41 appear to be a function of the stability of P28, or vice-versa. The levels of P24 were related to the presence but not the levels of P41 in H9, I-2, and C1, where levels of P41 varied, but P24 remained consistently reduced. In contrast to P41 stabilization, HMW2Δmid had no effect on the stabilization of P24, despite increased levels of P41.

We demonstrated that the C-terminus of HMW2 is required to maintain wild-type partitioning of HMW2 into the TX-insoluble fraction and to stabilize cytadherence accessory proteins HMW3 and P65. Interestingly, the C-terminus of HMW2 may be necessary, but is not sufficient for maintaining other specific functions in the cell,

including stabilization of HMW1, localization of P1, cytadherence, motility, and maintenance of normal cellular morphology.

WT and C1R1 were the only strains tested which stabilized HMW1. Thus, since the translational start sites for P28 were deleted in C1R1 and no P28 was made, this protein is not required for HMW1 stabilization. Furthermore, the only differences between C1R1 and the strains I-2, H9, and C1, which did not stabilize HMW1, was the presence of the C-terminus and the predicted trimeric coiled-coil region 10 in C1R1, implicating one or both of these regions as essential for HMW1 stabilization. Interestingly, although these regions are present in HMW2Δmid, this construct failed to stabilize HMW1 in either I-2 or C1, indicating that these regions are not sufficient to stabilize HMW1. In contrast, HMW2Δmid stabilized HMW3 and P65 in I-2 and C1, apparently due to the presence of the C-terminus, indicating distinct requirements for stabilization of these proteins compared to HMW1. Thus, the C-terminus and predicted trimeric coiled-coil 10 may be required, but are not sufficient to stabilize HMW1, suggesting that additional regions are required. These could include leucine repeats 3 and 4, predicted dimeric coiled-coils 5 and 6, and/or cysteine 3, which are absent in I-2 and HMW2Δmid but present in C1 and C1R1. However, because HMW1 is not stabilized in C1/HMW2Δmid, which contains all of the necessary domains including the C-terminus and predicted trimeric coiled-coil 10, albeit not contiguously, this suggests that these regions must be contained within a single molecule. Recent data indicate that a reciprocal relationship exists between HMW1 and HMW2 (Willby *et al.*, 2004) and these results are consistent with the hypothesis that HMW1 and HMW2 may interact directly. No experiments to examine a potential direct interaction of these two proteins,

such as a yeast two-hybrid, have been done, and additional studies will be necessary to explore this possibility further and to determine if these regions of HMW2 are essential because of an interaction that occurs, for example with HMW1, at specific amino acids within these regions and/or they are required for maintaining a certain spatial position within the attachment organelle.

In previous studies, HMW1 has been shown to be required for P1 clustering at the terminal organelle (Hahn *et al.*, 1998). Our P1 localization data demonstrating that the same strains that do not stabilize HMW1 (I-2, H9, and I-2/HMW2Δmid) did not localize P1, supports that hypothesis. P1 localization studies in C1R1 have not been performed, but because HMW1 is stabilized, we predict that P1 is localized. The ability to glide follows this same pattern, where strains I-2 and C1 exhibit no satellite growth; gliding was not restored by HMW2Δmid in strains I-2 and C1. Wild-type gliding was apparent in C1R1 (Hasselbring and Krause, unpublished data). Thus, the regions essential for HMW1 stabilization are also required for P1 localization and gliding motility.

Because P1 is the major adhesin in *M. pneumoniae*, it was not surprising that in most of the strains that did not localize P1 to the attachment organelle (I-2, H9, C1, and C1/HMW2Δmid), cytadherence was reduced. Surprisingly, I-2/HMW2Δmid did not stabilize HMW1 or localize P1 yet exhibited intermediate hemadsorption, where erythrocytes attached to the edges of the colonies, but not the center. Several factors were considered as possibly contributing to the difference in cytadherence between I-2 and C1 when producing HMW2Δmid. We first considered the possibility that reversion in I-2 contributed to the increased cytadherence, but a revertant population would have most likely also restored normal cytadherence localization of P1 and this was not the

case. Secondly, we considered that the difference in cytadherence might be due to wild-type levels of P28. However, mutant C1R1 fails to produce P28, but is able to cytadhere at intermediate levels. Thus, the increased levels of P28 in I-2/HMW2Δmid probably did not contribute to its intermediate cytadherence phenotype. Lastly, a shorter but more stable HMW2 derivative is made in I-2 than in C1. The greater stability of the HMW2 derivative might allow for better interaction with HMW2Δmid, and thus allow for increased cytadherence, as was shown for HMW2 stability. Cellular morphology is restored in the same pattern, where mutants I-2 and H9 have an aberrant morphology, unlike I-2/HMW2Δmid, whose morphology resembles wild-type cells. Based on these results, the regions required for cytadherence and normal cellular morphology may be distinct from those required for HMW1 stability, P1 localization, and gliding motility. The C-terminus and predicted trimeric coiled-coil 10 are necessary, but do not have to be contiguous with HMW2 and the region including leucine repeats 3 and 4, predicted dimeric coiled-coils 5 and 6, and cysteine 3 is not required. For complete restoration of cytadherence, an additional region of HMW2, predicted trimeric coiled-coil 7, which is absent in C1R1, may be required.

TEM analysis of thin sections demonstrated that the C-terminus of HMW1 and the C-terminus and/or predicted trimeric coiled-coil domain 10 of HMW2, but not P28, were essential for normal core formation. Furthermore, production of HMW2Δmid in I-2 and C1 allowed for rare and no cores, respectively. Western immunoblot data suggested that a small revertant population exists in I-2, consistent with the presence of a few cores. However, an interaction with HMW2Δmid, as predicted above, may have also allowed for a few cores to form in I-2/HMW2Δmid and seems consistent with HA

data and SEM analysis for this transformant. This would also explain the lack of cores in the C1/HMW2Δmid transformant, where no interaction is predicted to occur.

TEM analysis of TX fractions allowed us to refine our predictions and pinpoint more precisely the regions of HMW2 that affect core formation, based on a less obstructed view of the details of the core. In contrast to thin-section results, TX fractions of C1 revealed an intact core that appeared to be structurally unstable. A region containing two predicted dimeric coiled-coils (8-9) and leucine repeats (3-4) are present in C1 but absent in the HMW2 derivative strains that fail to form cores (I-2 and H9) and may contribute to core formation. Leucine repeat 5 was also present in C1, but was not considered to be essential for core formation because of its absence in C1R1, which forms a stable core. Thus, leucine zipper 5 is not further discussed. HMW2Δmid was not sufficient to stabilize the core in C1, substantiating the conclusion that probably no interaction is occurring between the two HMW2 derivatives. However, our prediction that the HMW2 derivative in I-2 and HMW2Δmid interact to form infrequent normal cores appears to be unfounded; the two predicted dimeric coiled-coils (8-9) and leucine repeats (3-4) that are thought to be required for core formation are absent in both HMW2 derivatives, thus a stable core would not be formed. The infrequent cores seen in I-2 and I-2/HMW2Δmid therefore probably reflect a small revertant population. C1R1 contains all three regions implicated in HMW2 function and forms a core that is wild-type-like in most respects. However, the appearance of the core in C1 and C1R1 suggest a step-wise assembly, with core stabilization perhaps occurring in two steps. The first step allows for partial stabilization of the core with the presence of the two predicted dimeric coiled-coils (5-6) and leucine repeats (3-4), such that unstably

associated core segments are present. Deletion or amino acid substitutions of specific leucine repeats within HMW2 could allow us to test our hypothesis concerning stabilization of the core by leucine zipper interactions. The second step completes the stabilization process, where predicted trimeric coiled-coil 10 and/or the C-terminus stabilizes the core in a wild-type configuration. While the cores present in C1R1 had a wild-type appearance, they were not wild-type in length. This deficit in length appears to be due to the absence of P28 and/or predicted trimeric coiled-coil region 1 of HMW2, which are absent in C1R1.

Our initial model for core formation suggests that HMW2 and P28 monomers interact in a lengthwise manner (Figure 2.1), predicting that a truncated HMW2 would form a shorter core (Balish *et al.*, 2003b). However, finding a difference only in the length of the cores of C1R1 and no complete core formation with truncated HMW2 derivatives was inconsistent with that model.

In an effort to understand how HMW2 contributes to core structure, we examined the localization of HMW2 using immunoelectron microscopy, demonstrating that the N- and C- terminus of HMW2 localize to the periphery of the core. Previously, images of wild-type cryo thin sections demonstrated the presence of spoke-like structures that were found on either side of the core, appearing to connect the core to the membrane (Hegermann *et al.*, 2002). The localization of gold to the periphery of the core seemed to indicate that HMW2 may correspond to these spoke-like structures surrounding the core. An obvious limitation to localization of HMW2 in TX fractions is that since TX extraction precedes fixation in our fraction preparation, there is potential for movement of cell structures that are normally anchored by the membrane. In hopes of obtaining

an unaltered view of the position of the spokes in comparison with the position of the gold particles labeling HMW2, we first fixed the mycoplasmas to the grid, then extracted them with TX. Unfortunately, immunogold labeling of HMW2 in these fractions appeared to have been obstructed on account of minimal gold labeling when compared with our previous gold-labeling experiments. An electron cryotomography study did not seem to support our conclusion that HMW2 corresponds to the spoke-like structures because spokes were not apparent along the periphery of the cores in intact wild-type cells when viewed in solution (Henderson and Jensen, 2006). However, the absence of spokes in these images could be attributed to the lack of a post-stain in sample preparation for electron cryotomography studies. Spokes were also not apparent in freeze fracture analysis of wild-type cells (Wall *et al.*, 1983). Unlike those studies, the spokes were readily visible in many of our transmission electron micrographs of TX fractions as well as images from other studies (Hegermann *et al.*, 2002), and thus, we did not regard them as electron microscopy artifacts.

Recent studies of the *M. pneumoniae* terminal organelle by electron cryotomography examined only intact wild-type cells in suspension. In that study, the 3-D rendering clearly revealed that the rods of the core are not identical, with one significantly thicker than the other (Henderson and Jensen, 2006). Our TEM analysis only allowed for an occasional view of the thin rod adjacent to the thick rod of the core. Because of this limited view, our HMW2 localization analysis did not allow us to determine a possible bias of gold distribution along the periphery of the core. However, we are able to conclude that since the thick rod is what we primarily see, HMW2 is not part of that rod, but could be a component of the thin rod. Our preliminary

measurements of the average width of the initial, unstable core structure of the C1 mutant strain (23 ± 6nm) indicated that its width is too large to be the thin rod, based on comparison with the predicted widths of both rods (~8nm and 13-31nm for the thin and thick rods, respectively) in another study (Henderson and Jensen, 2006).

Based on the evidence that suggests that HMW2 is not a component of the thick rod, that it localizes to the periphery of the core, and that there is no bias of HMW2 localization along the edge of the core, we suggest that HMW2 is a component of the thin rod of the core. Furthermore, because there is no bias in immunogold labeling of the N- or C-terminus of HMW2, we propose that the N- and C- terminus of HMW2 stack together to form the thin rod and the remaining central portion of HMW2 comprises the spoke-like structures surrounding the core. We have established several specific regions of HMW2 that are required for core stabilization in this study and which may be essential for establishing proper spatial positioning between the N- and C-termini of HMW2, such that the central portion of HMW2 could form the spokes and the termini would stack correctly. In addition, in the HMW2 derivative strains that form cores, C1 and C1R1, leucine repeats (3-4), absent in HMW2 derivative strains lacking a core, is present in these strains. We propose that the spatial positioning of the required coiled-coils [two dimeric coiled-coils (5-6)] and predicted trimeric coiled-coil (2) may allow for positioning of leucine repeats (3-4) to form leucine zippers for further stabilization of the core and possibly for interaction with proteins in the membrane that would tether the core to the membrane and form the spoke-like structures that have been reported previously (Hegermann *et al.*, 2002). Cysteine residue 3 is also present in the region with predicted dimeric coiled-coils and leucine repeats (3-4). The disulfide bond

predictor program DISULFIND (Department of Systems and Computer Science, Universita'di Firenze, Italy) predicted that the first two cysteines in HMW2 bind to each other while the third does not form a disulfide bond within the protein and is presumably available for disulfide bonding to other proteins (data not shown). We considered the possibility that cysteine 3 in HMW2 allows for tethering to a membrane protein. However, treatment of wild-type cores with 13% β-mercaptoethanol as part of our TX extraction procedure did not inhibit core formation (data not shown). Thus, the cysteines are not required for core stabilization, but may be required for interactions with other proteins that localize in the attachment organelle. In addition, a predicted disulfide-linked dimer of HMW2, HMW5 (Stevens and Krause, 1990), is also not required for core formation. Furthermore, we predict a role for P28, or more specifically its predicted trimeric coiled-coil 2, to stabilize the core structure by interacting with the C-terminal ends of HMW2 to form the trimeric coiled-coil. For a trimeric interaction to occur, two predicted trimeric coiled-coils would have to be present (one from each C-terminus of HMW2), along with the predicted trimeric coiled-coil region in P28 or two from P28 monomers and one from HMW2. In addition, the predicted dimeric coiled-coil located near the N-terminus of HMW2 could link to the same region on another HMW2 monomer. These multimeric interactions could stabilize the structure of the thin rod. The C1R1 mutant does not produce P28 and assembles cores that are about 20% shorter than the wild-type core. Thus, it is possible that the loss of P28 could prevent the trimeric coiled-coil interaction with the C-terminus of HMW2 from occurring, such that the length of the core is reduced, but still allows a normal core to be formed. Presumably, continued formation of the dimeric coiled-coil interactions and leucine

zipper interactions (3-4) would prevent the core from falling apart. Finally, a recent hypothesis suggested that leucine repeats within HMW2 may have a role in interacting with leucine repeats in either DnaK or the J-domain protein CapJ to allow for correct positioning of a chaperone complex within the attachment organelle (Cloward and Krause, unpublished data).

To summarize our current model for HMW2 organization and core formation, several scenarios comparing full-length HMW2 with the HMW2 derivatives are portrayed in Fig. 5.2. For wild-type *M. pneumoniae*, the N-and C-termini of HMW2 monomers are stacked on top of each other, such that the N- terminus is adjacent to another N-terminus with the C-termini are adjacent to each other, with the central portion of the protein folding to potentially form the spokes. Predicted trimeric interactions with coiled coil 10 between the C-termini and P28 could stabilize the thin rod, along with a trimeric interaction with coiled-coil 7 of two HMW2 monomers and P28, creating a second layer of stability for the C-termini. Predicted dimeric coiled-coil 1 is near the N-terminal domain and could also provide stability to the rod if a dimeric interaction occurs with another HMW2 monomer. The remaining folded portion of HMW2 could allow for leucine zipper interactions 2, 3, and 4 of adjacent HMW2 monomers to interact, thereby stabilizing them (Fig. 5.2A). For I-2 and H9, the C-terminus of HMW2 is absent, and thus the predicted trimeric coiled-coils are absent, as well. Therefore, the N-termini of HMW2 monomers stack on top of each other and a predicted dimeric interaction could form nearby. However, this complex is not stable, and because it is missing leucine repeats 3 and 4, the thin rod is unable to maintain a higher-ordered structure and falls apart or is unrecognizable by TEM (Fig. 5.2B).

Figure 5.2. Schematic model for core formation. The yellow rectangle represents the thick rod of the core. The boxes with N and C indicate the N- and C-termini of HMW2. The black lines are the central portion of HMW2. The blue boxes represent the predicted trimeric coiled-coil interactions and the green boxes represent the predicted dimeric coiled-coil interactions. The leucine zippers are indicated by the red boxes. The numbers in white on each box correspond to the structure in Fig. 5.1.

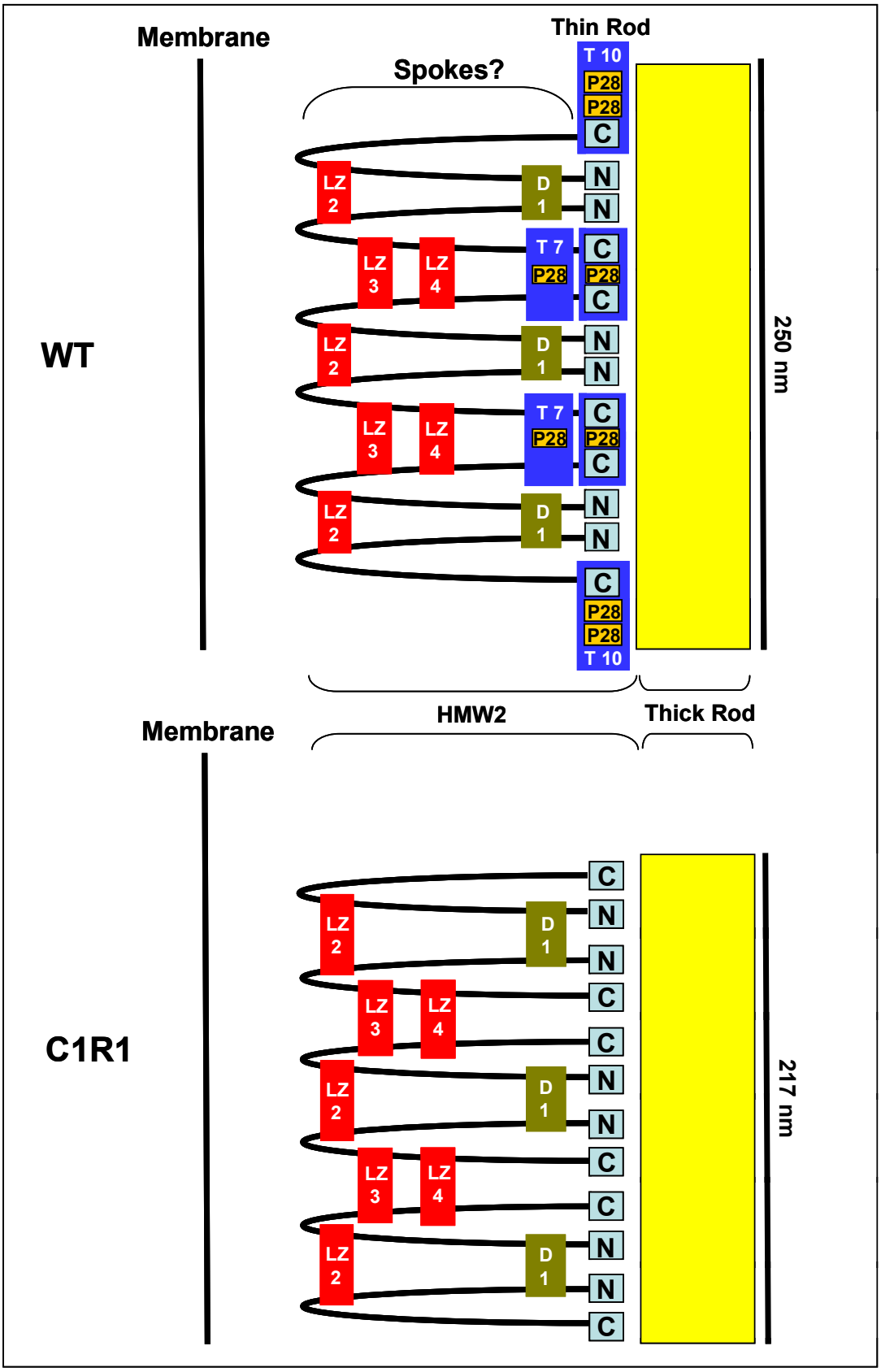
Membrane
Thin Rod
Spokes?
T 10
P28
P28
C
LZ 2
D 1
N
N
LZ 3
LZ 4
T 7
P28
C
P28
C
250 nm
WT
HMW2
Thick Rod
Membrane
C1R1
217 nm

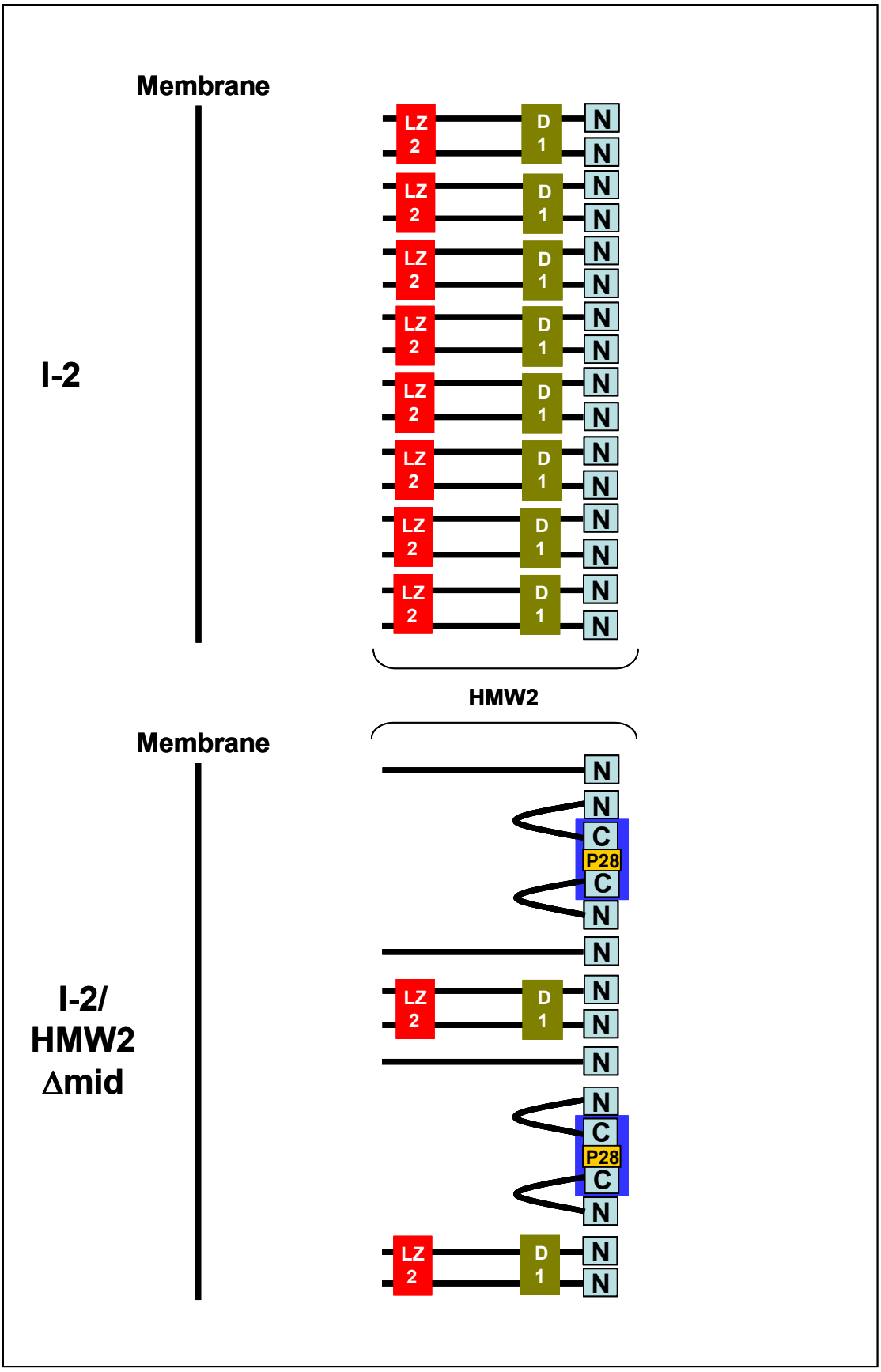
Membrane
I-2
LZ 2
D 1
N
HMW2
Membrane
I-2/
HMW2
Δmid
C
P28

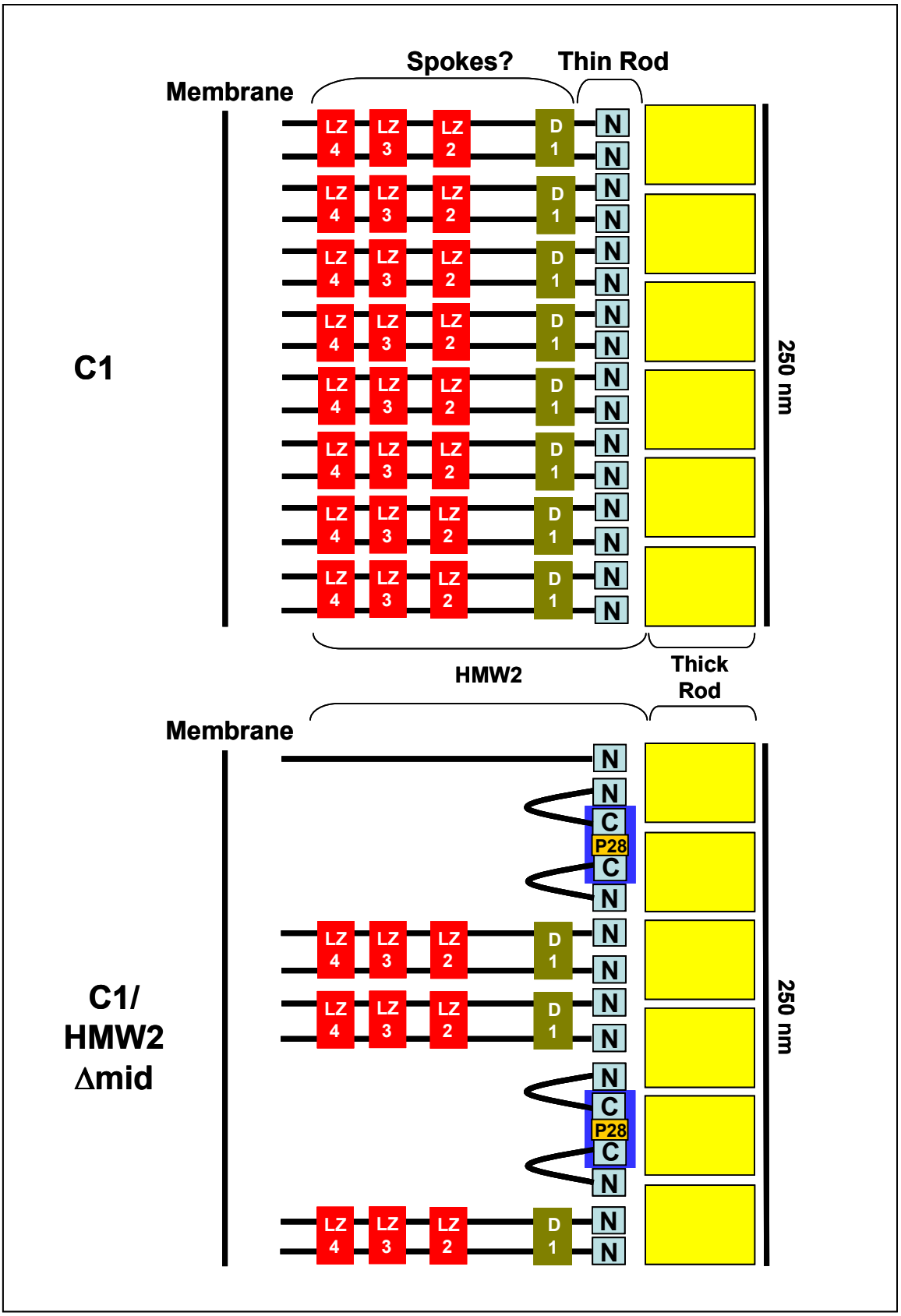
Spokes?
Thin Rod
Membrane
C1
LZ 4
LZ 3
LZ 2
D 1
N
250 nm
HMW2
Thick Rod
Membrane
C1/ HMW2 Δmid
C
P28
250 nm

Because of the instability of the thin rod, HMW2Δmid can easily interact with the rod between the HMW2 monomers, which are loosely bound to each other, and offers some stability by allowing for the formation of trimeric coiled-coil interactions between the C-termini and P28. However, this construct has no leucine repeats and thus, does not provide enough support for the thin rod to be stabilized in the region of the spokes (Fig. 5.2C). For the C1 mutant, the N-termini are stacked on top of each, as in I-2 and H9. However, the leucine repeats 3 and 4 are present, and thus partially stabilize the existing structure of the thin rod and allow for a semi-stable core to be apparent (Fig. 5.2D). Transformation of HMW2Δmid into C1 would provide a trimeric coiled-coil region and C-terminus, but the presence of the leucine zipper interactions 2, 3, and 4 in C1 may provide a level of stability that limits interactions with HMW2Δmid, as discussed previously with cytadherence (Fig. 5.2E). For the C1R1 mutant, the core structure is arranged as in wild-type, except that P28 is not present. Here, the lack of trimeric coiled-coil between the C-termini presumably decreases the length of the thin rod, giving the appearance of a shorter core in transmission electron micrographs of TX fractions of this strain (Fig. 5.2F). In this model, the thin rod would act as a scaffold to allow for formation of the thick rod. This would explain why no core is apparent in the absence of HMW2, where if HMW2 is not forming a thin rod, the thick rod either never forms or is very unstable. Interactions of the thin rod with membrane proteins could help to tether the core to the membrane, but no evidence of this is apparent at this time, other than the reciprocal relationship between HMW2 and HMW1.

HMW2 stability is independent of core formation. Thus, the HMW2 derivative in H9 was stable but did not form a core, while C1 produced a less stable HMW2

derivative but did form cores. However, core formation is dependent on stable interactions of HMW2 monomers, where as shown in the model, step-wise specific interactions stabilize the core. In I-2 and H9, the C-terminus, predicted trimeric coiled-coil 10, predicted dimeric coiled-coils 5 and 6, and leucine repeats (3-4) are missing, and thus prevent stabilizing interactions from occurring, such that the core falls apart or is not apparent. The presence of these regions allows for stable core formation. The regions required for stabilization of the core are also required for other cellular processes, linking core stability with normal functions of the cell. For example, for normal HMW1 stabilization, P1 localization, and gliding, the regions required for normal core formation, predicted trimeric coiled-coil 10, predicted dimeric coiled-coils (5-6), and leucine repeats (3-4), are essential. Leucine repeat domain 5 was also part of the region absent in strains that could not stabilize HMW1, localize P1, or glide; however, based on its absence in C1R1, which forms cores and stabilizes HMW1, as described above, it was not considered to contribute significantly to these processes. Another region that further stabilizes the core is predicted trimeric coiled-coil 7, which provides an additional interaction between HMW2 monomers near the C-terminal domain. This region, along with predicted trimeric coiled-coil 10 and the C-terminus of HMW2, allowed for normal hemadsorption and cellular morphology, as well.

Identification of the Components of the Core-Enriched Fraction

In order to define all components of the electron-dense core, we pursued various extractions to determine which yielded the purest cores. We generated a core-enriched fraction (CEF) with a series of treatments that included 2% TX/0.6 M KCl, 0.6 M KI/20%

sucrose, and 1 M guanidine-HCl. Analysis for membrane removal following each treatment in our core enrichment protocol, where ^{3}H-palmitic acid was used as a marker for the membrane, indicated that 99.9% of the membrane material was removed after extraction with 2% TX/0.6 M KCl. Our SDS-PAGE/silver stain analysis of the insoluble fraction following these three treatments demonstrated that the final insoluble fraction was much simpler than these resulting from 2% TX only, 2% TX/0.6 M KCl, or the 0.6 M KI/20% sucrose treatment. We analyzed this fraction by LC-MS/MS and identified 149 proteins as possible components of the core. One protein match was removed from this 149 based on poor peak score. In addition, fifty protein matches were removed based on the presence of a transmembrane domain, indicating association with the membrane and thus possible contaminants within the CEF. Finally, 9 ribosomal protein matches were removed as potential contaminants based on data showing that no ribosomes are present within the attachment organelle (Biberfeld and Biberfeld, 1970; Henderson and Jensen, 2006; Wilson and Collier, 1976). Thus, 89 proteins remained as components of the CEF. This was a surprisingly large number considering that a previous LC-MS/MS study only identified 41 proteins as components of the TX insoluble fraction (Regula *et al.*, 2001). We assumed that our CEF would contain less proteins than were found in the original TX-insoluble fraction. Interestingly, only 19 of the 41 proteins previously identified in the TX-insoluble fraction were identifical to proteins identified as components of the CEF. The discrepancy between the two studies can most likely be attributed to two factors. First, in our study, the CEF was loaded onto a C-18 column through the use of a nitrogen gas bomb. This prevents dilution of the sample that normally occurs when running a traditional liquid chromatography full-length C-18

column, as was done previously (Regula *et al.*, 2001). Second, our peptide readings were measured by an LTQ linear ion trap mass spectrometer, which has better peptide coverage and protein identification, greater sensitivity, higher confidence values, and requires less time than the LCQ linear ion trap mass spectrometer used in the previous study (Regula *et al.*, 2001).

Because the core-enriched fraction admittedly only enriches for cores and does not isolate them completely, not all of the components isolated as part of that fraction are necessarily components of the core. Because we predicted that the cytadherence accessory protein HMW2 forms the thin rod, it was not surprising that HMW2 was the most abundant protein in the CEF. Thus, we predict that other proteins within the CEF comprise the remaining portion of the core, which includes the terminal button, thick rod, and wheel-like base. Predictions, based on previous data, allowed us to suggest which proteins or groups of proteins could conceivably form the core.

Several cytadherence associated proteins were found to be part of the CEF, including HMW1, HMW3, P41, and P200. We considered each of these individually as to their significance in the fraction. First, HMW1 localizes along the edge of the attachment organelle associated with the membrane, on the surface and inside the cell. Based on this localization pattern, HMW1 has not been predicted to be part of the core, thus its inclusion in the CEF could merely be attributed to interactions with protein components of the core (Stevens and Krause, 1991). Recently, a reciprocal relationship was demonstrated between HMW1 and HMW2, based on the presence of reduced levels of each in the absence of the other (Willby *et al.*, 2004). HMW1 contains two cysteine residues that have been predicted, based on DISULFIND, to bind to each

other. However, in the presence of free cysteine residues in HMW2, disulfide exchange might result in bond formation between HMW1 and HMW2, such that HMW1 would be associated with the CEF. Based on previous treatments of cores with 2-mercaptoethanol, where cores remained intact, disulfide bonding between HMW1 and HMW2 does not contribute to stabilization of the core. However, the fact that a core is not formed in the absence of stable HMW1 suggests that interactions with HMW1, not necessarily involving its cysteine residues, contribute to core stabilization (Figs. 2.8, 2.9). Although the C-terminus of HMW1 is required for HMW2 stability and localization in the attachment organelle (Willby *et al.*, 2004), two dimeric coiled-coils near the C-terminus of HMW1 (784-816, 849-877aa) may provide a means for HMW1 to interact with HMW2 and stabilize the core. Despite a possible interaction with HMW2 to stabilize the core, HMW1 levels are reduced in the C1/HMW2∆mid mutant, which forms an unstable core. We have established that certain regions of HMW2 must be contiguous for HMW1 stabilization. This may indicate that certain spatial positioning of HMW2 in the core is required for HMW1-HMW2 interactions to occur, since we assume that electron-lucent space on either side of the core would physically separate HMW1 from HMW2 and a specific length of HMW2 may be needed to cross this barrier. Second, HMW3 localizes to the terminal button, a component of the core, and is predicted to wrap around the core (Stevens and Krause, 1992). Furthermore, a core is present in the absence of HMW3, although the core appears as a chevron-shape, where the two rods are split apart at the base (Willby *et al.*, 2004). Thus, HMW3 is not required for core stability, but for maintaining a normal core conformation. The close proximity of HMW3 to the core, and thus HMW2, could explain why fewer regions of

HMW2 are required for HMW3 stabilization than for HMW1 and why an unstable core in C1/HMW2Δmid can stabilize HMW3, but not HMW1. HMW3 stabilizes P65 (Willby and Krause, 2002), most likely due to the position of HMW3 in the attachment organelle near the extreme tip of the cell, where P65 is localized. Thus, the same regions of HMW2 required for HMW3 stabilization are required for P65. Third, P41 localizes to the base of the core, possibly as the wheel-like structure considered to be a component of the core (Hasselbring and Krause, 2007; Seto and Miyata, 2003). Continued TEM analysis of strains without cores and the P41- strain (Hasselbring and Krause, 2007) may allow us to determine if the core or the wheel can form without the other. Lastly, P200 has been localized to the attachment organelle (Jordan *et al.*, 2007) and thus, cannot be excluded as a component of the core.

Because no ribosomes are apparent in the attachment organelle (Biberfeld and Biberfeld, 1970; Wilson and Collier, 1976), we predict that protein synthesis must take place elsewhere in the cell. Furthermore, if protein synthesis does not occur in the attachment organelle, it would seem inefficient of the cell to transcribe mRNA in the attachment organelle. Thus, the proteins and enzymes specifically related to transcription and translation may not be localized to the core structure. However, the evidence is clear that they are present in our CEF. Perhaps because of the size of the RNA polymerase complex, its sedimentation along with the core-enriched fraction could explain its presence. Decreased length of centrifugation of the fraction may be necessary to prevent this from occurring. In addition, passage of the CEF through a sucrose cushion may remove the complex as well, or any other large complexes that are not part of the core. Based on the prediction that protein synthesis occurs outside

of the tip structure, proteins that localize to the attachment organelle must be transported to this structure. Thus, the presence of transport proteins and chaperones within the CEF seems reasonable for proper localization and protein folding to occur. However, these types of proteins would most likely be located all over the cell and not restricted to the thick rod of the core.

Recently, the RNA degradosome was isolated as a new cytoskeletal component in *E. coli* in a study to identify proteins that interact with MinD (Taghbalout and Rothfield, 2007). The degradosome includes RNaseE, RNA helicase B, polynucleotide phosphorylase, and enolase and is responsible for degrading mRNAs and for processing tRNA and rRNA (Taghbalout and Rothfield, 2007). It was shown to form a helical structure along the length of the cell extending to the cell poles, reminiscent of the localization pattern of other cytoskeletal proteins in *E. coli*, MinD and MreB (Shih *et al.*, 2003) and MreB in *B. subtilis* (Jones *et al.*, 2001), which also helically wind along the length of the cell. This RNaseE is thought to be the backbone onto which the degradosome forms and although RNaseE was found to interact with MinD, this complex is formed independent from MinD and MreB (Taghbalout and Rothfield, 2007). One of the component proteins of the RNA degradosome, enolase in *E. coli*, was found in the CEF of *M. pneumoniae*, but was discarded because of its predicted membrane association, based on the presence of a transmembrane domain. However, ribonuclease R was present, but unlike PNPase, has been shown in *E. coli* to act independently of a helicase, and thus independent of the formation of a complex of enzymes for normal mRNA degradation to occur.

DNA replication machinery could associate with the core, considering that cell division begins with the formation of a new tip structure (Hasselbring *et al.*, 2006a; Seto, 2000), and presumably a core. A previous study in *M. gallisepticum* indicating that a DNA complex was present in the bleb, the attachment organelle equivalent (Maniloff and Quinlan, 1974), is evidence in support of the presence of DNA replication proteins and transcription factors in that region. Although a DNA complex is not an integral part of the core of *M. pneumoniae*, based on treatments of the cores with DNase where the core remains intact (this study), DAPI-stained DNA is apparent behind P1 in another study (Seto *et al.*, 2001). This could suggest that the DNA complex of *M. pneumoniae* is located in the cell body adjacent to the attachment organelle. Since cell division originates in the attachment organelle with replication of the core, if DNA attaches to the core for separation of daughter chromosomes, then the DNA replication and transcription proteins in the CEF would have easy access to the DNA complex.

Previously, the idea of an “enzoskeleton” was proposed in a study of *E. coli*, which is a predicted superstructure that forms due to linkages between complexes of metabolic enzymes, membranes, nucleic acids, and cytoskeletal structures, resembling those in eukaryotes, within the cell (Norris *et al.*, 1996). Metabolic enzymes were identified in the CEF of *M. pneumoniae*, including enzymes involved in glycolysis and a component of both the pyruvate dehydrogenase complex and the ATP synthase complex. However, we do not know at present if these enzymes are part of an enzoskeleton-like structure.

Although the cytoskeleton of *M. pneumoniae* was first described over 25 years ago, only recently have proteins been identified that comprise this ultrastructural feature

of the cell (Regula *et al.*, 2001). Even then, the proteins were not assigned to specific structures of the cytoskeleton. This study is the first attempt to determine the precise components of the electron-dense core, a major structural element of the cytoskeleton. Previously, cytoskeletal proteins, which confer specific functions in the cell, have been identified in other organisms. MreB, actin homolog, found in *E. coli* and *B. subtilis* has been shown to be essential for maintaining cell shape and form helical structures along the length of the cell (Jones *et al.*, 2001; Shih *et al.*, 2003). The MreB protein in *Caulobacter crescentus* has been shown to have a role in determination of the polarity of bacterial cells (Gitai *et al.*, 2004). In addition, the MinCDE proteins in *E. coli* also form a helical structure, along the length of the cell and oscillate between the cell poles to prevent premature or displaced division of the cell (Shih *et al.*, 2003). *Spiroplasma melliferum* has two cytoskeletal proteins MreB and a 55-kDa fibril protein that comprise the filaments that run the length of the cell and are thought to allow for cell movement (Kurner *et al.*, 2005). No actin, MreB, or MinCDE homologs have been identified in *M. pneumoniae* and because of this, its cytoskeleton appears to be unlike those for other genera of bacteria (Balish and Krause, 2006). The lack of known cytoskeletal proteins in *M. pneumoniae* suggests that this scaffold of the cell may consist of novel cytoskeletal proteins. However, the minimalist nature of mycoplasmas raises the possibility that some proteins may have evolved to have more than 1 function. For instance, elongation factor Tu and the E1 β subunit of the pyruvate dehydrogenase complex have been hypothesized to act as additional adhesin proteins in *M. pneumoniae*, based on their ability to bind to fibronectin (Dallo *et al.*, 2002). Thus, it remains to be seen if other proteins in *M. pneumoniae* also have dual functions, one of

which is to form the cytoskeleton. Further studies will hopefully identify these and novel proteins specifically, along with their function as components of the cytoskeleton to shed new light on cytoskeletons in mycoplasmas, and bacteria in general.

Futher experiments will be required for a more precise identification of the components of the core. LC/MS-MS of other HMW2 mutants that do not have cores, as well as analysis of further purified samples, may allow for better differentiation of exactly which components are part of the core structure. In the age of electron cryotomography, further examination of HMW2 mutant strains would allow for a more detailed view of the core and may identify the presence of cores or core elements that were not localized to the correct location in the attachment organelle (Henderson and Jensen, 2006). This detailed view of the core may also allow us to see differences in the cores that were not visible by TEM analysis. Production of fluorescent protein fusions for specific proteins found in the CEF would be useful for localization experiments in wild-type and mutant strains of *M. pneumoniae* to determine if the core components are present elsewhere in the cell. Then, time studies with the protein fusions could allow us to visualize the assembly of the core, both the order and timing. Finally, solving the crystal structure for HMW2 and the proteins that form the core, may aid in our understanding of core formation.

CHAPTER VI

REFERENCES

Alexander, E.R., Foy, H.M., Kenny, G.E., Kronmal, R.A., McMahan, R., Clarke, E.R., MacColl, W.A., and Grayston, J.T. (1966) Pneumonia due to *Mycoplasma pneumoniae*. Its incidence in the membership of a co-operative medical group. *N Engl J Med* 275: 131-136.

Alvarez-Manilla, G., Atwood, J., 3rd, Guo, Y., Warren, N.L., Orlando, R., and Pierce, M. (2006) Tools for glycoproteomic analysis: size exclusion chromatography facilitates identification of tryptic glycopeptides with N-linked glycosylation sites. *J Proteome Res* 5: 701-708.

Balish, M.F., Hahn, T.W., Popham, P.L., and Krause, D.C. (2001) Stability of *Mycoplasma pneumoniae* cytadherence-accessory protein HMW1 correlates with its association with the triton shell. *J Bacteriol* 183: 3680-3688.

Balish, M.F., and Krause, D.C. (2002) Cytadherence and the Cytoskeleton. In *Molecular Biology and Pathogenicity of Mycoplasmas*. Razin, S., and R. Herrmann (ed). New York: Kluwer Academic/Plenum Publishers, pp. 491-518.

Balish, M.F., Ross, S.M., Fisseha, M., and Krause, D.C. (2003a) Deletion analysis identifies key functional domains of the cytadherence-associated protein HMW2 of *Mycoplasma pneumoniae*. *Mol Microbiol* 50: 1507-1516.

Balish, M.F., Santurri, R.T., Ricci, A.M., Lee, K.K., and Krause, D.C. (2003b) Localization of *Mycoplasma pneumoniae* cytadherence-associated protein HMW2 by fusion with green fluorescent protein: implications for attachment organelle structure. *Mol Microbiol* 47: 49-60.

Balish, M.F., and Krause, D.C. (2006) Mycoplasmas: a distinct cytoskeleton for wall-less bacteria. *J Mol Microbiol Biotechnol* 11: 244-255.

Baseman, J.B., Cole, R.M., Krause, D.C., and Leith, D.K. (1982) Molecular basis for cytadsorption of *Mycoplasma pneumoniae*. *J Bacteriol* 151: 1514-1522.

Baseman, J.B., Morrison-Plummer, J., Drouillard, D., Puleo-Scheppke, B., Tryon, V.V., and Holt, S.C. (1987) Identification of a 32-kilodalton protein of *Mycoplasma pneumoniae* associated with hemadsorption. *Isr J Med Sci* 23: 474-479.

Biberfeld, G., and Biberfeld, P. (1970) Ultrastructural features of *Mycoplasma pneumoniae*. *J Bacteriol* 102: 855-861.

Boguslavsky, S., Menaker, D., Lysnyansky, I., Liu, T., Levisohn, S., Rosengarten, R., Garcia, M., and Yogev, D. (2000) Molecular characterization of the *Mycoplasma gallisepticum* pvpA gene which encodes a putative variable cytadhesin protein. *Infect Immun* 68: 3956-3964.

Bove, J.M. (1999) The one-hundredth anniversary of the first culture of a mollicute, the contagious bovine peripneumonia microbe, by Nocard and Roux, with the collaboration of Borrel, Salimbeni, and Dujardin-Baumetz. *Res Microbiol* 150: 239-245.

Bredt, W. (1968) Motility and multiplication of *Mycoplasma pneumoniae.* A phase contrast study. *Pathol Microbiol (Basel)* 32: 321-326.

Carson, J.L., H. Ping-Chuan, A.M. Collier (1992) Cell Structural and Functional Elements. In *Mycoplasmas: Molecular Biology and Pathogenesis*. Maniloff, J., R.N. McElhaney, L.R. Finch, J.B. Baseman (ed). Washington, D.C.: American Society for Microbiology, pp. 63-72.

Chanock, R.M., Hayflick, L., and Barile, M.F. (1962) Growth on artificial medium of an agent associated with atypical pneumonia and its identification as a PPLO. *Proc Natl Acad Sci U S A* 48: 41-49.

Chanock, R.M. (1963) *Mycoplasma pneumoniae*: proposed nomenclature for atypical pneumonia organism (Eaton agent). *Science* 140: 662.

Cloward, J., and Krause, D.C. (unpublished data).

Clyde, W.A., Jr. (1961) Demonstration of Eaton's agent in tissue culture. *Proc Soc Exp Biol Med* 107: 715-718.

Clyde, W.A., Jr. (1979) *Mycoplasma pneumoniae* infections of man. In *The mycoplasmas II: Human and animal mycoplasmas*. Vol. II. Tully, J.G.a.W.R.F. (ed). New York: Academic Press, pp. 275-306.

Collier, A.M., and Clyde, W.A. (1971) Relationships Between *Mycoplasma pneumoniae* and Human Respiratory Epithelium. *Infect Immun* 3: 694-701.

Collier, A.M., and Baseman, J.B. (1973) Organ culture techniques with mycoplasmas. *Ann. N. Y. Acad. Sci.* 225: 277-289.

Collier, A.M., Hu, P.C., and Clyde, W.A., Jr. (1983) Location of attachment moiety on *Mycoplasma pneumoniae*. *Yale J Biol Med* 56: 671-677.

Dallo, S.F., Su, C.J., Horton, J.R., and Baseman, J.B. (1988) Identification of P1 gene domain containing epitope(s) mediating *Mycoplasma pneumoniae* cytoadherence. *J Exp Med* 167: 718-723.

Dallo, S.F., Chavoya, A., and Baseman, J.B. (1990) Characterization of the gene for a 30-kilodalton adhesion-related protein of *Mycoplasma pneumoniae*. *Infect Immun* 58: 4163-4165.

Dallo, S.F., Lazzell, A.L., Chavoya, A., Reddy, S.P., and Baseman, J.B. (1996) Biofunctional domains of the *Mycoplasma pneumoniae* P30 adhesin. *Infect Immun* 64: 2595-2601.

Dallo, S.F., Kannan, T.R., Blaylock, M.W., and Baseman, J.B. (2002) Elongation factor Tu and E1 beta subunit of pyruvate dehydrogenase complex act as fibronectin binding proteins in *Mycoplasma pneumoniae*. *Mol Microbiol* 46: 1041-1051.

Dandekar, T., B. Snel, S. Schmidt, W. Lathe, M. Suyama, M. Huynene, P. Bork (2002) Comparative Genome Analysis of the Mollicutes. In *Molecular Biology and Pathogenicity of Mycoplasmas*. Razin, S., and R. Herrmann (ed). New York: Kluwer Academic/Plenum Publishers, pp. 255-278.

Dhandayuthapani, S., Rasmussen, W.G., and Baseman, J.B. (1999) Disruption of gene mg218 of *Mycoplasma genitalium* through homologous recombination leads to an adherence-deficient phenotype. *Proc Natl Acad Sci U S A* 96: 5227-5232.

Dhandayuthapani, S., Rasmussen, W.G., and Baseman, J.B. (2002) Stability of cytadherence-related proteins P140/P110 in *Mycoplasma genitalium* requires MG218 and unidentified factors. *Arch Med Res* 33: 1-5.

Dienes, L. (1940) Cultivation of pleuropneumonia-like organisms from female genital organs. *Proc. Soc. Exp. Biol. Med.* 44: 468-469.

Dirksen, L.B., Krebes, K.A., and Krause, D.C. (1994) Phosphorylation of cytadherence-accessory proteins in *Mycoplasma pneumoniae*. *J Bacteriol* 176: 7499-7505.

Dirksen, L.B., Proft, T., Hilbert, H., Plagens, H., Herrmann, R., and Krause, D.C. (1996) Sequence analysis and characterization of the hmw gene cluster of *Mycoplasma pneumoniae*. *Gene* 171: 19-25.

Domermuth, C.H., Nielsen, M.H., Freundt, E.A., and Birch-Andersen, A. (1964) Ultrastructure of *Mycoplasma species*. *J Bacteriol* 88: 727-744.

Dorigo-Zetsma, J.W., Wilbrink, B., Dankert, J., and Zaat, S.A. (2001) *Mycoplasma pneumoniae* P1 type 1- and type 2-specific sequences within the P1 cytadhesin gene of individual strains. *Infect Immun* 69: 5612-5618.

Dybvig, K. (1990) Mycoplasmal genetics. *Annu Rev Microbiol* 44: 81-104.

Dybvig, K., and Voelker, L.L. (1996) Molecular biology of mycoplasmas. *Annu Rev Microbiol* 50: 25-57.

Eaton, M.D. (1965) Pleuropneumonia-like organisms and related forms. *Annu Rev Microbiol* 19: 379-406.

Edward, D.G., and Freundt, E.A. (1956) The classification and nomenclature of organisms of the pleuropneumonia group. *J Gen Microbiol* 14: 197-207.

Edward, D.G., Freundt, E.A., Chanock, R.M., Fabricant, J., Hayflick, L., Lemcke, R.M., Rezin, S., Somerson, N.L., and Wittler, R.G. (1967) Recommendations on nomenclature of the order Mycoplasmatales. *Science* 155: 1694-1696.

Feldner, J., Gobel, U., and Bredt, W. (1982) *Mycoplasma pneumoniae* adhesin localized to tip structure by monoclonal antibody. *Nature* 298: 765-767.

Fisseha, M., Gohlmann, H.W., Herrmann, R., and Krause, D.C. (1999) Identification and complementation of frameshift mutations associated with loss of cytadherence in *Mycoplasma pneumoniae*. *J Bacteriol* 181: 4404-4410.

Franzoso, G., Hu, P.C., Meloni, G.A., and Barile, M.F. (1993) The immunodominant 90-kilodalton protein is localized on the terminal tip structure of *Mycoplasma pneumoniae*. *Infect Immun* 61: 1523-1530.

Freundt, E.A., and Razin, S. (1984) Mycoplasma. In *Bergey's Manual of Systemic Bacteriology*. Vol. I. Holt, J.G. (ed). Baltimore: Williams and Wilkins, pp. 742-770.

Gerstenecker, B., and Jacobs, E. (1990) Topological mapping of the P1-adhesin of *Mycoplasma pneumoniae* with adherence-inhibiting monoclonal antibodies. *J Gen Microbiol* 136: 471-476.

Gitai, Z., Dye, N., and Shapiro, L. (2004) An actin-like gene can determine cell polarity in bacteria. *Proc Natl Acad Sci U S A* 101: 8643-8648.

Gobel, U., Speth, V., and Bredt, W. (1981) Filamentous structures in adherent *Mycoplasma pneumoniae* cells treated with nonionic detergents. *J Cell Biol* 91: 537-543.

Goh, M.S., Gorton, T.S., Forsyth, M.H., Troy, K.E., and Geary, S.J. (1998) Molecular and biochemical analysis of a 105 kDa *Mycoplasma gallisepticum* cytadhesin (GapA). *Microbiology* 144 (Pt 11): 2971-2978.

Goodburn, G.M., Marmion, B.P., and Kendall, E.J. (1963) Infection with Eaton's primary atypical pneumonia agent in England. *Br Med J* 5340: 1266-1270.

Hackett, K.J., and Whitcomb, R.F. (1995) Cultivation of spiroplasmas in undefined and defined media. In *Molecular and diagnostic procedures in mycoplasmology*. Vol. 1. Razin, S., and J.G. Tully (ed). New York: Academic Press, Inc., pp. 41-54.

Hahn, T.W., Krebes, K.A., and Krause, D.C. (1996) Expression in *Mycoplasma pneumoniae* of the recombinant gene encoding the cytadherence-associated protein HMW1 and identification of HMW4 as a product. *Mol Microbiol* 19: 1085-1093.

Hahn, T.W., Willby, M.J., and Krause, D.C. (1998) HMW1 is required for cytadhesin P1 trafficking to the attachment organelle in *Mycoplasma pneumoniae*. *J Bacteriol* 180: 1270-1276.

Hahn, T.W., Mothershed, E.A., Waldo, R.H., 3rd, and Krause, D.C. (1999) Construction and analysis of a modified Tn4001 conferring chloramphenicol resistance in *Mycoplasma pneumoniae*. *Plasmid* 41: 120-124.

Hansen, E.J., Wilson, R.M., and Baseman, J.B. (1979a) Isolation of mutants of *Mycoplasma pneumoniae* defective in hemadsorption. *Infect Immun* 23: 903-906.

Hansen, E.J., Wilson, R.M., and Baseman, J.B. (1979b) Two-dimensional gel electrophoretic comparison of proteins from virulent and avirulent strains of *Mycoplasma pneumoniae*. *Infect Immun* 24: 468-475.

Hansen, E.J., Wilson, R.M., Clyde, W.A., Jr., and Baseman, J.B. (1981) Characterization of hemadsorption-negative mutants of *Mycoplasma pneumoniae*. *Infect Immun* 32: 127-136.

Hasselbring, B.M., Jordan, J.L., and Krause, D.C. (2005) Mutant analysis reveals a specific requirement for protein P30 in *Mycoplasma pneumoniae* gliding motility. *J Bacteriol* 187: 6281-6289.

Hasselbring, B.M., Jordan, J.L., Krause, R.W., and Krause, D.C. (2006a) Terminal organelle development in the cell wall-less bacterium *Mycoplasma pneumoniae*. *Proc Natl Acad Sci U S A* 103: 16478-16483.

Hasselbring, B.M., Page, C.A., Sheppard, E.S., and Krause, D.C. (2006b) Transposon mutagenesis identifies genes associated with *Mycoplasma pneumoniae* gliding motility. *J Bacteriol* 188: 6335-6345.

Hasselbring, B.M., and Krause, D.C. (2007) Cytoskeletal protein P41 is required to anchor the terminal organelle of the wall-less prokaryote *Mycoplasma pneumoniae*. *Mol Microbiol* 63: 44-53.

Hasselbring, B.M., and Krause, D.C. (unpublished data).

Hasselbring, B.M., Sheppard, E.S., and Krause, D.C. (unpublished data).

Hayflick, L. (1965) Tissue cultures and mycoplasmas. *Tex Rep Biol Med* 23: Suppl 1:285+.

Hedreyda, C.T., Lee, K.K., and Krause, D.C. (1993) Transformation of *Mycoplasma pneumoniae* with Tn4001 by electroporation. *Plasmid* 30: 170-175.

Hedreyda, C.T., and Krause, D.C. (1995) Identification of a possible cytadherence regulatory locus in *Mycoplasma pneumoniae*. *Infect Immun* 63: 3479-3483.

Hegermann, J., Herrmann, R., and Mayer, F. (2002) Cytoskeletal elements in the bacterium *Mycoplasma pneumoniae*. *Naturwissenschaften* 89: 453-458.

Henderson, G.P., and Jensen, G.J. (2006) Three-dimensional structure of *Mycoplasma pneumoniae*'s attachment organelle and a model for its role in gliding motility. *Mol Microbiol* 60: 376-385.

Henderson, G.P., and Jensen, G.J. (unpublished data).

Herrmann, H., and Wiche, G. (1983) Specific in situ phosphorylation of plectin in detergent-resistant cytoskeletons from cultured Chinese hamster ovary cells. *J Biol Chem* 258: 14610-14618.

Himmelreich, R., Hilbert, H., Plagens, H., Pirkl, E., Li, B.C., and Herrmann, R. (1996) Complete sequence analysis of the genome of the bacterium *Mycoplasma pneumoniae*. *Nucleic Acids Res* 24: 4420-4449.

Hu, P.C., Collier, A.M., and Baseman, J.B. (1975) Alterations in the metabolism of hamster tracheas in organ culture after infection by virulent *Mycoplasma pneumoniae*. *Infect Immun* 11: 704-710.

Hu, P.C., Collier, A.M., and Baseman, J.B. (1976) Interaction of virulent *Mycoplasma pneumoniae* with hamster tracheal organ cultures. *Infect Immun* 14: 217-224.

Hu, P.C., Collier, A.M., and Baseman, J.B. (1977) Surface parasitism by *Mycoplasma pneumoniae* of respiratory epithelium. *J Exp Med* 145: 1328-1343.

Hu, P.C., Cole, R.M., Huang, Y.S., Graham, J.A., Gardner, D.E., Collier, A.M., and Clyde, W.A., Jr. (1982) *Mycoplasma pneumoniae* infection: role of a surface protein in the attachment organelle. *Science* 216: 313-315.

Hu, P.C., Schaper, U., Collier, A.M., Clyde, W.A., Jr., Horikawa, M., Huang, Y.S., and Barile, M.F. (1987) A *Mycoplasma genitalium* protein resembling the *Mycoplasma pneumoniae* attachment protein. *Infect Immun* 55: 1126-1131.

Inamine, J.M., Denny, T.P., Loechel, S., Schaper, U., Huang, C.H., Bott, K.F., and Hu, P.C. (1988a) Nucleotide sequence of the P1 attachment-protein gene of *Mycoplasma pneumoniae*. *Gene* 64: 217-229.

Inamine, J.M., Loechel, S., and Hu, P.C. (1988b) Analysis of the nucleotide sequence of the P1 operon of *Mycoplasma pneumoniae*. *Gene* 73: 175-183.

Inamine, J.M., Loechel, S., Collier, A.M., Barile, M.F., and Hu, P.C. (1989) Nucleotide sequence of the MgPa (mgp) operon of *Mycoplasma genitalium* and comparison to the P1 (mpp) operon of *Mycoplasma pneumoniae*. *Gene* 82: 259-267.

Inamine, J.M., Ho, K.C., Loechel, S., and Hu, P.C. (1990) Evidence that UGA is read as a tryptophan codon rather than as a stop codon by *Mycoplasma pneumoniae*, *Mycoplasma genitalium*, and *Mycoplasma gallisepticum*. *J Bacteriol* 172: 504-506.

Jacobs, E., Rock, R., and Dalehite, L. (1990) A B cell-, T cell-linked epitope located on the adhesin of *Mycoplasma pneumoniae*. *Infect Immun* 58: 2464-2469.

Jones, L.J., Carballido-Lopez, R., and Errington, J. (2001) Control of cell shape in bacteria: helical, actin-like filaments in *Bacillus subtilis*. *Cell* 104: 913-922.

Jordan, J.L., Berry, K.M., Balish, M.F., and Krause, D.C. (2001) Stability and subcellular localization of cytadherence-associated protein P65 in *Mycoplasma pneumoniae*. *J Bacteriol* 183: 7387-7391.

Jordan, J.L., Chang, H.Y., Balish, M.F., Holt, L.S., Bose, S.R., Hasselbring, B.M., Waldo, R.H., 3rd, Krunkosky, T.M., and Krause, D.C. (2007) Protein P200 is Dispensable for *Mycoplasma pneumoniae* Hemadsorption but not Gliding Motility or Colonization of Differentiated Bronchial Epithelium. *Infect Immun* 75: 518-522.

Kahane, I., Tucker, S., Leith, D.K., Morrison-Plummer, J., and Baseman, J.B. (1985) Detection of the major adhesin P1 in triton shells of virulent *Mycoplasma pneumoniae*. *Infect Immun* 50: 944-946.

Keeler, C.L., Jr., Hnatow, L.L., Whetzel, P.L., and Dohms, J.E. (1996) Cloning and characterization of a putative cytadhesin gene (mgc1) from *Mycoplasma gallisepticum*. *Infect Immun* 64: 1541-1547.

Kenri, T., Taniguchi, R., Sasaki, Y., Okazaki, N., Narita, M., Izumikawa, K., Umetsu, M., and Sasaki, T. (1999) Identification of a new variable sequence in the P1 cytadhesin gene of *Mycoplasma pneumoniae*: evidence for the generation of antigenic variation by DNA recombination between repetitive sequences. *Infect Immun* 67: 4557-4562.

Kenri, T., Seto, S., Horino, A., Sasaki, Y., Sasaki, T., and Miyata, M. (2004) Use of fluorescent-protein tagging to determine the subcellular localization of *Mycoplasma pneumoniae* proteins encoded by the cytadherence regulatory locus. *J Bacteriol* 186: 6944-6955.

Kirchoff, H. (1992) Motility. In *Mycoplasmas: Molecular Biology and Pathogenesis*. Maniloff, J., R.N. McElhaney, L.R. Finch, J.B. Baseman (ed). Washington, D.C.: American Society for Microbiology, pp. 289-306.

Krause, D.C., and Baseman, J.B. (1982) *Mycoplasma pneumoniae* proteins that selectively bind to host cells. *Infect Immun* 37: 382-386.

Krause, D.C., Leith, D.K., Wilson, R.M., and Baseman, J.B. (1982) Identification of *Mycoplasma pneumoniae* proteins associated with hemadsorption and virulence. *Infect Immun* 35: 809-817.

Krause, D.C., Leith, D.K., and Baseman, J.B. (1983) Reacquisition of specific proteins confers virulence in *Mycoplasma pneumoniae*. *Infect Immun* 39: 830-836.

Krause, D.C., and Mawn, C.B. (1990) Physical analysis and mapping of the *Mycoplasma pneumoniae* chromosome. *J Bacteriol* 172: 4790-4797.

Krause, D.C., and Lee, K.K. (1991) Juxtaposition of the genes encoding *Mycoplasma pneumoniae* cytadherence-accessory proteins HMW1 and HMW3. *Gene* 107: 83-89.

Krause, D.C., and Taylor-Robinson, D. (1992) Mycoplasma which infect humans. In *Mycoplasmas: Molecular Biology and Pathogenesis*. Maniloff, J., McElhaney, R. N., Finch, L. R., Baseman, J.B. (ed). Wahsington, D.C.: American Society for Microbiology, pp. 417-444.

Krause, D.C. (1996) *Mycoplasma pneumoniae* cytadherence: unravelling the tie that binds. *Mol Microbiol* 20: 247-253.

Krause, D.C., Proft, T., Hedreyda, C.T., Hilbert, H., Plagens, H., and Herrmann, R. (1997) Transposon mutagenesis reinforces the correlation between *Mycoplasma pneumoniae* cytoskeletal protein HMW2 and cytadherence. *J Bacteriol* 179: 2668-2677.

Krause, D.C., and Balish, M.F. (2001) Structure, function, and assembly of the terminal organelle of *Mycoplasma pneumoniae*. *FEMS Microbiol Lett* 198: 1-7.

Krause, D.C., and Balish, M.F. (2004) Cellular engineering in a minimal microbe: structure and assembly of the terminal organelle of *Mycoplasma pneumoniae*. *Mol Microbiol* 51: 917-924.

Krause, D.C., Jordan, J.L., Chang, H.-Y., Park, H.K., and Krunkosky, T.M. (2007) Mycoplasma pneumoniae attachment and colonization of the respiratory mucosa. In *Virulence Mechanisms of Bacterial Pathogens*. Brogden, K.A., Minion, F.C., Stanton, T.B., Zhang, Q., Nolan, L., J., M. and Wannemuehler (eds). Washington, D.C.: ASM Press, In press.

Krebes, K.A., Dirksen, L.B., and Krause, D.C. (1995) Phosphorylation of *Mycoplasma pneumoniae* cytadherence-accessory proteins in cell extracts. *J Bacteriol* 177: 4571-4574.

Kurner, J., Frangakis, A.S., and Baumeister, W. (2005) Cryo-electron tomography reveals the cytoskeletal structure of *Spiroplasma melliferum*. *Science* 307: 436-438.

Laemmli, U.K. (1970) Cleavage of structural proteins during the assembly of the head of bacteriophage T4. *Nature* 227: 680-685.

Layh-Schmitt, G., and Herrmann, R. (1992) Localization and biochemical characterization of the ORF6 gene product of the *Mycoplasma pneumoniae* P1 operon. *Infect Immun* 60: 2906-2913.

Layh-Schmitt, G. (1993) The ORF6 gene product of the P1 operon of *Mycoplasma pneumoniae*. *Zentralbl Bakteriol* 278: 287-295.

Layh-Schmitt, G., and Herrmann, R. (1994) Spatial arrangement of gene products of the P1 operon in the membrane of *Mycoplasma pneumoniae*. *Infect Immun* 62: 974-979.

Layh-Schmitt, G., Hilbert, H., and Pirkl, E. (1995) A spontaneous hemadsorption-negative mutant of *Mycoplasma pneumoniae* exhibits a truncated adhesin-related 30-kilodalton protein and lacks the cytadherence-accessory protein HMW1. *J Bacteriol* 177: 843-846.

Layh-Schmitt, G., Himmelreich, R., and Leibfried, U. (1997) The adhesin related 30-kDa protein of *Mycoplasma pneumoniae* exhibits size and antigen variability. *FEMS Microbiol Lett* 152: 101-108.

Layh-Schmitt, G., and Harkenthal, M. (1999) The 40- and 90-kDa membrane proteins (ORF6 gene product) of *Mycoplasma pneumoniae* are responsible for the tip structure formation and P1 (adhesin) association with the Triton shell. *FEMS Microbiol Lett* 174: 143-149.

Layh-Schmitt, G., Podtelejnikov, A., and Mann, M. (2000) Proteins complexed to the P1 adhesin of *Mycoplasma pneumoniae*. *Microbiology* 146 (Pt 3): 741-747.

Mader, B., Hu, P.C., Huang, C.H., Schilz, E., and Jacobs, E. (1991) The mature MgPa-adhesin of *Mycoplasma genitalium*. *Zentralbl Bakteriol* 274: 507-513.

Mahairas, G.G., and Minion, F.C. (1989) Transformation of *Mycoplasma pulmonis*: demonstration of homologous recombination, introduction of cloned genes, and preliminary description of an integrating shuttle system. *J Bacteriol* 171: 1775-1780.

Maniloff, J., and Quinlan, D.C. (1974) Partial purification of a membrane-associated deoxyribonucleic acid complex from *Mycoplasma gallisepticum*. *J Bacteriol* 120: 495-501.

Maniloff, J. (2002) Phylogeny and Evolution. In *Molecular Biology and Pathogenicity of Mycoplasmas*. Razin, S., and R. Herrmann (ed). New York: Kluwer Academic/Plenum Publishers, pp. 31-43.

Marmion, B.P. (1990) Eaton agent--science and scientific acceptance: a historical commentary. *Rev Infect Dis* 12: 338-353.

May, M., Papazisi, L., Gorton, T.S., and Geary, S.J. (2006) Identification of fibronectin-binding proteins in *Mycoplasma gallisepticum* strain R. *Infect Immun* 74: 1777-1785.

Meiklejohn, G., Eaton, M.D., and van Herick, W. (1945) A Clinical Report on Cases of Primary Atypical Pneumonia Caused by a New Virus. *J Clin Invest* 24: 241-250.

Meng, K.E., and Pfister, R.M. (1980) Intracellular structures of *Mycoplasma pneumoniae* revealed after membrane removal. *J Bacteriol* 144: 390-399.

Mollenhauer, H.H., and Whaley, W.G. (1963) An observation on the functioning of the Golgi apparatus. *J Cell Biol* 17: 222-225.

Morrison-Plummer, J., Lazzell, A., and Baseman, J.B. (1987) Shared epitopes between *Mycoplasma pneumoniae* major adhesin protein P1 and a 140-kilodalton protein of Mycoplasma genitalium. *Infect Immun* 55: 49-56.

Morsy, M.A., Panangala, V.S., and Hu, P.C. (1993) Identification and characterization of a *Mycoplasma synoviae* 55,000-molecular-weight antigen associated with hemagglutination. *Avian Dis* 37: 1097-1104.

Nocard, and Roux (1990) The microbe of pleuropneumonia. 1896. *Rev Infect Dis* 12: 354-358.

Norris, V., Turnock, G., and Sigee, D. (1996) The *Escherichia coli* enzoskeleton. *Mol Microbiol* 19: 197-204.

Oakley, B.R., Kirsch, D.R., and Morris, N.R. (1980) A simplified ultrasensitive silver stain for detecting proteins in polyacrylamide gels. *Anal Biochem* 105: 361-363.

Ogle, K.F., Lee, K.K., and Krause, D.C. (1991) Cloning and analysis of the gene encoding the cytadherence phase-variable protein HMW3 from *Mycoplasma pneumoniae*. *Gene* 97: 69-75.

Ogle, K.F., Lee, K.K., and Krause, D.C. (1992) Nucleotide sequence analysis reveals novel features of the phase-variable cytadherence accessory protein HMW3 of *Mycoplasma pneumoniae*. *Infect Immun* 60: 1633-1641.

Papazisi, L., Frasca, S., Jr., Gladd, M., Liao, X., Yogev, D., and Geary, S.J. (2002) GapA and CrmA coexpression is essential for *Mycoplasma gallisepticum* cytadherence and virulence. *Infect Immun* 70: 6839-6845.

Pich, O.Q., Burgos, R., Ferrer-Navarro, M., Querol, E., and Pinol, J. (2006) *Mycoplasma genitalium* mg200 and mg386 genes are involved in gliding motility but not in cytadherence. *Mol Microbiol* 60: 1509-1519.

Pollack, J.D., Merola, A.J., Platz, M., and Booth, R.L., Jr. (1981) Respiration-associated components of Mollicutes. *J Bacteriol* 146: 907-913.

Pollack, J.D. (1992) Carbohydrate Metabolism and Energy Conservation. In *Mycoplasmas: Molecular Biology and Pathogenesis*. maniloff, J., R.N. McElhaney, L.R. Finch, J.B. Baseman (ed). Washington, D. C.: American Society for Microbiology, pp. 181-200.

Pollack, J.D., Williams, M.V., and McElhaney, R.N. (1997) The comparative metabolism of the mollicutes (Mycoplasmas): the utility for taxonomic classification and the relationship of putative gene annotation and phylogeny to enzymatic function in the smallest free-living cells. *Crit Rev Microbiol* 23: 269-354.

Pollack, J.D. (2002) Central Carbohydrate Pathways: Metabolic Flexibility and the Extra Role of Some "Housekeeping" Enzymes. In *Molecular Biology and Pathogenicity of Mycoplasmas*. Razin, S., and R. Herrmann (ed). New York: Kluwer Academic/Plenum Publishers, pp. 163-199.

Popham, P.L., Hahn, T.W., Krebes, K.A., and Krause, D.C. (1997) Loss of HMW1 and HMW3 in noncytadhering mutants of *Mycoplasma pneumoniae* occurs post-translationally. *Proc Natl Acad Sci U S A* 94: 13979-13984.

Powell, D.A., Hu, P.C., Wilson, M., Collier, A.M., and Baseman, J.B. (1976) Attachment of *Mycoplasma pneumoniae* to respiratory epithelium. *Infect Immun* 13: 959-966.

Proft, T., and Herrmann, R. (1994) Identification and characterization of hitherto unknown *Mycoplasma pneumoniae* proteins. *Mol Microbiol* 13: 337-348.

Proft, T., Hilbert, H., Layh-Schmitt, G., and Herrmann, R. (1995) The proline-rich P65 protein of *Mycoplasma pneumoniae* is a component of the Triton X-100-insoluble fraction and exhibits size polymorphism in the strains M129 and FH. *J Bacteriol* 177: 3370-3378.

Proft, T., Hilbert, H., Plagens, H., and Herrmann, R. (1996) The P200 protein of *Mycoplasma pneumoniae* shows common features with the cytadherence-associated proteins HMW1 and HMW3. *Gene* 171: 79-82.

Radestock, U., and Bredt, W. (1977) Motility of *Mycoplasma pneumoniae*. *J Bacteriol* 129: 1495-1501.

Razin, S., and Jacobs, E. (1992) Mycoplasma adhesion. *J Gen Microbiol* 138: 407-422.

Reddy, S.P., Rasmussen, W.G., and Baseman, J.B. (1995) Molecular cloning and characterization of an adherence-related operon of *Mycoplasma genitalium*. *J Bacteriol* 177: 5943-5951.

Regula, J.T., Boguth, G., Gorg, A., Hegermann, J., Mayer, F., Frank, R., and Herrmann, R. (2001) Defining the mycoplasma 'cytoskeleton': the protein composition of the Triton X-100 insoluble fraction of the bacterium *Mycoplasma pneumoniae* determined by 2-D gel electrophoresis and mass spectrometry. *Microbiology* 147: 1045-1057.

Reynolds, E.S. (1963) The use of lead citrate at high pH as an electron-opaque stain in electron microscopy. *J Cell Biol* 17: 208-212.

Roberts, D.D., Olson, L.D., Barile, M.F., Ginsburg, V., and Krivan, H.C. (1989) Sialic acid-dependent adhesion of *Mycoplasma pneumoniae* to purified glycoproteins. *J Biol Chem* 264: 9289-9293.

Rocha, E.P., and Blanchard, A. (2002) Genomic repeats, genome plasticity and the dynamics of Mycoplasma evolution. *Nucleic Acids Res* 30: 2031-2042.

Rodwell, A.W., and Mitchell, A. (1979) Nutrition, Growth, and Reproduction. In *The Mycoplasmas*. Vol. 1. Barile, M.F., Razin, S. (ed). New York: Academic Press, Inc. .

Rogers, M.J., Simmons, J., Walker, R.T., Weisburg, W.G., Woese, C.R., Tanner, R.S., Robinson, I.M., Stahl, D.A., Olsen, G., Leach, R.H., and et al. (1985) Construction of the mycoplasma evolutionary tree from 5S rRNA sequence data. *Proc Natl Acad Sci U S A* 82: 1160-1164.

Romero-Arroyo, C.E., Jordan, J., Peacock, S.J., Willby, M.J., Farmer, M.A., and Krause, D.C. (1999) *Mycoplasma pneumoniae* protein P30 is required for cytadherence and associated with proper cell development. *J Bacteriol* 181: 1079-1087.

Rudd, K.E. (2000) EcoGene: a genome sequence database for *Escherichia coli* K-12. *Nucleic Acids Res* 28: 60-64.

Ruland, K., Wenzel, R., and Herrmann, R. (1990) Analysis of three different repeated DNA elements present in the P1 operon of *Mycoplasma pneumoniae*: size, number and distribution on the genome. *Nucleic Acids Res* 18: 6311-6317.

Schaper, U., Chapman, J.S., and Hu, P.C. (1987) Preliminary indication of unusual codon usage in the DNA coding sequence of the attachment protein of *Mycoplasma pneumoniae*. *Isr J Med Sci* 23: 361-367.

Seto, S., Layh-Schmitt, G., Kenri, T., and Miyata, M. (2001) Visualization of the Attachment Organelle and Cytadherence Proteins of *Mycoplasma pneumoniae* by Immunofluorescence Microscopy. *J. Bacteriol.* 183: 1621-1630.

Seto, S., and Miyata, M. (2003) Attachment organelle formation represented by localization of cytadherence proteins and formation of the electron-dense core in wild-type and mutant strains of *Mycoplasma pneumoniae*. *J Bacteriol* 185: 1082-1091.

Seto, S., Kenri, T., Tomiyama, T., and Miyata, M. (2005) Involvement of P1 adhesin in gliding motility of *Mycoplasma pneumoniae* as revealed by the inhibitory effects of antibody under optimized gliding conditions. *J Bacteriol* 187: 1875-1877.

Seto, S., Layh-Schmitt, G., Kenri, T., Miyata, M. (2000) Formation schemes of the attachment organelle in *Mycoplasma pneumoniae*. *IOM Letters* 13: 149.

Shih, Y.L., Le, T., and Rothfield, L. (2003) Division site selection in *Escherichia coli* involves dynamic redistribution of Min proteins within coiled structures that extend between the two cell poles. *Proc Natl Acad Sci U S A* 100: 7865-7870.

Smiley, B.K., and Minion, F.C. (1993) Enhanced readthrough of opal (UGA) stop codons and production of *Mycoplasma pneumoniae* P1 epitopes in Escherichia coli. *Gene* 134: 33-40.

Starger, J.M., and Goldman, R.D. (1977) Isolation and preliminary characterization of 10-nm filaments from baby hamster kidney (BHK-21) cells. *Proc Natl Acad Sci U S A* 74: 2422-2426.

Steinert, P.M., Zimmerman, S.B., Starger, J.M., and Goldman, R.D. (1978) Ten-nanometer filaments of hamster BHK-21 cells and epidermal keratin filaments have similar structures. *Proc Natl Acad Sci U S A* 75: 6098-6101.

Stevens, M.K., and Krause, D.C. (1990) Disulfide-linked protein associated with *Mycoplasma pneumoniae* cytadherence phase variation. *Infect Immun* 58: 3430-3433.

Stevens, M.K., and Krause, D.C. (1991) Localization of the *Mycoplasma pneumoniae* cytadherence-accessory proteins HMW1 and HMW4 in the cytoskeletonlike Triton shell. *J Bacteriol* 173: 1041-1050.

Stevens, M.K., and Krause, D.C. (1992) *Mycoplasma pneumoniae* cytadherence phase-variable protein HMW3 is a component of the attachment organelle. *J Bacteriol* 174: 4265-4274.

Su, C.J., Tryon, V.V., and Baseman, J.B. (1987) Cloning and sequence analysis of cytadhesin P1 gene from *Mycoplasma pneumoniae*. *Infect. Immun.* 55: 3023-3029.

Su, C.J., Chavoya, A., Dallo, S.F., and Baseman, J.B. (1990) Sequence divergency of the cytadhesin gene of *Mycoplasma pneumoniae*. *Infect Immun* 58: 2669-2674.

Taghbalout, A., and Rothfield, L. (2007) RNaseE and the other constituents of the RNA degradosome are components of the bacterial cytoskeleton. *Proc Natl Acad Sci U S A* 104: 1667-1672.

Talkington, D.F., Waites, K.B., Schwartz, S.B., and Besser, R.E. (2001) Emerging from obscurity: understanding pulmonary and extrapulmonary syndromes, pathogenesis, and epidemiology of human *Mycoplasma pneumoniae* infections. In *Emerging Infections 5*. Scheld, W.M., W. A. Craig, J. M. Hughes (ed). Washington, D. C. : American Society for Microbiology, pp. 57-84.

Taylor, G., Taylor-Robinson, D., and Fernald, G.W. (1974) Reduction in the severity of *Mycoplasma pneumoniae*-induced pneumonia in hamsters by immunosuppressive treatment with antithymocyte sera. *J Med Microbiol* 7: 343-348.

Tham, T.N., Ferris, S., Bahraoui, E., Canarelli, S., Montagnier, L., and Blanchard, A. (1994) Molecular characterization of the P1-like adhesin gene from *Mycoplasma pirum*. *J Bacteriol* 176: 781-788.

Towbin, H., Staehelin, T., and Gordon, J. (1979) Electrophoretic transfer of proteins from polyacrylamide gels to nitrocellulose sheets: procedure and some applications. *Proc Natl Acad Sci U S A* 76: 4350-4354.

Tryon, V.V., and Baseman, J.B. (1987) The acquisition of human lactoferrin by *Mycoplasma pneumoniae*. *Microb Pathog* 3: 437-443.

Tully, J.G., Whitcomb, R.F., Clark, H.F., and Williamson, D.L. (1977) Pathogenic mycoplasmas: cultivation and vertebrate pathogenicity of a new spiroplasma. *Science* 195: 892-894.

van, I., and Ruys, A.C. (1960) The fine structure of the Mycoplasmataceae (microorganisms of the pleuropneumonia group PPLO). 1. Mycoplasma hominis, *M. fermentans* and *M. salivarium*. *J Ultrastruct Res* 3: 282-301.

Waites, K.B., and Talkington, D.F. (2004) *Mycoplasma pneumoniae* and its role as a human pathogen. *Clin Microbiol Rev* 17: 697-728, table of contents.

Waldo, R.H., 3rd, Popham, P.L., Romero-Arroyo, C.E., Mothershed, E.A., Lee, K.K., and Krause, D.C. (1999) Transcriptional analysis of the hmw gene cluster of *Mycoplasma pneumoniae*. *J Bacteriol* 181: 4978-4985.

Waldo, R.H., 3rd, Jordan, J.L., and Krause, D.C. (2005) Identification and complementation of a mutation associated with loss of *Mycoplasma pneumoniae* virulence-specific proteins B and C. *J Bacteriol* 187: 747-751.

Waldo, R.H., 3rd, and Krause, D.C. (2006) Synthesis, stability, and function of cytadhesin P1 and accessory protein B/C complex of *Mycoplasma pneumoniae*. *J Bacteriol* 188: 569-575.

Wall, F., Pfister, R.M., and Somerson, N.L. (1983) Freeze-fracture confirmation of the presence of a core in the specialized tip structure of *Mycoplasma pneumoniae*. *J Bacteriol* 154: 924-929.

Weatherly, D.B., Astwood, J.A., 3rd, Minning, T.A., Cavola, C., Tarleton, R.L., and Orlando, R. (2005) A Heuristic method for assigning a false-discovery rate for protein identifications from Mascot database search results. *Mol Cell Proteomics* 4: 762-772.

Weisburg, W.G., Tully, J.G., Rose, D.L., Petzel, J.P., Oyaizu, H., Yang, D., Mandelco, L., Sechrest, J., Lawrence, T.G., Van Etten, J., and et al. (1989) A phylogenetic analysis of the mycoplasmas: basis for their classification. *J Bacteriol* 171: 6455-6467.

Willby, M.J., and Krause, D.C. (2002) Characterization of a *Mycoplasma pneumoniae* hmw3 mutant: implications for attachment organelle assembly. *J Bacteriol* 184: 3061-3068.

Willby, M.J., Balish, M.F., Ross, S.M., Lee, K.K., Jordan, J.L., and Krause, D.C. (2004) HMW1 is required for stability and localization of HMW2 to the attachment organelle of *Mycoplasma pneumoniae*. *J Bacteriol* 186: 8221-8228.

Wilson, M.H., and Collier, A.M. (1976) Ultrastructural study of *Mycoplasma pneumoniae* in organ culture. *J Bacteriol* 125: 332-339.

Woese, C.R., Maniloff, J., and Zablen, L.B. (1980) Phylogenetic analysis of the mycoplasmas. *Proc Natl Acad Sci U S A* 77: 494-498.

Yoshida, S., Fujisawa, A., Tsuzaki, Y., and Saitoh, S. (2000) Identification and expression of a *Mycoplasma gallisepticum* surface antigen recognized by a monoclonal antibody capable of inhibiting both growth and metabolism. *Infect Immun* 68: 3186-3192.